Assessment of Human Trunk Kinetics Using a Multi-Segment Model: An Approach to Minimize the Propagation of Experimental Errors

by

Alireza Noamani

A thesis submitted in partial fulfillment of the requirements for the degree of

Master of Science

Department of Mechanical Engineering
University of Alberta

Abstract

Evaluating several pathological conditions such as low-back pain, scoliosis, herniated discs, and postural stability after spinal cord injury or chronic stroke requires a deep understanding of the inter-spinal interactions. Assessing the kinetics of the human head-arms-trunk (HAT) could provide useful information for clinical assessment during various motor tasks, and for designing prevention and rehabilitation strategies. Mathematical techniques such as linked-segment models of the HAT along with an inverse dynamics approach can be used to calculate the inter-segmental moments. Several studies have investigated the lumbosacral joint moment using a single-segment model of the trunk during different movements. However, methods for calculating joint moments at different levels of the spinal column have rarely been investigated. This is due to the fact that joint moment estimation using an inverse dynamics approach requires accurate estimation of the individual-specific body segment parameters (BSPs) (e.g., mass, center of mass, moments of inertia, and joint centers of rotation) of each segment, which is technically challenging for the multi-segment HAT due to the high inter-participant variability of these parameters for HAT segments. Moreover, this approach is prone to experimental errors due to inaccuracies in kinematic data induced by soft tissue artifacts and force plate measurement errors (such as center of pressure offsets). As a result, a methodology to estimate joint moments at different levels of the spinal column after minimizing above-mentioned inaccuracies is of great significance.

The objective of this thesis was to propose a methodology for accurate assessment of the three-dimensional (3D) inter-vertebral moments using a multi-segment HAT model via compensating errors in motion data (due to soft tissue artifacts), ground interaction force measurements (due to center of pressure offsets), and BSPs estimation for the HAT segments. Using the proposed methodology, this study also aimed to provide, for the first time, the inter-vertebral moment patterns during multi-directional trunk-bending motions using a multi-segment HAT model.

First, this study presented a nonlinear, multi-step, optimization-based, non-invasive method for estimating individual-specific BSPs and center of pressure offsets for calculating joint moments in a seven-segment HAT model. The collected motion data of eleven non-disabled individuals

participating in a seated trunk-bending experiment in the anterior direction (recorded by motion capture cameras and a force plate) were used. Initial estimates of the BSPs were adopted from cadaveric data and scaled for each individual. Two inverse dynamics approaches were used. Accurate inputs are expected to result in the same values for the net joint moment via both inverse dynamics approaches. Since scaling induces inaccuracies in the estimation of the BSPs, the inverse dynamics approaches were expected to result in different values for the net joint moments. Therefore, a set of BSPs and center of pressure offsets, that minimize the difference between the results of the two approaches, are expected to be more accurate compared to those which result in significantly larger differences. Our proposed method estimated the individual-specific BSPs and the center of pressure offsets that minimized the difference between the net joint moment calculated via both inverse dynamics approaches at all inter-segmental levels. The obtained results indicated that the proposed method significantly reduced the difference ($p < 0.01$) in the net joint moment estimation by 77.6 % (average among participants). The proposed method enabled more accurate estimation of individual-specific BSPs, and consequently more accurate assessment of the 3D kinetics of a multi-segment HAT model.

Second, this study presented a procedure for estimating joint moments at different inter-segmental levels during multi-directional trunk-bending motion after compensating two major sources of error: inaccuracy of individual-specific BSPs and soft tissue artifacts. The collected motion data of eleven non-disabled individuals participating in a seated trunk-bending experiment in five different directions and for three different speeds were used. We compensated for the errors in the motion data due to soft tissue artifacts based on a previously introduced technique. The effect of joint level, trunk-bending direction, and movement speed on the inter-segmental moments were investigated. The results showed significant effects ($p < 0.01$) of joint-level, bending-direction, as well as an interaction effect between joint-level and bending-direction. Moreover, we observed significant effects of joint-level and trunk-bending direction as well as their interaction effect on the net joint moment errors induced due to soft tissue artifacts. The results of this study reflected complex, task-specific patterns for the 3D inter-segmental moments at different joint-levels, which cannot be studied using single-segment models or without such error compensations.

The proposed procedure enables more accurate *in vivo* estimation of the inter-vertebral moments during various functional tasks. Interpretation of inter-vertebral moments can be of great importance for clinical evaluations and for developing injury prevention and rehabilitation strategies as well as identifying any clinically meaningful joint moment patterns for either non-disabled or disabled populations.

Preface

This thesis is an original work by Alireza Noamani. The research project, of which this thesis is a part, received research ethics approval from the Health Research Ethics Board of the University of Alberta, Project Name "Assessment of Dynamic Balance and Fall Risk in Sitting", study ID MS2_Pro00063998.

Chapter 3 of this thesis has been submitted as an original article (research paper) to the *Journal of Biomechanical Engineering (Transactions of the ASME)*, titled **"Optimal Estimation of Anthropometric Parameters for Quantifying Multi-Segment Trunk Kinetics"**.

Chapter 4 of this thesis has been submitted as an original article (full paper) to *Gait and Posture*, titled **"Quantification of Multi-Segment Trunk Kinetics during Multi-Directional Trunk Bending"**.

Chapters 3 and 4 present a methodology development and data analysis and interpretation applied on previously collected data. The collected data were presented in the *Journal of Electromyography & Kinesiology, vol. 20, no. 5, pp. 823–832, 2010* and the *Journal of Applied Biomechanics, vol. 26, no. 3, pp. 265–272, 2010* that addressed different research questions.

Parts of this thesis were presented as a poster at the *17th Annual Alberta Biomedical Engineering Conference 2016 (Banff, Canada)* and selected for a five-minute presentation competition at the same conference.

Dedicated to

My parents,

Sadaf, my twin sister,

And

Shiva, my love.

Acknowledgments

I would like to express my sincere gratitude to my supervisors, Dr. Hossein Rouhani and Dr. Albert H. Vette for their encouragement, patience, motivation, and immense knowledge. Their guidance helped me tremendously in all the time of research and writing this thesis.

I would like to thank Dr. Milos Popovic and Dr. Richard Preuss for their contribution in data collection and their insightful comments on this research. I would like to thank my lab colleagues for their contribution. I would like to thank Ms. Gabriela Ueno for her help in image processing of the Male Visible Human images. I would like to especially thank Kshitij Agarwal for helping me during the experiments. Many thanks also go to Fatemeh Gholibeigian for always being there for me when I needed her and for offering his help whenever I needed assistance. I would also like to thank Justin Lewicke and Darrell Goertzen for lending their expertise and answering many questions that I had about the motion capture system. I am extremely grateful to Andy Williams, Jordan Arthur, Sofia Medina Pando, and Azhali Arellano Lopez for helping me in designing and performing the experiments. I could always count on Milad Nazarahari, Hooman Bahari, and Niloufar Ahmadian to help me whenever I needed assistance.

I would like to thank my parents and my sister who have been extremely supportive throughout the process. And finally, I would like to thank my love, Shiva Zamani, for her love, patience, and endurance, none of this could have been possible without your support.

This project was made possible through the generous support of the Faculty of Engineering of the University of Alberta, the Faculty of Graduate Studies and Research, University of Alberta; Alberta Innovates Technology Futures, and the Natural Sciences and Engineering Research Council of Canada.

Table of Contents

List of Tables

List of Figures

Nomenclature

3D	three-dimensional
A	anterior
AL	anterior-lefts
AR	anterior-right
BSPs	body segment parameters
COM	center of mass
COP	center of pressure
CV	coefficient of variation
GRFs	ground reaction forces
HAT	head-arms-trunk
JCR	joint center of rotation
L	left
R	Right
RMS	root mean square
RMSE	root mean square error

Chapter 1

1 Introduction

1.1 Trunk Kinetics and Applications

Spinal cord and back injuries frequently occur due to various conditions such as occupational, athletic, and accidental incidences. Accurate risk assessment, prevention, and treatment evaluation for such injuries require assessment of the kinematics and kinetics of the spinal column [1]. Such assessments require an accurate and reliable estimation of trunk muscle forces and spinal interactions [1]. Intervertebral interactions such as relative movements between vertebrae, and spinal loads are of great importance for clinical evaluation of a wide range of pathological conditions such as scoliosis [2]–[5], low back pain [6]–[12], spinal cord injury [13]–[16], ankylosing spondylitis [17], and herniated disks [18]. Measurement of the inter-spinal interactions is also employed for medical decision making and for designing pre- and post-surgical treatments [19].

Various techniques have been used for accurate measurement of the intervertebral motion such as percutaneous skeletal trackers, inserted bone pins [20], [21], and medical imaging [22]. However, any technique that involves surgery or inserting pins increases the risk of spinal cord injury or may cause infection [19]. Besides, medical imaging techniques are subject to radiation exposure [19]. Non-invasive motion tracking systems have been extensively used to capture the motion of different body parts during various motor tasks. Motion tracker systems use skin-mounted active or passive markers and infrared cameras to record the instantaneous three-dimensional (3D) coordinates of the anatomical landmarks. This measurement technique presents no risk and is used as a gold-standard reference tool for human movement studies as well as for clinical decision-making purposes. Mathematical techniques have been introduced and employed along with the gold-standard motion capture systems to study biomechanical mechanisms of various motor tasks.

Linked-segment models of the human body, as a mathematical technique, have facilitated *in vivo* studying of intervertebral interactions. Biomechanical studies have widely used motion capture systems along with linked-segment models to study the spinal kinematics and the spine's or trunk's stability [23], [24]. Furthermore, clinical studies have employed such biomechanical model approaches in investigating pathological conditions such as hemiplegia and Parkinson's disease [25], chronic stroke [26], and multiple sclerosis [27]. 3D kinematics of the upper body have so far been studied using single-segment [28] and multi-segment [29] models of the head-arms-trunk (HAT). To investigate the effect of movements produced and maintained by neuro-musculoskeletal systems on postural stability, assessment of the HAT kinetics has also been used in biomechanics and rehabilitation research [30]. Moreover, measuring the net joint forces and moments is needed for calculating muscle forces, finding best rehabilitation techniques, evaluation of disability and impairment, or prostheses design [31]. Hence, assessing the accuracy and reliability of the kinetic analysis of the HAT is of great importance for many real-world applications as inaccurate measurements may result in wrong medical decisions, morbidity, and even permanent health conditions. Direct *in vivo* measurement of the reaction forces and moments at the body joints as generated by muscles requires very small and minimal invasive transducers [30] inserted among or around the spine, which is not practical in real-world clinical measurements. Therefore, indirect computation of kinetic variables (i.e., intervertebral forces and moments) via mathematical techniques such as inverse dynamics along with linked-segment models has become the preferred approach.

Inverse dynamics, as a iterative algorithm, is a computational approach to determine inter-segmental forces and moments. Using an inverse dynamics formulation, the inter-segmental reaction forces and moments can be calculated in a linked-segment model of the HAT based on non-invasive motion capture data. For this purpose, measurement of the inter-segmental kinematics, accurate estimation of anthropometric parameters, and force interaction between the body and the base of support are required. Although inverse dynamics is a commonly-used approach for biomechanical studies, it is prone to inaccurate results due to propagation of errors in measurement data. Several studies addressed the sources of error in kinetic analyses and suggested that inaccuracies in measurement of (a) kinematic parameters [32]–[34], (b) force plate data [35], and (c) anthropometric properties of body segments (hereafter referred to as body

segment parameters (BSPs)) [36]–[38] make major contributions to uncertainties in net joint moment estimations. Some studies investigated the effect of joint center locations, segment orientation, external forces and their point of application, linear acceleration, and inertial parameters of the segments on the estimated joint moments [39], [40] in the lower limbs and suggested that inaccuracies in (a) BSPs and (b) the segments' motion are the main sources of uncertainty [37], [40]. Therefore, accurate results of an inverse dynamics approach require compensation of above-mentioned errors. Such compensation techniques are not trivial, and have not been developed yet, particularly for assessing the kinetics of multi-segment models of the HAT, because of its specific technical challenges [31]. As a result, utilizing such assessment of multi-segment HAT kinetics in clinical evaluation is currently not possible and reliable due to the induced errors in kinematics data, inaccuracies in estimating individual-specific BSPs, and systematic errors in force plate measurements due to calibration with motion capture cameras. Therefore, an approach that could minimize the propagation of the above-mentioned experimental errors could enable the assessment of HAT kinetics for clinical evaluation of a wide range of pathological conditions.

Kinematic data required as input for the inverse dynamics formulation oftentimes are obtained from motion tracking systems which require marker placement on anatomical landmarks for capturing the motion of different body segments during a motor task. Therefore, three types of error could affect the kinematic measurements: (a) instrumentation inaccuracy (e.g., calibration of cameras), (b) marker misplacement on the bony anatomical landmarks, and (c) soft tissue artifacts (STA), i.e., the relative movement between skin-mounted markers and underlying bony landmarks [41]–[43]. These errors propagate in segment motion and joint angle calculations and could affect the computation of the intervertebral forces and moments when using inverse dynamics. Previous studies have investigated the effect of kinematic inaccuracies such as soft tissue artifacts on the kinematics and kinetics assessment of the lower limbs [44]–[46]. Besides, some studies assessed such effects on the kinematics of scapula [47], lumbar spine vertebrae [48], spine curvature [49], and the multi-segment HAT [19]. However, to the best of our knowledge, no study investigated the effect of soft tissue artifacts on the kinetics of a multi-segment HAT model.

The inverse dynamics approach requires accurate estimation of BSPs. Previous studies have highlighted the necessity of an individual-specific set of BSPs [38]. Medical imaging techniques such as magnetic resonance imaging, gamma-ray scanning, and dual-energy X-ray absorptiometry have been used to more accurately measure individual-specific BSPs. Although these methods are more accurate, they cannot be used for daily clinical analyses due to the significant cost, complexity, and radiation exposure. Regression equations [50] based on medical images of a small sample population or based on a limited number of cadavers [51] were also proposed to estimate individual-specific BSPs. All these efforts enable scaling approaches to estimate BSPs for different individuals based on the body weight and height; however, such methods could result in significant errors greater than 40% in joint moment estimation [52]. Optimization approaches have been proposed to estimate individual-specific BSPs for the lower limbs. These studies used the overdetermined nature of the traditional inverse dynamics formulation to find an optimal set of BSPs that minimizes the error in joint moment estimation by minimizing the difference between the joint moments calculated via different inverse dynamic approaches [52], [53]. Accurate inputs are expected to result in the same values for the net joint moment via different inverse dynamics approaches. Therefore, a set of BSPs, that minimizes the difference between the results of the approaches, are expected to be more accurate compared to those which result in significantly larger differences. However, the proposed methods only targeted the anthropometric data of the lower limbs when assuming the HAT as a single rigid body. To the best of our knowledge, there is currently no optimization-based study that investigates individual-specific BSPs for the upper body. More accurate and reliable estimation of individual-specific BSPs could enable more accurate measurement of the intervertebral moments, and consequently the characterization of postural balance and of the response of HAT to impact loads, the evaluation of the surgical approaches, and the design of neuroprostheses [51].

Using single-segment kinematic models, the interaction forces between the body and ground, and anthropometric parameters (i.e., BSPs), the intervertebral joint moment at the lumbosacral level has been investigated in the past [1], [31], [39], [54], [55]. The key challenge in extending this approach to the assessment of HAT kinetics using multi-segment models is the estimation of BSPs for several small-scale segments along the vertebral column. Recently, Vette et al. obtained BSPs for each vertebra based on high-quality images from a single Caucasian cadaver [56] and used

them for estimating cervical and lumbar spine joint moments based on kinematic data collected in another *in vivo* study. However, the BSPs obtained with one participant may not yield accurate joint moments based on kinematics data from another participant. In addition, the pattern of the joint moments at different levels of the spinal column is yet to be studied for various functional tasks.

To the best of our knowledge, not a single study has reported on quantitative, 3D kinetics of a multi-segment HAT model using accurate individual-specific BSPs, whose estimation is technically challenging due to the high inter-participant variability of the BSPs. Consequently, a new approach to compensate the above-mentioned inaccuracies and address a reliable, quantitative approach for more accurate estimation of the intervertebral reaction loads can significantly facilitate the assessment of HAT kinetics during movements using multi-segment models, and enable objective clinical evaluations and decision-making.

1.2 Thesis Objectives

The goal of this study is to provide a more accurate estimation of the 3D intervertebral moments at different levels of the spinal column using a multi-segmental HAT model. To address and compensate for the major sources of inaccuracies, a comprehensive methodology is proposed to compensate errors in: (a) kinematic data due to soft tissue artifacts, (b) interaction force measurement (i.e., center of pressure (COP) offsets), and (c) BSPs for several segments along the spinal column. This study also aims to apply, for the first time, the proposed methodology to assess the joint moment patterns along the spinal column during multi-directional trunk bending, facilitating the characterization of the effects of joint level, trunk bending direction, and movement speed on the joint moment (Figure 1).

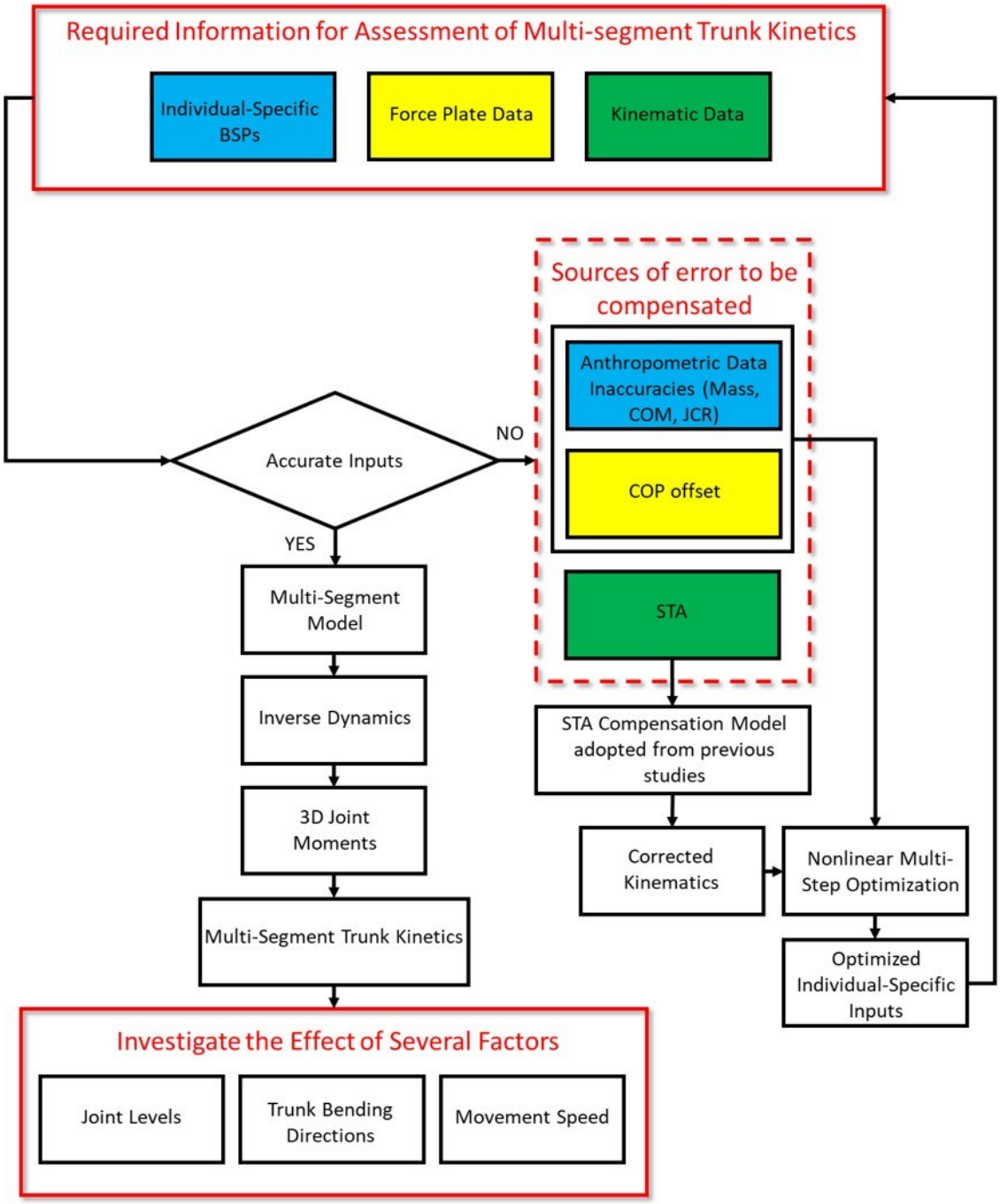

Figure 1. Thesis outline and summary of the proposed methodology: Multi-segment trunk kinetics have been calculated to investigate the effect of several factors after compensating inaccuracies in body segment parameters (BSPs), center of pressure (COP) offsets, and soft tissue artifacts (STA). BSPs include the segment's mass, center of mass (COM), and the joint center of rotation (JCR).

1.3 Thesis Outline

Chapter 2 reviews the literature that is relevant to this thesis: a review of human movement biomechanics and motion tracking systems; an overview of kinematics and kinetics descriptions for biomechanical analysis of human movement; a review of spinal column anatomy, trunk kinematic models and kinematic analysis; a review of trunk kinetics and its application in biomechanics; and an overview of errors in kinetic analyses of human movement and compensation methods. Chapter 3 presents a non-invasive, nonlinear optimization-based method to more accurately estimate a set of individual-specific BSPs and COP offsets for quantifying multi-segment trunk kinetics that minimizes the error in intervertebral joint moment estimation. Chapter 4 presents the effect of soft tissue artifacts on joint moments and provides the pattern of 3D joint moments at different levels of the spinal column during multi-directional seated trunk bending. Chapter 5 summarizes the key findings, provides conclusive remarks on the performed work, and describes future perspectives.

Chapter 2

2 Literature Review

2.1 Human Movement Biomechanics

The aim of human movement biomechanics is to assess human motion based on descriptive quantitative information obtained from raw measurements [57]. The quantitative evaluation of human movement requires raw data from capturing 3D coordinates of the body's anatomical landmarks to find the relative motions between body segments [30], [57]–[59]. The anatomical landmarks whose motions are tracked could be categorized as (a) the center of gravity of body segments, (b) joint centers of rotation, (c) extremes of limb segments, or (d) bony prominences [57]. Further processing of the raw measurements is required to calculate kinematic variables of the body segments such as linear or angular displacements, velocities, and accelerations. Selection of the body segments is based on the task or movement to be studied. Following kinematics analysis of the human movement, the data can be used to calculate the forces and moments, which causes the observed movement. Kinetics analysis of the human movement provides insight into the mechanisms, movement strategies, and contribution of the neural system to movement execution [57].

To track the 3D movements of the body segments, different techniques are used: optoelectronic stereophotogrammetry [59], [60], stereoradiography [61], electromagnetic tracking systems [62]–[64], inertial measurement units (IMUs) [65]–[70], and markerless motion capture systems [71]–[73]. Among all these types of motion tracking systems, stereophotogrammetric systems are most frequently used by researchers.

2.1.1 Stereophotogrammetric Systems

Optoelectronic stereophotogrammetric systems are widely used to capture the instantaneous position of the anatomical landmarks in a 3D measurement volume during various motor tasks.

Reconstruction of the trajectories of the landmarks could be based on photographs [74], radiographs [75], or video images [41], [76]. Several advantages of reconstructing the coordinates from video images such as lower cost, faster data processing , and less image distortion due to processing make the video-based optoelectronic systems the most efficient and common motion-tracking system for biomechanical studies [41]. Two types of markers are commonly used by video-based motion capture systems: retroreflective passive markers, and active markers. Passive markers are used along with cameras equipped with light-emitting diode arrays mounted around the lens of each camera that illuminate infrared light [41]. Pattern recognition software [77] or dedicated hardware circuits [78] are used to recognize the passive markers in the video frames. Active markers tracking is performed by sequential pulse timing of the markers themselves detected by the system [41]. This implies that the active marker systems are more accurate and with higher sampling frequencies compared to the passive marker systems; however, the presence of wires, batteries, and pulsing circuitry are the main disadvantages of these systems [41], [79].

For tracking the movement of a body part of interest, the instantaneous positions of a minimum of three non-aligned markers placed superficially on that segment are required [59]. To reconstruct 3D coordinates of a marker and prevent marker obscurity, simultaneous visibility by at least two cameras is needed [41]. Therefore, to minimize the possibility of missing a marker and to increase the robustness of data acquisition, some studies suggest using at least four markers per segment. This enables the reconstruction of the segment in case one of the markers becomes obstructed.

2.1.2 Limitations of Stereophotogrammetric Systems

Stereophotogrammetric systems are subject to several sources of errors that could affect the measured marker coordinates, including instrumental errors [41], soft tissue artifacts [19], [43], and anatomical landmark misplacement [42], [80]. Instrumental errors could be propagated either systematically, due to inaccuracies in system calibration or nonlinearities, or randomly because of marker flickering, or electronic noise [41]. Soft tissue artifacts (STA) are defined as the relative movement of a skin-mounted marker with respect to underlying bone due to skin deformation and/or muscle contraction [19], [43]. The error induced by STA is shown to be task-specific, and not consistent among individuals [43]. The STA effect on the kinematics of the human movements is typically larger than the instrumental errors caused by the stereophotogrammetric system and,

hence, is a major source of inaccuracies [43]. Identification of the anatomical landmarks is a key requirement in human movement analysis using video-based stereophotogrammetric systems. Anatomical landmark determination could highly affect the joint kinematics in terms of reliability and interpretability [42]. The shape of the anatomical landmark, soft tissue thickness over the bony prominences, palpation procedure, and finally the researcher expertise can contribute to an accurate identification of an anatomical landmark [42].

Using stereophotogrammetric systems for movement analysis requires a great amount of time for participant preparation and attachment of markers and fixtures [73]. Moreover, it needs a trained operator to accurately find the anatomical landmarks for placing the skin-mounted markers. Markerless motion capture systems are a new technology that may enhance the study of movement biomechanics by eliminating the inter-operator variability and the experimental artifacts (e.g., STA and marker misplacement) [73], [81]. However, this method has longer processing times [73] and its accuracy is dependent on choosing the proper technical equipment and algorithms [81]. Hence, its validity and reproducibility must be assessed for clinical applications [82].

In addition, stereophotogrammetric systems require a dedicated laboratory volume for biomechanical analysis of conventionally designed observation-based tests. Hence, such systems are costly and can only be utilized to capture and analyze a brief series of tasks in a constrained environment. New emerging light-weight IMU-based technologies have been recently used for ambulatory assessment of human locomotion. Such wearable systems enable long-term continuous monitoring during natural, real-life activities [83], [84] and increase the feasibility of in-home monitoring for older adults and individuals with chronic conditions [85]. Wearable health monitoring systems could facilitate early diagnosis and better treatment of medical conditions [86]. However, further biomechanical and clinical research is required to overcome challenges and issues associated with wearable systems for becoming a reliable technology and being accepted by clinicians and patients as an enhanced healthcare system [83]–[87] compared to gold-standard motion capture systems.

2.2 Kinematics and Kinetics Descriptions

2.2.1 Kinematic Data Acquisition and Processing

Capturing the trajectory of the skin-mounted markers using a motion capture system allows reconstructing the body segments of interest during the execution of a motor task [59]. The 3D rotation and translation of each rigid body segment are determined by at least three non-collinear markers or a cluster of markers attached superficially to the segment. The location of the markers is determined based on the experimental task and anatomical landmarks of the segment. This approach enables the measurement of kinematic variables that describe the body segment's motion as non-deformable rigid bodies. The kinematic variables are determined either by measurement or estimation using mathematical models of the musculoskeletal system [59]. A multi-body kinematics model can describe the kinematics of body segments represented as a chain of links (rigid body segments) connected to each other via joints. The number of the segments, the number of degrees of freedom in the model, and constraints imposed by the joints are dependent on the goal of the study to achieve an accurate estimation of the human movement that could mimic the function of the musculoskeletal system [30], [59]. As such, the kinematic variables of the body segments in the linked-segment model can be obtained based on the measurements of the motion tracking system. For this purpose, frames of reference should be first introduced.

2.2.2 Global and Local Frames

In a laboratory equipped with a stereophotogrammetric system for human movement analysis, a global reference frame is arbitrarily defined through a calibration procedure. The global frame (lab-fixed frame) is a set of orthogonal axes $(\vec{X}_g, \vec{Y}_g, \vec{Z}_g)$ in which the instantaneous coordinates of the markers are provided by the motion capture system [59], [88]. A local frame (body-fixed frame) (Figure 2) is a segment-specific frame fixed to the rigid segment and is defined based on the instantaneous positions of the markers placed on that segment [57], [59], [88]. When the markers defining a local frame are superficially placed with respect to the underlying anatomical landmark, the local frames are also called bone-embedded anatomical frames [30]. Using this standard approach, the associated segment local frame is repeatedly identifiable, which is required

for achieving high intra- and inter-participant repeatability [59]. Nonetheless, a point of interest can be expressed with respect to either a local or global frame (Figure 2) [57].

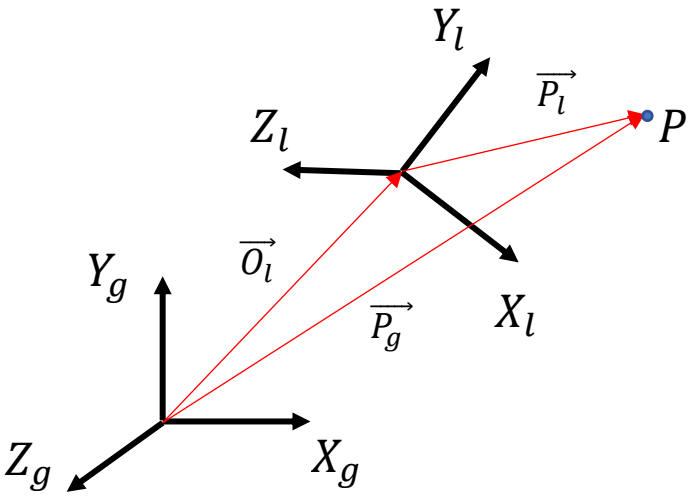

Figure 2. The position of a point of interest expressed in a global frame $(\vec{X}_g, \vec{Y}_g, \vec{Z}_g)$ or a local frame $(\vec{X}_l, \vec{Y}_l, \vec{Z}_l)$ as $\vec{P}_g$ and $\vec{P}_l$, respectively. $\vec{O}_l$ is a vector that shows the origin of the local frame in the global frame.

2.2.3 Coordinate Transformation

To define the local frame (coordinate system) of a segment, the instantaneous coordinates of three markers placed on that segment with respect to the global frame are required. $\vec{a}_1$, $\vec{a}_2$, and $\vec{a}_3$ are the position vectors of the segment's markers in the global reference frame (Figure 3). The local frame can be defined as a set of three orthogonal unit vectors expressed in the global frame as follows:

$$\vec{X}_l = \frac{\vec{a}_2 - \vec{a}_1}{|\vec{a}_2 - \vec{a}_1|},\ \vec{Y}_{aux} = \frac{\vec{a}_1 - \vec{a}_3}{|\vec{a}_1 - \vec{a}_3|},\ \vec{Z}_l = \frac{\vec{X}_l \times \vec{Y}_{aux}}{|\vec{X}_l \times \vec{Y}_{aux}|},\ \vec{Y}_l = \frac{\vec{Z}_l \times \vec{X}_l}{|\vec{Z}_l \times \vec{X}_l|} \quad \text{(Eq. 2.1)}$$

where $\vec{X}_l$, $\vec{Y}_l$, and $\vec{Z}_l$ are the unit vectors constituting the local frame of a segment, expressed in the global frame. The orientation of a rigid body in space with respect to the global frame is defined using an instantaneous rotation matrix denoted as follows:

$$ {}^{global}_{local}R = [\vec{X}_l, \vec{Y}_l, \vec{Z}_l] = \begin{bmatrix} \vec{X}_g.\vec{X}_l & \vec{X}_g.\vec{Y}_l & \vec{X}_g.\vec{Z}_l \\ \vec{Y}_g.\vec{X}_l & \vec{Y}_g.\vec{Y}_l & \vec{Y}_g.\vec{Z}_l \\ \vec{Z}_g.\vec{X}_l & \vec{Z}_g.\vec{Y}_l & \vec{Z}_g.\vec{Z}_l \end{bmatrix} = \begin{bmatrix} \cos\theta_{\vec{X}_g\vec{X}_l} & \cos\theta_{\vec{X}_g\vec{Y}_l} & \cos\theta_{\vec{X}_g\vec{Z}_l} \\ \cos\theta_{\vec{Y}_g\vec{X}_l} & \cos\theta_{\vec{Y}_g\vec{Y}_l} & \cos\theta_{\vec{Y}_g\vec{Z}_l} \\ \cos\theta_{\vec{Z}_g\vec{X}_l} & \cos\theta_{\vec{Z}_g\vec{Y}_l} & \cos\theta_{\vec{Z}_g\vec{Z}_l} \end{bmatrix} \quad \text{(Eq. 2.2)} $$

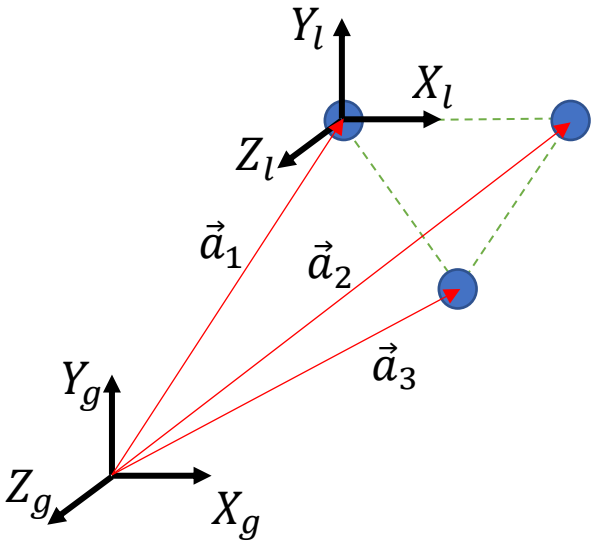

Figure 3. Coordinate transformation from a local frame to the global frame. The orientation of a segment of interest can be defined by a time-varying rotation matrix consisting of three columns of unit vectors and constructed using the instantaneous positions of at least three markers placed on the segment.

where the components of each column of this matrix are the projection of each axis of the local frame onto the unit directions of the global frame. The dot product of two unit vectors gives the cosine of the angle between them. To obtain the position vector of an arbitrary point on a segment during movement in the global reference frame, a transformation between two coordinate systems is required as denoted in (Eq. 2.3):

$$ \vec{P}_g = {}^{global}_{local}R.\vec{P}_l + \vec{O}_l \quad \text{(Eq. 2.3)} $$

where $\vec{P}_l$ and $\vec{P}_g$ are the position vectors in the local and global frames, respectively, $\vec{O}_l$ the position vector of the local frame origin expressed in the global frame, and ${}^{global}_{local}R$ is the instantaneous rotation matrix that describes the segment orientation with respect to the global frame [89].

2.2.4 Inverse Dynamics

By knowing the location of each segment's center of mass (COM) and its inertia tensor, the effect of the mass distribution of the link (segment) is determined [89]. The motion resulted from a set of forces and initial conditions can be computed via forward-dynamics [90]. However, in biomechanics, we oftentimes calculate the forces and moments that cause a particular movement using a motion capture system and anthropometric (inertial and geometric) parameters. This process is called inverse dynamics [90]. The forces and moments can be internal and external: internal forces are imposed by contraction of muscles, ligaments, or the friction in the muscles and joints [57]; external forces are applied by the ground or external loads [57]. Methods, such as iterative Newton-Euler dynamics algorithm, can be used to compute the forces and moments that correspond to a given body segment's motion. The algorithm is composed of outward and inward iterations [89]. For a given n-link model, the outward iterations compute the linear and rotational velocity and the linear and rotational acceleration of the COM of each link starting from link one and moving consecutively to link n. Subsequently, the inertial force and moment acting at the COM of each link are calculated. Having the load at the link's COM, the inward iteration computes the interaction joint forces and moments based on the force and moment balance equations for each link recursively from link n back to link one. The iterative formulation of Newton-Euler equations, adopted from [89], is summarized as follows:

Outward iterations: (Eq. 2.4)

$$^{i+1}\dot{v}_{i+1} = {}^{i+1}_{i}R(\ {}^{i}\dot{\omega}_i \times {}^{i}P_{i+1} + {}^{i}\omega_i \times (\ {}^{i}\omega_i \times {}^{i}P_{i+1}) + {}^{i}\dot{v}_i)\ ,$$

$$^{i+1}\dot{v}_{COM_{i+1}} = {}^{i+1}\dot{\omega}_{i+1} \times {}^{i+1}P_{COM_{i+1}} + {}^{i+1}\omega_{i+1} \times \left({}^{i+1}\omega_{i+1} \times {}^{i+1}P_{COM_{i+1}}\right) + {}^{i+1}\dot{v}_{i+1}\ ,$$

$$^{i+1}F_{i+1} = m_{i+1}\,{}^{i+1}\dot{v}_{COM_{i+1}},$$

$$^{i+1}N_{i+1} = {}^{COM_{i+1}}I_{i+1}\,{}^{i+1}\dot{\omega}_{i+1} + {}^{i+1}\omega_{i+1} \times {}^{COM_{i+1}}I_{i+1}\,{}^{i+1}\omega_{i+1}\ .$$

Inward iterations: (Eq. 2.5)

$$^{i}f_i = {}^{i}_{i+1}R\,{}^{i+1}f_{i+1} + {}^{i}F_i\ ,$$

$${}^{i}n_i = {}^{i}N_i + {}^{i}_{i+1}R^{i+1}n_{i+1} + {}^{i}P_{COM_i} \times {}^{i}F_i + {}^{i}P_{i+1} \times {}^{i}_{i+1}R^{i+1}f_{i+1}\,.$$

Where i is the index of the link that connects the distal and proximal joints i and $i+1$, ω is the angular velocity, v is the joint linear velocity, $\dot{v}$ is the joint linear acceleration, P is the joint position, P_{COM} is the segment COM position, v_{COM} is the segment COM linear velocity, $\dot{v}_{COM}$ is the segment COM linear acceleration, R is the rotation matrix, ${}^{COM}I$ is the moment of inertia tensor, m is the mass of the segment, F and N are the inertial forces and moments acting on the segment COM, and f and n are the forces and moments at the joints.

For an arbitrary segment i with the distal joint i and proximal joint $i+1$, ${}^{COM_i}I_i$ is expressed in the segment-fixed frame with the origin at the segment's COM, ${}^{i}P_{COM_i}$ is the position of the segment's COM expressed in the segment-fixed frame with the origin at joint i. Moreover, the angular velocity and acceleration of the segment (${}^{i}\omega_i$ and ${}^{i}\dot{\omega}_i$), linear acceleration of the joint (${}^{i}\dot{v}_i$), and the segment's COM linear acceleration (${}^{i}\dot{v}_{COM_i}$) are also expressed in the segment-fixed frame with the origin at joint i. ${}^{i}_{i+1}R$ is a rotation matrix from the segment-fixed frame at joint $i+1$ to joint i. Using this notation, the force and moment at joint i are calculated via (Eq. 2.5) at the segment-fixed frame with the origin at joint i.

The instantaneous angular velocity of each segment at time t is calculated based on the rotation matrices at time t and $(t-1)$ as follows:

$${}^{G}_{L}R(t) = {}^{G}_{L}R(t-1)\,.\,\left(\frac{1}{f_s}S(\vec{\omega})\right) \qquad \text{(Eq. 2.6)}$$

$$S(\vec{\omega}) = f_s\,.\,{}^{G}_{L}R(t-1)^{-1}\,.\,{}^{G}_{L}R(t) \qquad \text{(Eq. 2.7)}$$

$$S(\vec{\omega}) = \begin{bmatrix} 0 & -\omega_z(t-1) & \omega_y(t-1) \\ \omega_z(t-1) & 0 & -\omega_x(t-1) \\ -\omega_y(t-1) & \omega_x(t-1) & 0 \end{bmatrix} \qquad \text{(Eq. 2.8)}$$

where f_s is the sampling frequency of the system, $S(\omega)$ is the skew-symmetric matrix applied on vector of angular velocity $\vec{\omega}$.

Note that the position vectors and angular and linear velocities are calculated from the kinematics of the body segments recorded by the motion tracking system (e.g., optoelectronic, IMU-based, etc.). The instantaneous rotation matrices are calculated based on the concepts introduced in section 2.2.3 from the instantaneous position of the skin-mounted markers, which are used to transfer all joint forces and moments to the global frame.

2.3 Trunk Kinematics

Trunk kinematics have been extensively studied using various linked-segment models based on the region of interest and the accuracy needed to capture the relative motion between different levels of the spinal column.

2.3.1 Anatomy of the Human Trunk

The trunk of the human body refers to all body segments between the base of the neck and the hip; however, it does not include the arms [60]. The spinal column consists of the vertebral column, sacral bones, and coccyx. The vertebral column consists of twenty-four vertebrae including seven vertebrae of the cervical spine ($C1\ to\ C7$), twelve of the thoracic spine ($T1\ to\ T12$), and five of the lumbar spine ($L1\ to\ L5$) (Figure 4). The adjacent vertebrae are attached to each other by intervertebral discs composed of the fibrocartilaginous joint, which ties the vertebrae together while providing slight relative movements. Due to the elastic connection and the muscles extended along the spinal column, the spine is flexible for bending toward different directions, but relatively stiff against vertical loading [30]. The sacral region located inferior of the lumbar spine, and the coccyx located inferior of the sacral region, are two rigid bony segments (sacrum ($S1\ to\ S5$) and coccyx (Co1 to Co4)) that are attached to the spinal column.

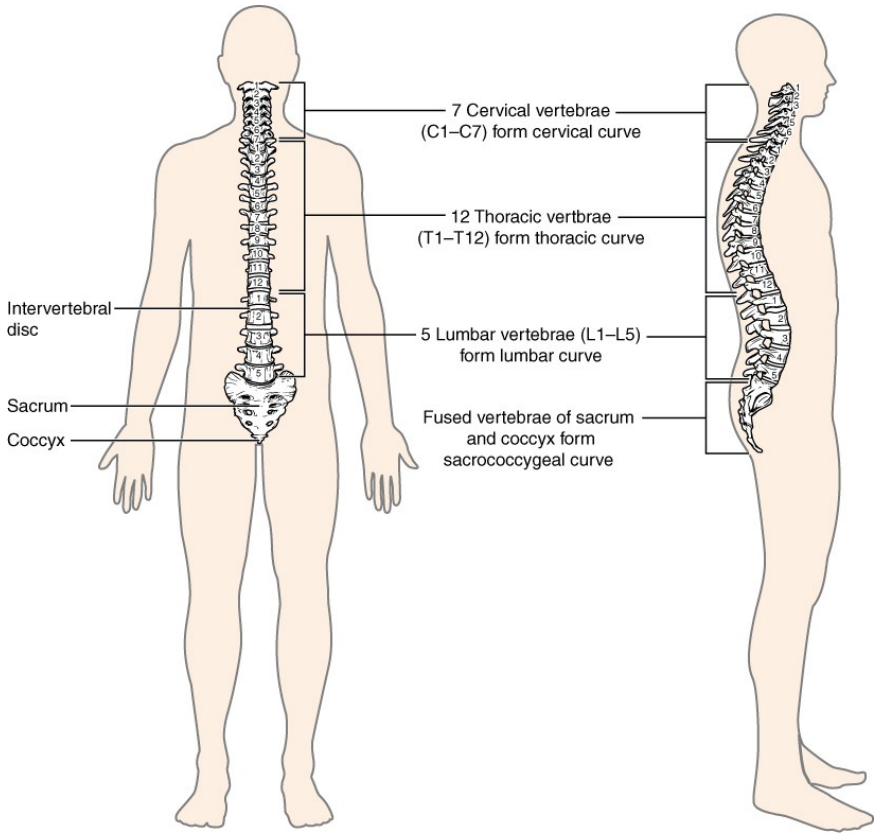

Figure 4. Anatomy of the spinal column. It consists of seven cervical, twelve thoracic, and five lumbar vertebrae. Sacrum and coccyx are two rigid bones attached inferior of the lumbar spine (adopted from: https://upload.wikimedia.org/wikipedia/commons/8/82/715_Vertebral_Column.jpg , access date: October 15, 2017).

2.3.2 Single-Segment Trunk Models

The kinematics of the human trunk have been studied using a one-segment model. Previous studies have considered the trunk as a single rigid body and calculated its angle with respect to the pelvis acting as an inverted pendulum. Some studies used single-segment trunk models to investigate the motion of the lumbar [28], [91] and thoracic spine [92]. Troke et al. [93] generated a comprehensive, gender-specific normative database of the lumbar spine's ranges of motion based on data from 405 non-disabled individuals. Static and dynamic balance has been investigated using a single-segment of the trunk as an inverted pendulum to predict the region of stability [94], [95] and loss of balance, as well as for fall assessment [96]–[100]. Other studies have explored human postural control using a single-segment of the trunk [101]–[119]. Goodworth and Peterka [120]

characterized the control of the upper body orientation with respect to the pelvis in response to external perturbations consisting of both pelvis and visual surround tilts. They also used a feedback model for investigating the contribution of the sensorimotor modalities such as the vestibular, visual, and proprioceptive systems to spinal stabilization [120], [121]. Some studies investigated intrinsic trunk stability [122]–[125]. Granata and Marras [122] proposed an EMG (electromyography)-based model of the lumbar spine and predicted the trunk extension moment generated by muscles forces as a function of trunk flexion angle for each individual. They also showed that spinal compressive and shear loading increased with trunk asymmetry during free dynamic lifting [123]. Granata and Wilson [124] investigated the effect of trunk posture on spinal stability. They showed that spinal stability was affected by trunk posture and that asymmetrical posture due to low back pain decreased the control of spinal stability. Panjabi et al. [126] evaluated the risk of injury during whiplash and its effect on cervical spine curvature. This approach has been extensively used to study the orientation of the trunk during walking [27], [127]–[129]. Mazza et al. [130] used an IMU attached to the lower trunk and tuned a Kalman filter to estimate the orientation of the trunk during treadmill walking. They validated their results by a stereophotogrammetric system. Grimpampi et al. [25] obtained the lower trunk angle with a single IMU during level walking for a group of patients with hemiplegia and Parkinson's disease. They stated that trunk angle assessment during abnormal gait could provide insight into motor control impairment and help decision-making in rehabilitation strategies [25]. Huntley et al. [26] evaluated the utility and robustness of three models (13-segment whole body, head-trunk-pelvis, and one-segment pelvis models) for clinical gait assessment among stroke survivors.

Although the use of a single-segment model facilitates capturing the trunk kinematics by using only three or four markers, it ignores the relative motion among different levels of the spinal column during a motor task. Hence, multi-segment trunk models can shed light on our understanding of how relative movements between adjacent vertebral segments could affect execution of motor functions.

2.3.3 Multi-segment Trunk Models

The number of studies that modeled the human trunk as multiple segments is still limited. An ideal multi-segment trunk model would allow tracking the motion of each spinal unit consisting of an

intervertebral disc and the adjacent vertebrae [131]. However, non-invasive measurement of the motion of each unit is not feasible by using current motion capture technology. This is due to the fact that palpable bony surfaces around each spinal unit are too small and, thus, the ability to place a required number of skin-mounted markers on each spinal unit is limited [131]. As a result, previous studies suggest to consider two or more vertebrae as a single rigid body and define them as a single trunk segment by proper marker configuration whose motion could be captured by the motion capture system [30], [131].

Syczewska et al. [132] used a seven-segment model of the spine between $C7$ and $S2$. They investigated the inter-segmental movement patterns during treadmill walking with normal pace and showed a significant effect of such movements in the reduction of energy consumption during gait. Gatton and Pearcy [133] studied the effect of inter-vertebral joint motions during lumbar flexion tasks by placing five position sensors over the lumbar vertebrae. They identified no unique sequence among their participants [133]. Al-Eisa et al. [134] examined the relationship between pelvic asymmetry and trunk motion patterns in non-disabled individuals and those with low back pain. They used a three-segment model of the trunk and suggested that functional impairment in those with low back pain could be better identified by asymmetrical movement of the lumbar spine rather than absolute range of motion [134]. A three-segment kinematic model was used by Konz et al. [131] to assess the spinal motion during walking. They concluded that the relationship between the lower limb motion and spinal motion during walking could be useful for preoperative decision-making to recover normal alignment and balance with least impact on gait. Preuss and Fung [135] used a four-segment biomechanical model of the trunk while EMG electrodes were bilaterally attached to seven trunk muscles. They used a horizontal support surface translation test using a perturbation platform moving in eight different directions for both standing and sitting postures. They observed relative movements between the segments in both test postures. Moreover, for both biomechanical and neuromuscular aspects of the trunk response, significant effects of the perturbation direction and posture (sitting or standing) as well as interaction effects between these factors were observed. Preuss and Popovic [136] proposed a seven-segment model of the trunk and pelvis as the next step. Using a multi-directional trunk bending experiment, they reported significantly different patterns of inter-segmental motions among participants at different levels of the spinal column. They also concluded that the inter-segmental spine motion was task-

specific, complex with inconsistent distribution among the joint levels. Leardini et al. [60] compared eight previously-proposed biomechanical models which were different in terms of marker-set, anatomical frame definition, and joint convention. They reported that the patterns and ranges of motion obtained by these models were significantly different. Hence, marker-set and frame definition must be carefully reviewed prior to any clinical decision-making [60]. Moreover, they proposed a five-segment model of the trunk for different routine daily activities [29]. They found high intra-participant repeatability; however, significant participant-specific motion was detected at each inter-segmental level in three anatomical planes. A more recent study investigated spinal motion during staircase walking outside a lab volume by using inertial and magnetic sensors placed on the pelvis, lumbar spine, and thoracic spine [69]. Their results showed significant differences in motion pattern and range of motion of the spine between staircase and level walking [69]. Kinematic and kinetic stability indices were introduced and evaluated using a multi-segment trunk model and a force plate, respectively. The motion of different spinal regions including lumbar spine, lower and upper thorax were recorded during non-dominant single leg standing for control and recurrent low back pain individuals [137]. Participants with recurrent low back pain showed higher lumbar stability compared to the other spinal regions in the eyes-open condition because of a proposed pain prevention strategy. In contrast, the stability decreased in eyes-closed condition, implying they were more reliant on visual information from the surrounding compared to proprioceptive information. A recent study investigated the spinal kinematics during gait across different age groups [138]. This study showed age-dependent kinematics of the spine and showed that lumbar lordosis (exaggerated lumbar spine curve) and thoracic kyphosis (exaggerated thoracic spine curve) increase throughout adolescence. Moreover, they showed a higher range of motion of the lumbar spine for adults compared to adolescents.

All above-mentioned studies have used multi-segment trunk models and investigated differences between the spinal motions at different levels. These studies showed that the spinal motion is task-dependent and complex along the spinal column at different inter-vertebral joints, which cannot be observed using a single-segment model of the trunk. This implies that the quantification of kinematics using multi-segmental trunk models plays a significant role in the biomechanical analysis of human movements, and that accurate assessment of the relative motion between the spinal segments is needed.

2.4 Trunk Kinetics

Kinetics assessment based on a linked-segment model requires measurements of the inter-segmental motions, accurate estimation of the BSPs (anthropometric data), and ground reaction forces (GRFs) as the inputs of an inverse dynamics approach. Several studies employed linked-segment models of the human body along with BSPs to estimate forces and moments at various body joints during different motor tasks. Trunk kinetics using a single-segment model have been studied to calculate 3D lumbo-sacral ($L5/S1$) joint forces and moments. Kingma et al. [55] developed a 3D linked-segment model of the body with a single trunk segment and calculated the lumbo-sacral joint moment. They derived BSPs from regression equations and proved the validity of the model by comparing the lumbo-sacral joint moment obtained via both bottom-up and top-down inverse dynamics approaches. The bottom-up inverse dynamics approach uses kinematics data and BSPs of the body segments measurd by a motion capture system as well as kinetics (GRFs and COP) measured by a force plate, along with a linked-segment model. It starts with computation of the joint forces and moments from the inferior most segment and proceeds successively upward with assuming the force plate data as the boundary condition for the bottom-most segment. The top-down inverse dynamics approach uses only the kinematics data and BSPs of the body segments in a linked-segment model. It considers an unloaded condition (or a known load as the boundary condition) for the top most segment and starts calculation from the superior-most segment and proceeds downward consecutively. Plamondon et al. [54] and Desjardins et al. [39] used lower body and upper body kinematic models for estimating the lumbo-sacral joint moment. The lower body kinematic model included the feet, shanks, thighs, and pelvis, whereas the upper body model included the hands, forearms, upper arms, head, and trunk. They used the data provided by Winter [57] and regression equations to estimate the mass, COM, and moments of inertia of the trunk segment. Plamondon et al. [54] examined the validity of the bottom-up and top-down inverse dynamics approaches to estimate the net moment at the lumbo-sacral ($L5/S1$) joint during lifting tasks for lower body and upper body kinematic models, respectively. They showed 95% correlation between the results obtained by both bottom-up and top-down approaches [54]. Desjardins et al. [39] quantified the sensitivity of the bottom-up and top-down inverse dynamics approaches to experimental errors [39]. Their results suggested that the external forces (bottom-up approach) and mass of the segments (top-down approach) are the major contributors to the

differences in the sensitivity of the lumbo-sacral joint moment about the transverse axis [39]. Larivière and Gagnon [139] compared both bottom-up and top-down approaches based on two biomechanical models for estimating the 3D lumbo-sacral joint moment. The lower and upper body biomechanical models were the same as in a previous study [39]. Their results demonstrated good agreement between the two approaches for static tasks, but disparity for dynamic tasks. They also investigated the sensitivity of the lumbo-sacral joint moment to measurement errors when both bottom-up and top-down approaches were used for motion analysis during lifting tasks [40]. Their results revealed that the main source of variability for both models was the orientation of the anatomical frames and joint centers of rotation (JCR). Moreover, they suggested that the bottom-up approach requires precise measurement of the COP and the top-down approach needs accurate estimation of BSPs and the upper body segment accelerations [40]. Consequently, they concluded that error minimization in kinetics assessment of the spinal column is of great importance. In a different application, Callaghan et al. [140] explored the effects of walking speed and arm swing on loads, motion, and muscle activation at the lumbar spine. They used a linked-segment kinematic model, regression equations for BSPs estimation, and a bottom-up approach to obtain the $L4/L5$ forces and moments. Subsequently, they partitioned these moments amongst the muscles based on the EMG signals by using an EMG-driven model [140]. Some studies benefited from the quantification of kinetics using linked-segment spine models in investigating chronic low back pain [141] and balance recovery [31]. Arjmand et al. [1] utilized both bottom-up and top-down approaches to estimate the net moment at the $L5/S1$ intervertebral disc. Recent studies investigated the effect of unilateral lower limb amputation on the kinetics of the low back at the lumbo-sacral level during walking [142], sitting and standing [143]. They showed that altered trunk motion and lumbo-sacral kinetics may play a significant biomechanical role in start and/or recurrence of low-back pain [143] and may contribute to risk of low-back injury in individuals with lower limb amputation [142]. In a recent study, Faber et al. [144] used a full-body ambulatory inertial motion capture system to estimate lumbo-sacral joint moments and GRFs via the top-down approach. They validated their results via the bottom-up approach using measurements from a force plate and motion capture cameras [144].

All above-mentioned studies have investigated the moments and forces at the lumbo-sacral joint using a one-segment HAT model. Multi-segment HAT models have been rarely used to study

inter-spinal joint kinetics. Just recently, Seay et al. [145] proposed an inverse dynamics approach along with a two-segment HAT model (thoracic and lumbar segments) to estimate joint moments and forces acting on the lumbo-sacral ($L5/S1$) and thoraco-lumbar ($T12/L1$) joints during running at different stride lengths. They considered the thorax segment a cylinder and computed the lumbar segment's anthropometric parameters (BSPs) according to Pearsall et al. [146]. Vette et al. [56] incorporated the BSPs from a single cadaver into an inverse dynamics approach for calculating the joint moments at the cervical and lumbar spinal joints for another male individual during perturbed sitting.

The majority of the above-mentioned studies investigated the lumbo-sacral joint moment using a single-segment trunk model. Few studies were found that investigated the kinetics of the spinal column using multi-segment kinematic models. Previous studies showed that assessing the kinetics of single-segment trunk models is error-prone, and reported the sources of inaccuracies in the trunk kinetics; however, to the best of our knowledge, not a single study has proposed a multi-segment assessment of human trunk kinetics along with compensation for experimental errors. The major sources of error are due to inaccuracies in (a) kinematics data, (b) BSPs, and (c) force plate data. Errors in kinematics were introduced in section 2.1.2. In the following section, errors in BSPs and force plate data are introduced.

2.5 Errors in Human Movement Kinetics Analysis

Generally, kinetics analysis of human movement using a linked-segment model and an inverse dynamics approach requires kinematic variables of the rigid segments, accurate estimation of the BSPs, and force plate measurements (GRFs and position of the COP). Although inverse dynamics approaches have been extensively used to calculate the forces and moments at various body joints, previous studies suggested that these approaches are prone to errors caused by inaccuracy in (a) segment motion (rotation and translation) measurements, (b) BSPs estimation, (c) force plate measurements, and (d) location of JCRs [34]. Riemer et al. [37] showed that the above-mentioned inaccuracies could lead to substantial uncertainties in joint moment estimation varying from 6% to 232% of the moment magnitude for the lower limb joints. They also suggested that inaccuracies in segment orientation and BSPs are the major sources of these uncertainties [37].

2.5.1 BSPs Errors

Many studies have investigated the effect of inaccuracy in BSPs estimation on the calculated joint moments during human movement. Lenzi et al. [147] determined the influence of inaccuracies in BSPs estimation and modeling assumptions on the instantaneous position of COM by simulating the BSPs error as ±10% variation in the parameters. They assumed the anatomical structure of the whole body as a set of four rigid segments with a single trunk segment and assigned the BSPs by using scaling equations provided by Winter [57] based on body weight and height [147]. They showed that, although some BSPs are more critical for different COM trajectory estimation methods, sensitivity and error propagation are task-specific [147]. Rao et al. [36] investigated the influence of different models for estimating BSPs on the calculated joint moments via inverse dynamics during gait in a three-segment lower limb model (foot, shank, and thigh). Six often-used estimation models (one geometric model, two cadaveric models, and three in vivo mass-scanning models) were used along with a bottom-up inverse dynamic approach. Their results indicated that estimated BSPs were highly dependent on the model used for estimating BSPs and deviated from 9.73% to 60% of the mean value estimated by the six models across different segments. They reported that the peak value of the flexion/extension moment at the hip joint varied up to 20.11% within the models when using different models for estimating BSPs, which implies that the effect of BSPs on the joint moment estimation cannot be neglected [36]. A Monte Carlo simulation was used by Nguyen and Reynolds [148] to simulate the effect of variability and uncertainty in BSPs on joint moments and suggested little effect of BSPs estimation on joint moments for slow and repeatable movement such as gait except for the swing phase. Some researchers studied the effect of BSPs estimation on kinetics assessment of gait [149], [150], quiet standing, squatting, and level walking [151]. Ganley and Powers [149]and Kay Lee et al. [150] investigated the effect of BSPs variations on joint moment calculation at the lower limbs (foot, shank, thigh) during gait and concluded that motor tasks with high acceleration could be more affected by inaccuracy of BSPs. Chen et al. [151] used a sixteen-segment model of the body (head, neck, upper arms, forearms, thighs, shanks, trunk, pelvis, hands, and feets) during quiet standing, squatting, and gait using BSPs from four estimation methods. They assessed the difference between the calculated and measured GRFs and COP as error. They reported significant differences between the error induced by the BSPs estimation methods. Hence, individual-specific BSPs are essential for evaluation of

several motor tasks. At the same time, accurate estimation of BSPs can only be achieved by imaging techniques which are not always practical for clinical assessments. Although different sets of BSPs [57], [152], [153] are routinely used for estimating inertial parameters in gait laboratories, many studies extensively discussed various concerns regarding the use of previously-published datasets for BSPs, particularly when the individual falls outside the originally studied population for which the BSPs were estimated [36], [38], [55], [154], [155]. This is even more critical for pathological groups with limb asymmetry, since applying existing BSPs datasets could result in substantially different joint forces and moments during gait [38].

Several techniques have been used to accurately estimate individual-specific BSPs. Medical imaging techniques such as magnetic resonance imaging [156]–[159], gamma-ray scanning [160], dual-energy X-ray absorptiometry [149], [150], [152], [161]–[163], and computed tomography [146] have been used to estimate individual-specific sets of BSPs. Although these methods have high accuracy and errors of 5% or less [52], they require medical imaging equipment which is too expensive and involves radiation exposure. Consequently, they are not an adequate approach for routine clinical evaluation of human movement [163]. Therefore, other researchers employed previously collected data from medical images and provided regression equations to estimate BSPs [160]. Hinrichs [50] developed a set of regression equations to estimate moments of inertia for body segments. However, the equations were based on a very small sample population, which implies that using them could result in large errors, especially for individuals who fall outside the population in terms of body weight and height. Durkin and Dowling [163] used BSPs obtained from dual-energy X-ray absorptiometry of four human populations and developed linear regression equations for estimating BSPs of five body segments in the frontal plane. They reported significant differences among the populations for all segments and BSPs. Nevertheless, they claimed that their proposed regression equations were generally best when compared to other sources. Yet, there is currently no single data set for all BSPs, populations, and body segments with globally high accuracy. Simple geometric models such as elliptical zones with known densities [164] and circular cylinders based on the segment length and circumference [163] were used with constant density to estimate BSPs. However, more complex geometric models which consider density changes and mass distribution characteristics of the segment are needed to enhance the accuracy of such methods [163]. Most of previously introduced predictive equations are not able to obtain

BSPs for 3D kinetics assessment. Moreover, they frequently assumed that the COM and the endpoints of the segment are aligned and the moments of inertia tensor is principal with respect to the anatomical axes of the segments [165]. Dumas et al. [165] adjusted the equations provided by previous studies and provided adjusted scaling equations that could be directly used for 3D kinetics assessments. Another study obtained the BSPs from a limited number of cadavers which allows individual-specific scaling based on the body weight and height [151]. Recently, Vette et al. [51] provided a comprehensive set of BSPs for the human trunk, with segments associated with every single vertebra, head, and upper limbs segments. Based on high-resolution images of the Male Visible Human, they digitally reconstructed the anatomical structures of a single cadaver and identified the 3D COM coordinates, mass, and moments of inertia for all vertebral trunk segments and four upper limbs (two per arm) as well as the 3D JCRs for spinal intervertebral discs [51]. All above-mentioned studies employed mathematical techniques along with medical images of either small populations or a limited number of cadavers to estimate individual-specific BSPs. However, an accurate method for estimating individual-specific BSPs during *in vivo* experiments using non-invasive radiation-free methods is still required.

Some studies employed force plate data to estimate individual-specific BSPs. These studies calculated the mass and COM position of a segment based on the changes in the mean body COP and force plate data in two different postures (e.g., standing and lying) when the segment is displaced [155]. Pataky et al. [166] proposed an *in vivo* method to determine body segment masses by using a force plate. They asked participants to lay on a board placed on a force plate and perform different specific postures. The mass of their limbs was subsequently estimated by using the COP positions from the force plate [166]. Their method can provide a quick approach to obtain individual-specific mass information which could be used to avoid erroneous biomechanical analyses for clinical assessments. Damavandi et al. [155] presented a method for estimating mass and COM location of the body segments from COP positions. Their method was sensitive in detecting the difference between individuals of different morphology and their results were within the range of previously-proposed methods. Hansen et al. [167] proposed a method for estimating BSPs in a fifteen-rigid-link model of the whole body. They identified the BSPs and recalculated the GRFs via an inverse dynamics approach and validated the calculated values against those obtained by the force plate. They also compared their results with the method proposed by Dumas

et al. [165]. As a different approach, some studies employed optimization techniques to estimate BSPs. Riemer et al. [52] used a two-step optimization approach to estimate BSPs. A four-segment model of the body with a single trunk segment was used and, by considering BSPs as optimization variables, their objective function minimized the least square difference between calculated GRFs via a top-down approach and known GRFs from a force plate. Chen et al. [151] proposed an optimization-based, non-invasive method for estimating individual-specific BSPs by using a motion capture system and two force plates. They used a sixteen-rigid-link model of the whole body with the trunk modeled as a single ellipsoidal segment during quiet standing and an optimization procedure. Using the BSPs as variables, their cost function minimized the sum of squared distances between the calculated and measured COP in stationary postures. Using common standard motion laboratory set-up, non-invasive optimization methods can be used for estimating BSPs for routine clinical evaluations especially for patients whose anthropometric data fall outside reported BSPs. Although some studies employed optimization techniques to estimate optimized individual-specific BSPs, they targeted only the lower limbs and/or considered the HAT as a single rigid segment. Due to high inter-participant variability of the shape and size of HAT segments, there is currently no comprehensive database for estimating individual-specific BSPs for the multi-segment HAT. Therefore, a non-invasive, radiation-free optimization-based algorithm that could provide individual-specific BSPs for the HAT segments is still needed.

2.5.2 Force Plate Measurements Errors

The influence of errors in COP and GRFs measured by a force plate on joint moments have been studied. McCaw and DeVita [35] quantified the effect of errors in alignment of foot coordinates, measured by motion capture cameras, and COP, measured by a force plate, on ankle, knee, and hip joint moments during the stance phase of gait. They considered ±0.5 and ±1.0 cm shifts in the anterior-posterior location of the COP and investigated its effect on the estimation of the joint moments using inverse dynamics. They showed that shifting COP caused 7% to 14% change in the maximum estimated joint moment [35]. Heiss and Pagnacco [168] suggested that the relationship between COP and COM trajectories captures aspects of the standing balance control strategy employed by the central nervous system and, therefore, minimizing their measurement error is of great importance in our ability to use them for comprehending balance control strategies [168]. They proposed an optimization method to find the location of the trunk COM and/or COP

that minimized the difference between the whole-body COM and COP positions in the horizontal plane during quiet standing. They assumed that the projection of the body COM position on the horizontal plane coincides with the COP during quiet standing. They showed that optimizing the COP and compensating its systematic error could significantly improve the optimization results in minimizing the difference between COM and COP positions in the horizontal plane. Karlsson and Frykberg [169] compared various force plate measures for evaluation of postural stability. They recorded force plate data from stroke survivors and compared the force plate measures and clinical balance test outcomes (Berg balance test) for each individual. They concluded that the force plate measures could quantify a different aspect of human balance during standing. Their results also indicated that the vertical force and the Berg balance test show the same aspects of postural stability. COP excursion has been widely used as an indicator of postural stability in standing. Ruhe et al. [170] explored the reliability of the COP measures for postural balance assessment by reviewing previously-published studies. They concluded that bipedal static COP measures could be reliable for postural stability evaluation and provided recommendations for increasing the reliability of using COP measures by applying specific conditions [170]. Thus, error compensation strategies that suppress systematic errors in force plate measurements (GRFs and COP position) are essential for characterizing postural stability and would lead to more accurate and reliable clinical evaluations. Some studies investigated the effect of erroneous force plate measures on the uncertainty of parameters calculated via inverse dynamics during gait [37], [171]. Riemer et al. [37] showed that, during the stance phase of the gait cycle, inaccuracies in the shank and thigh segment angles and the distance between the COP and ankle JCR were the major sources of uncertainties in the hip joint moment estimation. Pàmies-Vilà et al. [171] analyzed uncertainties in BSPs, kinematics, and force plate measurements on the kinetics of human gait obtained via inverse dynamics. They added a proportional error with respect to the full-scale output of the force plate and showed that inaccurate force plate readings could affect the joint moment estimation even more than inaccuracy of BSPs. Schmiedmayer and Kastner [172] explored the parameters that affect the accuracy of the COP, measured by piezoelectric force plates and derived an algorithm which describes the COP error. They also showed that the accuracy enhancement in COP position depends on the load distribution on the force plate. They concluded that accurate error compensation for COP position with correction formula can only be obtained for forces with a small area of distribution [173]. Therefore, the COP measured by the force plate during several

functional tasks and postures, particularly sitting that involve a distributed load on the surface of the force plate (compared to walking or standing) may result in erroneous readings. This could affect the kinetics assessment of various body segments during static/dynamic sitting and, thus, an error compensation method is required to obtain more accurate joint moments.

In this chapter, a review of the literature that is relevant to this thesis was presented. This review revealed that the quantification of multi-segment HAT kinetics has rarely been studied. The major technical challenge in this assessment has been uncertainty in the calculated inter-vertebral moments due to inaccuracy of kinematic data of the segments (due to soft tissue artifacts), high inter-participant variability of BSPs, and systematic error in the force plate measurement. Based on this review, no study has investigated the effect of soft tissue artifacts on the kinetics assessment of a multi-segment model of a HAT. Moreover, There is currently no reliable, non-invasive, radiation-free method for accurate estimation of individual-specific BSPs for HAT segments. Therefore, estimation of inter-vertebral moments is still technically challenging, and a new reliable approach that compensates for above-mentioned inaccuracies can significantly facilitate kinetics assessment of the HAT movements using multi-segment models, and enable objective clinical evaluations and decision-making.

Chapter 3

3 Optimized Body Segment Parameters Estimation

The material presented in this chapter has been submitted as a research paper to the Journal of Biomechanical Engineering. The majority of content of this chapter is identical to the material presented in the publication except for the text formatting which was done according to University of Alberta requirements.

A. Noamani, A. H. Vette, R. Preuss, M. R. Popovic, H. Rouhani, "Optimal Estimation of Anthropometric Parameters for Quantifying Multi-Segment Trunk Kinetics", submitted to Journal of Biomechanical Engineering (Transactions of the ASME).

3.1 Abstract

Kinetics assessment of the human head-arms-trunk (HAT) complex using a multi-segment model is required for clinical evaluation of several pathological conditions. Inaccuracies in body segment parameters (BSPs) is a major source of uncertainty in the estimation of the joint moments associated with the multi-segment HAT. Given the large inter-subject variability, there is currently no comprehensive database for the estimation of BSPs for the HAT. We propose a nonlinear, multi-step, optimization-based, non-invasive method for estimating individual-specific BSPs and calculating joint moments in a multi-segment HAT model. Eleven non-disabled individuals participated in a trunk-bending experiment, and their body motion was recorded using cameras and a force plate. A seven-segment model of the HAT was reconstructed for each participant. An initial guess of the BSPs was obtained by individual-specific scaling of the BSPs calculated from the Male Visible Human images. The inter-segmental moments were calculated using both bottom-up and top-down inverse dynamics approaches. Accurate kinematic parameters, BSPs, and force plate measurement are expected to result in the same values for the net joint moment via both inverse dynamics approaches. Since scaling induces inaccuracies in the estimation of the BSPs,

the inverse dynamics approaches were expected to result in different values for the net joint moments. Therefore, a set of BSPs and center of pressure offsets, that minimize the difference between the results of the two approaches, are expected to be more accurate compared to those which result in significantly larger differences. Our proposed method adjusted the scaled BSPs and center of pressure offsets to estimate optimal individual-specific BSPs that minimize the difference between the moments obtained by top-down and bottom-up inverse dynamics approaches. Our results indicate that the proposed method reduced the error (the difference between the net joint moment calculated via bottom-up and top-down approaches) in the net joint moment estimation by 77.59% (average among participants). Our proposed method enables more accurate estimation of individual-specific BSPs and, consequently, more accurate assessment of the three-dimensional kinetics of a multi-segment HAT model.

Keywords: Inverse dynamics; Joint moments; Multi-segment model; Optimization; Trunk kinetics.

3.2 Introduction

Evaluation of several conditions such as lower back pain [7], scoliosis [4], and spinal cord injury [15] requires kinematics and kinetics assessment of the spinal column. Since in vivo measurement of inter-spinal interaction (i.e., relative motion and load) is challenging, linked-segment models have been suggested as mathematical means to estimate the inter-segmental motions and moments during trunk motion. This approach has been extensively used to study the spine kinematics [29], [131], [138], vertebral trunk kinetics [56], and trunk stability [174]. Clinical studies have also evaluated the inter-segmental motions and moments of the trunk by using segmental models to investigate low back pain [7] and spinal cord injury [15]. Trunk kinematics have been investigated using one-segment and multi-segment models of the head-arms-trunk (HAT) complex [136]. Trunk kinetics have been studied using a one-segment [139] or multi-segment [56] HAT models based on kinematics measurement using a one-segment HAT model and estimation of the inter-segmental motions. To the best of our knowledge, no study has provided an individual specific, quantitative, three-dimensional (3D) kinetics assessment of the HAT based on independent motion measurement of several HAT segments. This particularly requires an individual-specific

estimation of body segment parameters (BSP) for each HAT segment in an inverse dynamics formulation, that is technically challenging and error-prone [52], especially for the multi-segment HAT because of the significant inter-subject variability of the BSPs.

In general, body kinetics assessment using linked-segment models and an inverse dynamics approach requires: (a) the capture of inter-segmental kinematics; and (b) accurate measurement of mass-inertia parameters and ground reaction forces (only for bottom-up inverse dynamics approach) [56]. Inverse dynamics is a computational approach that uses anthropometric, kinematic, and kinetic data as the input to calculate the forces and moments at various body joints [52]. Although the inverse dynamics approach is commonly used for biomechanical analysis of human movement, this procedure is error-prone. Riemer et. al [37] showed that the uncertainties in the estimated net joint moments derived from inverse dynamics could be significant, varying from 6% to 232% of the estimated moment magnitude. They also suggested that inaccuracies in BSPs and estimated segment angles are the major sources of these uncertainties [37]. As such, obtaining an accurate estimation of the BSPs including the 3D coordinates of the joint's center of rotation (JCR), 3D center of mass (COM) coordinates, mass, and moments of inertia for each segment, is a key requirement for kinetics assessment of the multi-segment body. Medical imaging techniques have been used to obtain individual-specific anthropometric data such as magnetic resonance imaging [158], gamma-ray scanning [160], and dual-energy X-ray absorptiometry [163]. Despite their high accuracy, such methods are usually expensive, too complex for routine clinical motion analysis, and subject to radiation [163]. Other studies used data obtained by medical imaging and suggested predictive equations to obtain BSPs [50], [160], [163]. Some studies obtained the anthropometric data from a limited number of cadavers and normalized them, which allowed for an individual-specific estimation of BSPs based on the participant's body weight and segment length [151]. However, such methods are prone to error when the data are applied to individuals with a different range of age, body type, sex and ethnicity [50], [166]. In fact, the estimation of BSPs based on cadaveric data may have error larger than 40% [52], implying that there is currently no method to accurately obtain BSPs for the multi-segment HAT.

In the past, concurrent derivation of top-down and bottom-up inverse dynamics formulation has been used to minimize errors mentioned above in joint moment calculation for lower limbs [175]–

[177]. In the top-down formulation, the dynamic equilibrium equations are solved starting from the most superior segment, proceeds downward for each consecutive segment, and requires only BSPs and kinematic data as the input. In the bottom-up formulation, these equations are solved from the most inferior segment, proceeds upward, and uses the force plate data in addition to the BSPs kinematic data. Therefore, the system is over-determined since the boundary conditions are known for the most inferior segment. Because of BSPs and kinematic data inaccuracies, the net joint moments obtained by both top-down and bottom-up formulations differ. Hence, a more accurate estimation of anthropometric and kinematic data results in smaller differences between net joint moments obtained by both formulations.

For the lower limb joints, optimization methods have been employed to minimize the effects of the BSPs' inaccuracy. Vaughan et. al [53] utilized a gradient projection algorithm for estimating BSPs. They considered the BSPs as the optimization variables and the difference between the measured and calculated ground reaction forces (GRF) under the feet as the cost function. Their approach required an initial estimate of the BSPs and did not target the minimization of the joint moment errors directly. Kuo [32] proposed a least-squares estimation approach for inverse dynamics computations to reduce the errors in joint moments by around 30% and eliminated constant biases in data. Cahouet et al. [33] addressed uncertainties in the acceleration data and their effect on the estimated joint moments using a weighted least-squares optimization approach. Cappozzo [178] and Mazza and Cappozzo [179] proposed an optimization algorithm for joint kinematics based on the GRF data; however, they did not consider errors in BSPs. Riemer et. al [34] presented a constrained nonlinear optimization to improve the accuracy of joint moments estimation by optimizing the angular position data. Their cost function minimized the difference between the measured and computed GRFs. They also proposed a two-step optimization method for improving the accuracy of the calculated joint moments [52]. All studies mentioned above provide an optimization-based method for calculating net joint moments at different lower limb joints in the sagittal plane during running, long jumping, kicking, gait, squatting and standing.

To the best of our knowledge, no study has proposed a comprehensive multi-segment model of the HAT for 3D joint moment estimation based on individual-specific BSPs. Therefore, the present

study proposes a nonlinear optimization-based, non-invasive method for estimating individual-specific BSPs in 3D kinetics assessment of the HAT using a multi-segment model.

3.3 Method

The experimental protocol and data collection were described in detail in a previous study [136] and, thus, are only briefly described here.

3.3.1 Experiment protocol

Eleven non-disabled individuals (4 females; age: 28.5±3.3 years; trunk height: 0.75±0.04 m) with no history of persistent back pain, spine-related musculoskeletal impairments, or any neurological, vestibular, or other balance-related disorders participated in the data collection. All individuals provided written consent prior to performing the experiment. Research Ethics Board approval was received from the local ethics committee.

Participants sat naturally on a rigid elevated surface, and the lower legs freely hung with no further constraints or support to restrict their movement. Each participant was instructed to lean forward and then return to the initial upright sitting position, three times in self-selected comfortable pace. Each participant performed an angular trunk motion of 45° to reach a physical target located in front of him/her by the head (Figure 5). The arms were crossed motionless over the chest throughout each trunk-bending trial. To avoid a counterweight effect of the lower legs during trunk movement, participants were asked to keep their lower legs vertically downwards throughout the experiment.

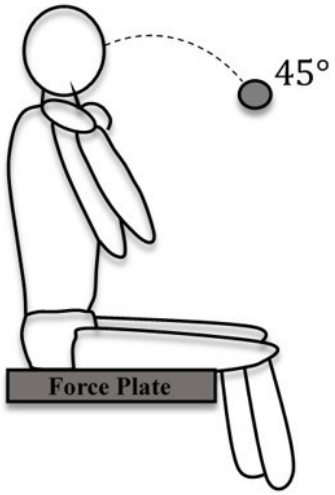

Figure 5. Targets for the trunk-bending task were placed at participant-specific distances and heights representing an angular motion of 45° of the trunk.

3.3.2 Data acquisition

Twenty-two reflective markers (10 mm diameter) were placed over and around the participant's spine, representing a seven-segment model of the trunk (Figure 6). Six motion capture cameras (Vicon, Oxford, UK) recorded the trajectory of the markers at a sampling rate of 120 Hz. The obtained time series were subsequently low-pass filtered by employing a dual-pass 8^{th}-order Butterworth filter at a cut-off frequency of 2 Hz. A force plate (AMTI, Watertown, MA, USA) was used to record the GRF and the position of the center of pressure (COP) at a sampling frequency of 1,000 Hz.

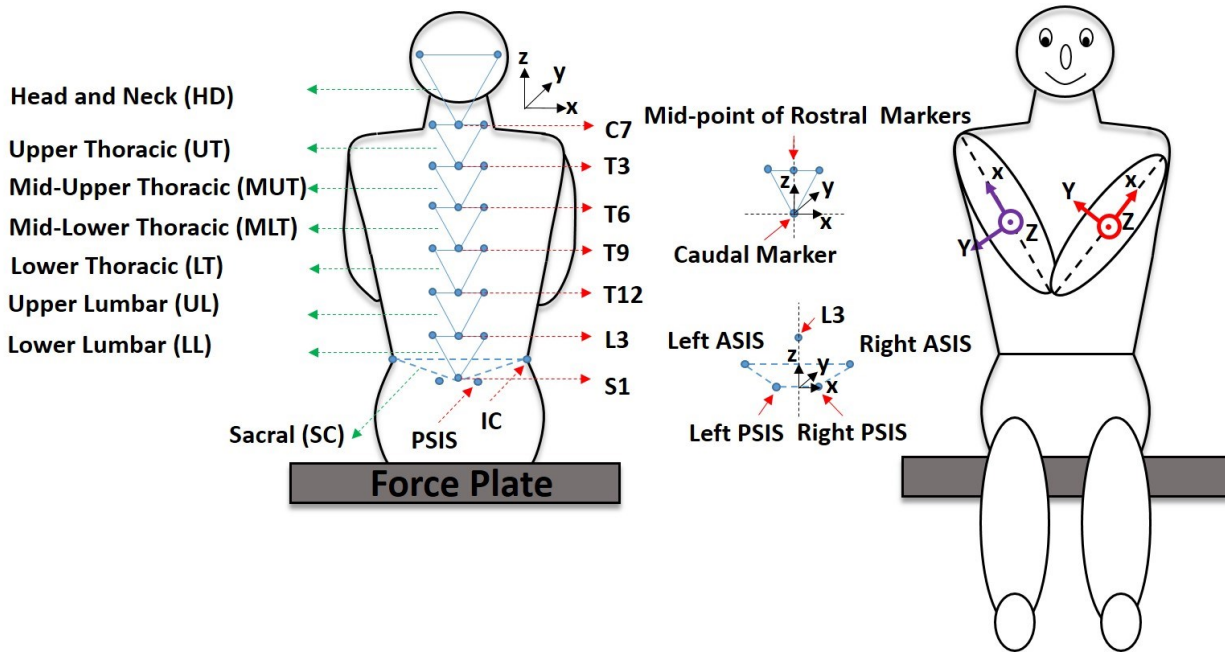

Figure 6. Markers were placed over the participant's spinal column to form a seven-segment trunk model: Head and neck (HD), upper thoracic (UT), mid-upper thoracic (MUT), mid-lower thoracic (MLT), lower thoracic (LT), upper lumbar (UL), lower lumbar (LL) and sacral (SC) segments In addition, the local frame of all HAT segments is depicted.

3.3.3 Multi-segment modeling of the head-arms-trunk (HAT) complex

According to Figure 6, the multi-segment model of the HAT consisted of seven rigid bodies representing the head and neck segment (HD), four thoracic segments (UT, MUT, MLT, and LT) and two lumbar segments (UL and LL). Each segment was defined by a marker placed centrally on the spinous process of the caudal vertebra and two markers placed at 5 cm lateral of the spinous process of the rostral vertebra. The LL trunk segment was located above the pelvis segment (SC), which was used to define the inertial reference frame of the body. These segments were assumed rigid and connected to each other by 3D revolute joints located at the center of respective inter-vertebral discs. Since the arms were assumed rigidly connected to the UT segment in the trunk-bending trials, their inertial properties were incorporated into the UT segment. For each trunk segment, a segment-fixed frame was defined according to Table 1a, and obtained based on the trajectory of markers placed on it. The X-, Y-, and Z-axes of each segment-fixed frame represented flexion/extension, lateral bending, and axial rotation, respectively. A segment-fixed frame was defined for the arm segments according to Table 1b, and was used to incorporate the anthropometric data of the arm segments into the UT segment (see Section 3.3.4).

3.3.4 Anthropometric data

The initial estimates of the mass, COM, and moments of inertia of the HAT segments were obtained from digital reconstructions of anatomical structures via high-resolution images of the Male Visible Human (MVH) from the body of a 38-year-old white male (height: 1.80 m and weight: 90 kg). Vette et al. have already calculated the 3D coordinates of the COM and JCR, mass and moment of inertia tensor for each of the 24 vertebral trunk segments and four arm segments [51]. We used these data to obtain the BSPs for our proposed seven-segment model of the trunk. First, the 3D coordinates of the inter-vertebral joints were identified using the MVH images and used as the JCRs in the proposed multi-segment model. Second, the coordinates associated with the anatomical landmarks of the pelvis including the left and right anterior superior iliac spine (ASIS) and the left and right posterior superior iliac spine (PSIS) were identified. Third, the mass, COM, and the moment of inertia tensor of each individual segment in the proposed model were calculated based on the parameters obtained in [51] as follows:

$$Mass_{segment} = \sum_{k=caudal\ subsegment,1}^{rostral\ subsegment,n} mass_k \qquad \text{(Eq. 3.1)}$$

$$COM_{segment} = \frac{\sum_{k=caudal\ subsegment,1}^{rostral\ subsegment,n} mass_k COM_k}{Mass_{segment}} \qquad \text{(Eq. 3.2)}$$

$$I_{segment} = \sum_{k=caudal\ subsegment,1}^{rostral\ subsegment,n} J^k,\ \ J^k = \begin{bmatrix} J_{11}^k & J_{12}^k & J_{13}^k \\ J_{21}^k & J_{22}^k & J_{23}^k \\ J_{31}^k & J_{32}^k & J_{33}^k \end{bmatrix} \qquad \text{(Eq. 3.3a)}$$

where $I_{segment}$ is the moment of inertia tensor of the segment composed of subsegments $k = 1{:}n$ with the moment of inertia tensor of J^k about the segment's COM expressed in the reference frame fixed to the pelvis of the cadaver Table 1c.

The components of J^k of subsegment k were calculated based on parallel axis theorem as follows:

$$J_{ij}^k = \ I_{ij}^k + mass_k\left(|R|^2\delta_{ij} - R_iR_j\right) \quad i,j = 1,2,3 \qquad \text{(Eq. 3.3b)}$$

$$\vec{R} = R_1\hat{x} + R_2\hat{y} + R_3\hat{z}$$

$$\delta_{ij} = \begin{cases} 1 & i = j \\ 0 & i \neq j \end{cases}$$

where I_{ij}^{k} denotes the components of inertia tensor of subsegment k about the subsegment's COM, $\vec{R}$ is the displacement vector from the subsegment's COM to segment's COM, and $\delta_{ij}$is the Kronecker delta function.

Application of inverse dynamics formulation requires obtaining the COM and JCR trajectories as well as the moments of inertia tensor of each segment throughout each trunk-bending trial with respect to a reference frame. However, all above-mentioned calculated parameters were expressed in a reference frame fixed to the pelvis defined by anatomical landmarks on the MVH images according to [51](Table 1c). It was needed to transform the anthropometric parameters to a lab-fixed frame during each trunk-bending trial. To this end, we used the reflective markers placed over the spinous processes to capture the motion of COM and JCR for each vertebral segment as a function of time. Image processing techniques were applied to the MVH images to obtain a set of vectors from the spinous processes to respective inter-vertebral spinal discs below the segment representing the JCR and from the spinous processes to the segment's COM. These vectors and the moment of inertia tensors were expressed in the segment-fixed frame and normalized to the MVH cadaver's body weight and trunk height. The vectors were then re-scaled by the participant's trunk height for the data collected in Section 2.3. The scaled moments of inertia tensors were also obtained based on the trunk height and the body weight of each individual. The trunk height was measured as the distance from the support surface to the base of the participant's occiput in an upright sitting posture. Then, we applied the instantaneous rotation matrix between the segment-fixed frame and the lab-fixed frame to obtain the two above-mentioned vectors expressed in the lab-fixed frame and subsequently the trajectory of each segment's COM and JCR in the lab-fixed frame. For each participant, we defined the lab-fixed frame based on anatomical landmarks of the pelvis during the motionless time interval at the beginning of each trial (Table 1d). The COM, JCR, moments of inertia tensor, GRF, COP, and angular kinematics were obtained for each segment with respect to this lab-fixed reference frame during each trunk-bending trial.

Table 1. Definition of implemented anatomical frames based on anatomical landmarks.

a) Segment-fixed frame for each spinal segment for trunk kinematics assessment

X-axis	Pointed from left to right, parallel to the two rostral markers
Z-axis	Pointed superiorly, parallel to the line between the caudal marker and the mid-point of two rostral markers
Y-axis	The cross-product of the Z and X axes, pointing anteriorly

b) Segment-fixed frame for arm segments

X-axis for each lower arm	Pointed distally from the elbow marker to the marker placed on the wrist (ulnar styloid process).
Z-axis for both upper and lower arms	Cross product of the X-axis of the lower and upper arm segments at each side of the body
Y-axis for each upper or lower arms	The cross-product of the Z and X axes, pointing anteriorly
X-axis for each upper arm	Pointed proximally from the elbow marker to the marker placed on the shoulder (acromion).

c) Pelvis-fixed frame for expression of anthropometric data in the MVH images [51]

Origin	Right ASIS
Y-axis	Pointing medially from the right ASIS to the left ASIS
X-axis	Pointing anteriorly perpendicular to the plane defined by two ASIS's and the midpoint of pubic tubercles
Z-axis	Pointing superiorly to form an orthogonal right-handed coordinate system

d) Lab-fixed frame defined based on pelvic landmarks during upright sitting

Origin	Midpoint of the two PSIS
X-axis	Pointing medially from the right PSIS to the left PSIS
Y-axis	Pointing anteriorly perpendicular to the plane defined by the X-axis and an auxiliary vector from mid-PSIS to L3 spinous process
Z-axis	Pointing superiorly to form an orthogonal right-handed coordinate system

3.3.5 Inverse dynamics

A custom-made algorithm for Newton-Euler recursive equations was employed as the inverse dynamics approach to calculate the net joint moments and forces at the inter-segmental levels in a multi-segment model of the HAT. Two inverse dynamics approaches were used: (1) bottom-up approach; and (2) top-down approach. The former approach used the force plate measurements, including GRF and COP position as the boundary condition of the dynamic chain in Newton-Euler recursive equations. The computation started from the most inferior segment and then proceeds upward. The latter approach only requires kinematic and BSPs data. In this approach, the inverse dynamics calculation started from the top-most segment and assumed the cross-sectional forces and moments to be zero at the top-most JCR as the boundary condition and proceeds downwards to the consecutive inferior segments.

3.3.6 Sensitivity to inertial terms

The Newton-Euler equations contain inertial terms such as the segments' angular and linear accelerations, obtained by the second time-derivative of the angular and linear positions, respectively. Due to the inherent noise of the motion capture system, differentiation leads to cumulative errors in the inverse dynamics computations. To investigate the effect of the inertial terms on the calculated net joint moments and forces, we assessed the sensitivity of the calculations to: (1) the linear accelerations, (2) the angular accelerations, and (3) both linear and angular accelerations. The error was defined as the difference between the net joint moment calculated with and without inertial terms via either the bottom-up or top-down approach. This error was calculated as the root mean square (RMS) error induced in the net moment calculation during each trial, relative to the net moment range calculated considering the inertial terms.

3.3.7 Optimization

The results computed by the two inverse dynamics approaches are commonly affected by errors. The major sources of error are: (1) the location of the JCR; (2) force plate measurement errors; (3) body segment parameters (BSPs) used for inverse dynamics computations; and (4) motion capture system noise and skin movement artifacts in kinematic data [34]. The top-down approach tends to be more sensitive to the inaccuracies from linear and angular acceleration data, compared to the

bottom-up approach that employs force plate measurements. Hence, the bottom-up approach leads to a more accurate estimation of joint moments and forces for the lower segments. Accordingly, the net joint moment obtained with these two approaches can differ. In this light, we developed a constrained nonlinear optimization algorithm to find an optimal (ideally error-free) set of measured parameters that minimizes the difference between the joint moments at all inter-segmental levels calculated by the bottom-up and top-down approaches. The cost function of this optimization, $\varphi(v)$, was defined as the least square of the difference between the norm of the 3D moment vector calculated from the top-down and the bottom-up approaches:

$$E_{i,j} = Norm(M_{i,j}^{td}(v) - M_{i,j}^{bu}(v)) \quad \text{(Eq. 3.4)}$$

$$\varphi(v) = \sum_{j=1}^{7}[\frac{1}{\sqrt{N}}(\sum_{i=1}^{N} {E_{i,j}}^2)^{0.5}] \quad \text{(Eq. 3.5)}$$

where v is the vector of optimization variables, i the time index, j the joint index, N the number of samples, M^{td} and M^{bu} are the 3D moment vectors obtained from the top-down and bottom-up approaches, respectively. We formulated a two-step optimization algorithm to find suboptimal solutions for fast convergence. In the first step, the offset error of the COP location measured by the force plate was minimized. The optimization variable was defined as a vector composed of two components of the offset error:

$$x_{COP} = \bar{x}_{COP} + \varepsilon_x \quad \text{(Eq. 3.6)}$$

$$y_{COP} = \bar{y}_{COP} + \varepsilon_y \quad \text{(Eq. 3.7)}$$

where $(\varepsilon_x, \varepsilon_y)$ is the bias, (x_{COP}, y_{COP}) the optimized COP location and $(\bar{x}_{COP}, \bar{y}_{COP})$ the initial COP location measured by the force plate.

In the second step, the errors due to scaled anthropometric data were aimed to be minimized. The position vectors of JCR and COM with respect to the spinal processes and mass of each segment were optimized for all segments to find the (ideally) error-free values. The optimization variables

were defined as these position vectors (assumed to be in the sagittal plane) and the segments' mass. Inequality constraints were applied as follows for obtaining anatomically sensible position vectors:

$$\left|Pos_{JCR_i} - \overline{Pos}_{JCR_i}\right| < \varepsilon_a \quad \text{(Eq. 3.8)}$$

$$\left|Pos_{COM_j} - \overline{Pos}_{COM_j}\right| < \varepsilon_b \quad \text{(Eq. 3.9)}$$

where i is the joint index, j is the segment index, Pos_{JCR} and Pos_{COM} are vectors from the reflective marker on the spinous process to the corresponding JCR and COM, respectively. $\overline{Pos}_{JCR}$ and $\overline{Pos}_{COM}$ are the initial values obtained using the MVH data. A genetic algorithm (MATLAB, MathWorks, Natick, MA, USA) was employed for the optimization (Figure 7). The RMS difference between the net joint moment time series obtained with top-down and the bottom-up approaches were calculated, both before and after optimization, and was used to evaluate the efficiency of our proposed method for minimizing the errors. Statistical analyses were performed to compare the following data (obtained among all participants):

(a) Sensitivity of the moments at each joint calculated via bottom-up compared to those calculated via top-down approaches, to inertial terms,
(b) Overall RMSE improvement achieved in step one compared to that achieved in step two of the optimization,
(c) Improvement of the moment estimations at each joint because of the optimization in the bottom-up approach compared to that in the top-down approach,
(d) RMS difference between the moment calculated via the bottom-up approach and that calculated via the top-down approach before optimization compared to this RMS difference after optimization (at each joint), and
(e) Comparison of RMS differences stated in (d) among all joints.

The Kolmogorov-Smirnov test rejected the null hypothesis that the data came from a normal distribution. Consequently, we used the non-parametric Wilcoxon Signed Rank test and Friedman test with significance level set at 0.05 for (a-d) and (e), respectively.

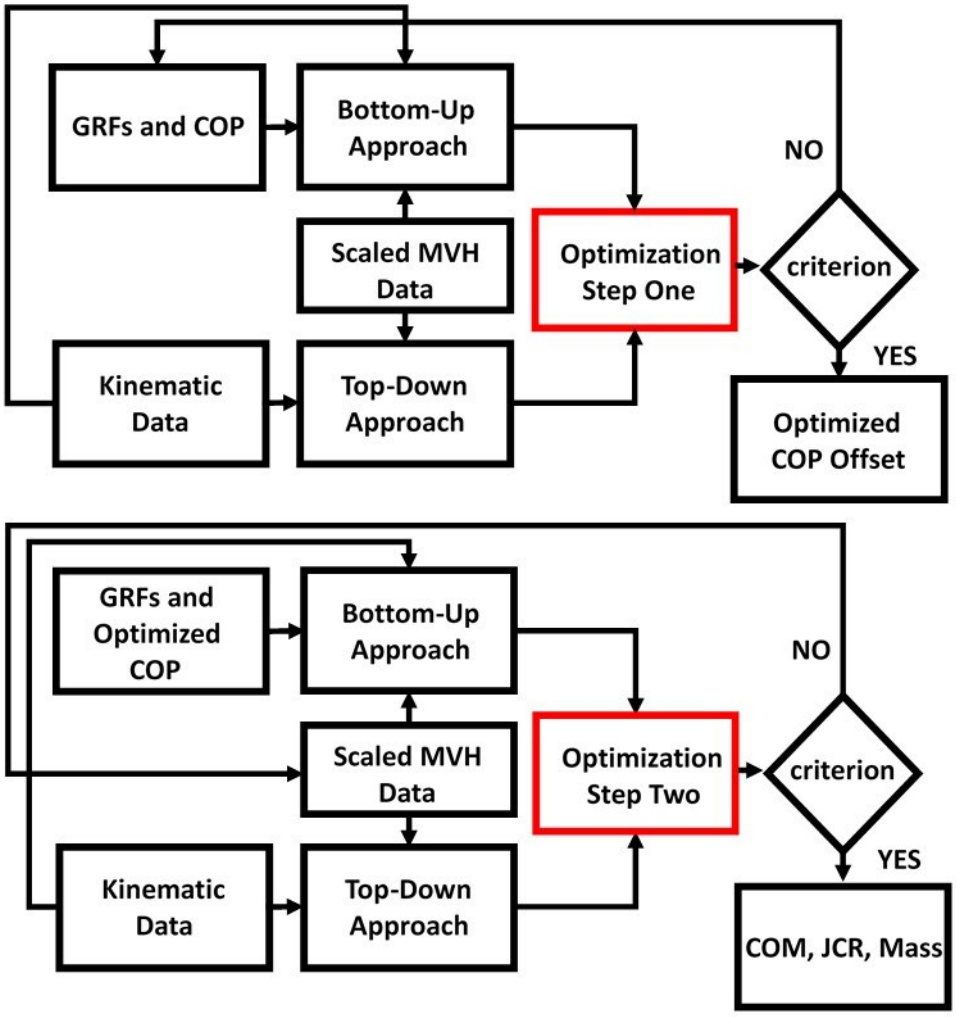

Figure 7. The two-step optimization algorithm to minimize the error between two traditional inverse dynamics approaches. The first step optimizes the offset error of the COP measured by the force plate. The second step uses the scaled anthropometric data from MVH and corrected COP from the previous step to find optimal individual-specific COM, JCR, and mass of each segment. At each step, optimization constraints were used as the criterion.

3.4 Results

The sensitivity of the bottom-up and the top-down approaches to inertial terms was investigated and presented in Table 2. According to Table 2, the median RMSE in the net joint moment relative

to its range varied from 0.58% to 4.76% and from 2.87% to 4.16% among all participants for bottom-up and top-down approaches, respectively. Table 2 also indicates that the top-down approach is significantly more sensitive to inertial terms compared to the bottom-up approach for joints SC-LL to MLT-MUT (p-value $\leq$ 0.005).

Table 2. Sensitivity of the inter-segmental joint moment to ignoring inertial terms in Newton-Euler equation (linear and angular acceleration terms set to zero). The induced errors are presented as normalized RMSE (in percentage), relative to the range of the net moment. The results are presented for both bottom-up and the top-down inverse dynamics approaches and for the seven intersegmental joints, as shown in Figure 6. The results are presented as percentile [25%, 50%, 75%] among all participants.

Joint	Bottom-Up	Top-Down	P-Value
SC~LL	[0.48, 0.58, 0.93]	[2.73, 2.99, 3.77]	0.001
LL~UL	[0.46, 0.63, 0.75]	[2.73, 2.88, 3.67]	0.001
UL~LT	[0.86, 0.98, 1.43]	[2.69, 2.87, 3.72]	0.001
LT~MLT	[1.33, 1.53, 2.22]	[2.85, 3.01, 3.91]	0.001
MLT~MUT	[1.87, 3.01, 4.20]	[3.18, 3.81, 5.04]	0.005
MUT~UT	[2.02, 3.33, 5.24]	[3.61, 4.16, 6.73]	0.083
UT~HD	[2.63, 4.76, 7.50]	[3.35, 4.12, 4.79]	0.413

The optimization algorithm converged for all participants and always reduced the cost function, with the RMS difference improving by 77.59% (on average, varying from 51.55% to 88.92% among all participants). This RMS difference at each step of the optimization reduced by 27.96% and 68.93% (average among participants) after the first and second steps, respectively (Table 3). Optimizing the COP (step one) has a smaller effect compared to the optimization of the BSPs (steps two) on reducing the RMS differences between results calculated via the two approaches (p-value < 0.001).

Table 3. Cumulative RMSE improvement (in percentage) after step 1 and step 2 of the optimization. The error was defined as the difference between the joint moments calculated by bottom-up and top-down approaches at each joint in the proposed multi-segment model of the HAT. The summation of RMSE at all joints was considered as the cumulative RMSE. The result is presented for all participants.

Participants	Step 1	Step 2	Total
1	23.00	69.36	76.41
2	13.54	43.97	51.55
3	13.90	50.03	56.98
4	48.23	58.76	78.65
5	24.90	85.01	88.74
6	36.56	73.65	83.28
7	26.35	84.96	88.92
8	22.34	73.28	79.25
9	45.72	54.11	75.09
10	31.96	80.12	86.47
11	21.07	84.98	88.14
Average	27.96	68.93	77.59
Standard deviation	11.56	14.98	12.61
Maximum	48.23	85.01	88.92
Minimum	13.54	43.97	51.55

The RMS differences between the net joint moment computed via bottom-up and top-down approaches were significantly smaller after optimization compared to those before optimization (p-value < 0.001 at each joint), and improved from 60.23% to 7.29% (79.25%) median among all participants (Table 4a). Among different joints, the improvement of the RMS differences varied from 75.59% to 82.27% (median among participants). Similarly, the RMS differences between the joint moments in the sagittal plane were reduced after optimization. This improvement had a median of 87.75% among all participants (Table 4b) and varied from 82.33% to 90.94% (p-value < 0.001 at each joint).

Table 4. The errors induced in the (a) net joint moment and (b) sagittal moment at each joint of the HAT multi-segment model. The errors are presented as RMS difference between the calculated moment via bottom-up and top-down inverse dynamics approaches, as percentile [25%, 50%, 75%] among all participants. The RMS differences are presented for both before and after optimization and for the seven intersegmental joints, as shown in Figure 6. The summation of RMS differences at all joints are presented as the cumulative RMSE.

(a) RMSE before and after optimization for net joint moment

Joint	Before	After	Improvement (%)
SC~LL	[4.86, 8.92, 10.80]	[0.92, 1.04, 2.64]	[75.05, 82.27, 85.33]
LL~UL	[4.86, 9.00, 10.75]	[0.91, 1.11, 2.64]	[74.44, 81.86, 85.68]
UL~LT	[4.69, 8.78, 10.61]	[0.84, 0.94, 2.48]	[76.50, 81.57, 88.03]
LT~MLT	[4.52, 8.62, 10.49]	[0.80, 0.86, 2.29]	[78.05, 81.41, 89.23]
MLT~MUT	[4.34, 8.44, 10.36]	[0.79, 0.91, 2.14]	[77.04, 80.50, 89.31]
MUT~UT	[4.29, 8.30, 10.26]	[0.80, 1.10, 2.21]	[71.43, 79.18, 88.56]
UT~HD	[4.35, 8.18, 10.18]	[0.93, 1.27, 2.46]	[61.12, 75.59, 85.87]
Cumulative RMSE	[31.62, 60.23, 73.46]	[6, 7.29, 16.81]	[75.42, 79.25, 87.72]

(b) RMSE before and after optimization for sagittal joint moment

Joint	Before	After	Improvement (%)
SC~LL	[4.68, 8.84, 10.61]	[0.49, 0.77, 2.24]	[78.78, 86.41, 89.41]
LL~UL	[4.67, 8.92, 10.54]	[0.51, 0.83, 2.24]	[78.62, 85.07, 89.65]
UL~LT	[4.47, 8.67, 10.38]	[0.43, 0.62, 2.03]	[80.27, 89.16, 90.49]
LT~MLT	[4.22, 8.48, 10.25]	[0.32, 0.47, 1.76]	[82.53, 90.94, 93.19]
MLT~MUT	[4.01, 8.26, 10.14]	[0.29, 0.54, 1.58]	[83.99, 90.46, 93.22]
MUT~UT	[4.05, 8.08, 10.01]	[0.33, 0.72, 1.52]	[83.29, 87.19, 92.05]
UT~HD	[4.08, 7.92, 9.90]	[0.59, 0.81, 1.64]	[70.50, 82.33, 90.18]
Cumulative RMSE	[29.21, 59.15, 71.70]	[2.83, 4.94, 12.61]	[82.15, 87.75, 89.33]

The statistical analysis of the net joint moment at each joint also revealed that the top-down approach can be significantly less affected by the BSPs' inaccuracy at the superior joints (joints UT-HD and MUT-UT) compared to the bottom-up approach (p-value < 0.001). Although there were no significant differences between the two approaches at the inferior joints (joints SC-LL and LL-UL), the bottom-up approach tends to be less affected by the BSPs' inaccuracy.

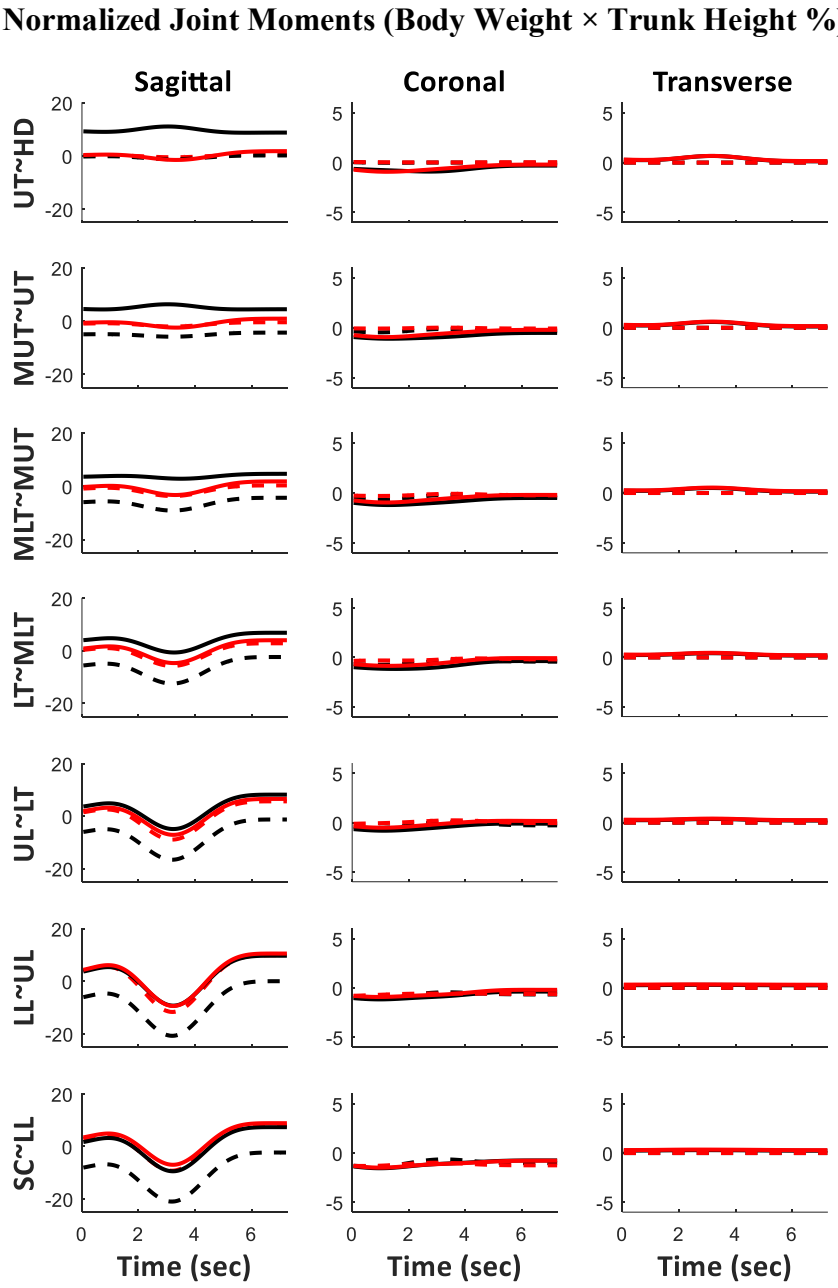

Figure 8. Normalized joint moments with respect to the body weight and trunk height (expressed in BWxTH%), for one of the participants. Results are presented for moments in sagittal, coronal, and transverse planes at all joints defined in Figure 6. The scale of moments in sagittal, coronal, and transverse planes are different. The moments calculated via the bottom-up approach are depicted as solid lines and those calculated via the top-down approach are depicted as dashed lines. Black lines indicate the moments obtained before optimization and the red lines indicates the moments obtained after optimization. As such, we expect that the distances between solid and dashed lines decrease after optimization.

Finally, Figure 8 represents the computed joint moment in the sagittal, coronal, and transverse planes at each joint before and after optimization using bottom-up and top-down inverse dynamics approaches for one participant and one trial. This figure demonstrates the extent of the capability of our proposed algorithm in reducing the error introduced by erroneous COP measurements and BSPs.

3.5 Discussion

Optimization-based inverse dynamics approaches have been proposed to compensate for the inaccuracy of BSPs in kinetics assessment of lower limbs during running [53], gait [32], squatting and standing sway [52]. However, to the best of our knowledge, no study has investigated the application of such an optimization-based approach specifically for kinetics assessment of the HAT complex when the trunk is modeled as multiple segments. Actually, a non-invasive estimation of individual-specific BSPs is a major prerequisite to kinetic assessment of multi-segment HAT. However, estimation of BSPs for multi-segment HAT based on typical anthropometric measurements is very challenging, because of the larger inter-subject variability of HAT segments compared to the lower limbs. Therefore, there is no comprehensive database for the BSPs of the multi-segment HAT. This study proposed a nonlinear optimization-based method for reducing the error in the joint moment calculation for the multi-segment HAT by estimating the COP offset and BSPs (i.e., JCR and COM locations and mass of each segment). Then, the proposed method was implemented on experimental data from a trunk-bending task to obtain the 3D joint moments among the HAT segment.

Both bottom-up and top-down approaches were insensitive to the linear and angular acceleration of the segments during the particular motion of trunk-bending (Table 2). As a result, the inertial terms were eliminated from the inverse dynamics formulation to reduce the computational cost during optimization. In previous studies, the difference between measured and calculated GRF at the distal extremity was defined as the cost function while BSPs were the optimization variables. In contrast, our proposed method included the difference between the magnitude of all net joint moments calculated using the top-down and the bottom-up approaches in the cost function of

optimization. As a result, these differences improved for all joint moments in the multi-segment HAT (Table 4).

Our proposed multi-step optimization enabled distinguishing the influence of estimation of BSPs from that of COP on the accuracy of the calculated joint moments in a multi-segment HAT model, and demonstrated the extent of the influence of inaccuracy of each of them. The optimization of BSPs (steps 2) improved the errors in joint moment calculation by 68.93% (average), which was larger than the improvement of these errors by optimization of the COP offset in step 1 (average: 27.96%). One interpretation can be the larger inaccuracy of the BSPs estimation compared to the COP offset. Indeed, the initial guess of the BSPs used for optimization was obtained from data of only one cadaver and then scaled for each participant with different body weight and height. Therefore, this initial guess of BSPs for different body shapes used for optimization might be more error-prone than the COP position that was recorded by the same force plate for all participants. In summary, adopting the anthropometric BSPs from data of only one cadaver might not be representative of all body shapes and populations and was a limitation of this study. A larger dataset for an initial guess of the BSPs may improve the accuracy of the estimated BSP's.

Alternatively, the joint moment calculation might be inherently more sensitive to BSPs inaccuracy than to COP inaccuracy. Notably, measurement errors of the BSPs, COP, GRF, and motion data (marker trajectories) may all propagate into the calculated joint moments, and the joint moment calculation can have different sensitivity to each parameter's inaccuracy. Our proposed method primarily focused on the improvement of errors due to individual-specific BSPs estimation and does not investigate the effect of inaccuracies in motion data (e.g., soft tissue artifact) and GRF measurements. Our previous studies demonstrated the effect of inaccuracies in motion data on the 3D kinematics assessment of the multi-segment HAT [19], [80]. Our future studies will investigate the effect of inaccuracies of each parameter (BSP's, force plate measures, motion data) on kinetics assessment of the multi-segment HAT.

The RMSE of the net joint moment (Table 4a) and its component in the sagittal plane (Table 4b) at all joints for all participants reduced after optimization. Actually, the errors of the sagittal component have a significant contribution towards the net moment error, because this component

is much larger than others when the trunk bends in the anterior direction. Therefore, our proposed optimization-based method can also be employed for trunk bending in directions other than the anterior direction to investigate the improvement of errors in the frontal and transverse components of the net joint moment.

The results revealed that the moment at inferior (superior) joints tended to be less affected by BSPs inaccuracy when calculated via bottom-up (top-down) approach compared to when they are calculated via top-down (bottom-up) approach. This could be justified as in each approach; the error propagation grows as the calculation proceeds toward joints farther from the segment on which the initial conditions are applied (Figure 8).

The proposed method is subject to other limitations as well. We employed a multi-segment model of the HAT with assuming each segment as a rigid body which may not be accurate during all body motions, especially high-impact motions. Nevertheless, our rigid body model was suitable for the performed exercise that consisted of slow motions without impact. Finally, we assumed that the body is symmetric in the frontal plane and, thus, the COMs and JCRs are in the sagittal plane. This assumption may not be valid especially in some pathological conditions.

3.6 Conclusion

Estimation of individual-specific BSP's for kinetics assessment of multi-segment HAT models is currently challenging. To address this challenge, (1) we assigned scaled BSPs for HAT segments obtained from cadaveric data to the body size of individuals who participated in an in-vivo experiment and approximated individual-specific BSPs; and (2) we proposed a method for minimizing the difference between the net joint moment calculated using top-down and bottom-up inverse dynamics formulations by estimating the BSPs and offset of COP. Using a multi-step nonlinear optimization approach, our method significantly reduced the differences between net joint moments calculated through the two inverse dynamics approaches among all HAT segments. Our proposed method can be used in the future to assess the sensitivity of the calculated trunk joint moments in a variety of daily tasks to a range of experimental errors including motion data, GRF, and BSP measurements. In addition, compensating the major source of error enables us to

accurately quantify the kinetics of the spinal column and facilitate finding inter-vertebral moment pattern at different levels of the spinal column in non-disabled or patient populations.

Chapter 4

4 Quantification of Multi-Segment Trunk Kinetics during Multi-Directional Trunk Bending

The material presented in this chapter has been submitted as a research paper to Gait & Posture. The majority of content of this chapter is identical to the material presented in the publication except for the text formatting which was done according to University of Alberta requirements.

A. Noamani, A. H. Vette, R. Preuss, M. R. Popovic, H. Rouhani, "Quantification of Multi-Segment Trunk Kinetics during Multi-Directional Trunk Bending", submitted to Gait & Posture

4.1 Abstract

Motion assessment of the body's head-arms-trunk (HAT) using linked-segment models along with an inverse dynamics approach can enable in vivo estimation of the inter-vertebral moments. However, such mathematical approach is prone to experimental errors due to inaccuracies in kinematic measurement associated with soft tissue artifacts and estimating individual-specific body segment parameters (BSPs). The inaccuracy of the BSPs is particularly challenging for the multi-segment HAT due to high inter-participant variability in the HAT's BSPs, implying that currently no study exists that has accurately identified the joint moments along the spinal column. This study characterized three-dimensional (3D) inter-segmental moments in a multi-segment HAT model during multi-directional trunk-bending, after minimizing the experimental errors. Eleven non-disabled individuals participated in a multi-directional trunk-bending experiment at five directions with three speeds. A seven-segment HAT model was reconstructed for each participant and its motion was recorded. After compensating the soft tissue artifacts induced error in kinematic data, and using optimized individual-specific BSPs and center of pressure offsets, the inter-segmental moments were calculated via inverse dynamics. Our results show a significant

effect of inter-segmental level and trunk-bending directions, and a two-way interaction effect between joint-level and bending-direction. Characterization of the net sagittal-coronal moment explained these effects. Our results indicate complex, task-specific patterns for the 3D moments with high inter-participant variability at different inter-segmental levels, which cannot be studied using single-segment models or without error compensation. Interpretation of inter-segmental moments after compensation of experimental errors can be of great importance for clinical evaluations and developing injury prevention and rehabilitation strategies.

Keywords: Inverse dynamics; Joint moments; Multi-segment model; Trunk kinetics.

4.2 Introduction

Accurate estimation of the inter-spinal loads is a key requirement for assessing the risk of injury during occupational and daily activities, designing prevention and treatment strategies [1], and pre- and post-treatment assessment [19]. Linked-segment models of the human body have been employed as a mathematical technique to facilitate in vivo studying of inter-vertebral interactions, in biomechanical studies to evaluate spine kinematics [136] and stability [24], and in the clinical evaluation of conditions such as low back pain [7], scoliosis [5], and spinal cord injury [15]. Using one-segment and multi-segment models of the head-arms-trunk (HAT), the three-dimensional (3D) kinematics of the upper body have been widely investigated [138]. Kinetics assessment of the HAT based on a linked-segment model using an inverse dynamics approach requires measurements of the inter-segmental motions and ground reaction forces (GRF) as well as accurate estimation of the body segment parameters (BSPs).

Although inverse dynamics is a commonly-used approach for kinetics assessment of the human body, this procedure is error-prone. Published studies suggest that major contributors to these errors are inaccuracy in (a) motion data [34], (b) force plate measurements [35], and (c) BSPs estimation [52]. Riemer et al. [37] showed that the above-mentioned inaccuracies could lead to significant errors ranging from 6 to 232% of the estimated peak moment. They also identified inaccuracies in estimated segment angles and BSPs as the main sources of these uncertainties.

Previous studies [19], [43] suggest that the relative motion between skin-mounted markers and bony prominences (anatomical landmarks), i.e., soft tissue artifacts (STA), during dynamic tasks causes inaccuracy in obtained joint angles. Hence, the assessment of the inter-vertebral moments via an inverse dynamics approach is likely affected by STA. Previous studies have shown the considerable impact of STA on the measurement accuracy of lower limb kinematics and kinetics [44], [46]. Some studies evaluated the effect of STA on kinematics measurements of the scapula [47] and spine [19]; however, to our knowledge, no study has quantified the STA effect on the inter-segmental joint moments of a multi-segment HAT model.

Moreover, kinetics assessment via an inverse dynamics approach requires accurate estimation of individual-specific BSPs, including the 3D center of mass (COM) coordinates, 3D coordinates of the joint's center of rotation (JCR) and the mass and moments of inertia for each segment. Although medical imaging techniques can be used to obtain highly accurate, individual-specific BSPs, they have the potential of radiation exposure [163]. Estimations of individual-specific BSPs using predictive equations based on medical imaging [163] and cadaveric data [151] were proposed; however, these estimations may induce errors of over 40% [52]. Optimization methods have been employed to minimize the effect of the BSPs' inaccuracy in calculating net joint moments at different lower limb joints in the sagittal plane [52]. However, to our knowledge, no study has estimated the 3D joint moments of a multi-segment HAT model based on optimized individual-specific BSPs.

Several studies have investigated the 3D reaction forces and moments at the lumbo-sacral ($L5/S1$) joint with a one-segment HAT model during various motor tasks such as walking [140], [142], lifting [141], balance recovery [31], and sit-to-stand [143], and for clinical evaluation of low-back pain [140], [141] and lower-limb amputation [142]. Regression equations [54], [55], [140], scaling equations [31], or geometrical models [1] have been widely used for estimating BSPs of a one-segment HAT model. Some studies have investigated the validity of using bottom-up and top-down approaches for calculating the lumbo-sacral joint moment [31], [54], [55], [141], [142]. Other studies particularly addressed the sensitivity of the lumbo-sacral joint moment computed to errors via bottom-up and top-down approaches [39], especially due to BSPs inaccuracy [31]. However, all these studies investigated the forces and moments at $L5/S1$ using one-segment HAT

model. None of them obtained the 3D inter-vertebral moments using a multi-segment HAT model due to technical complexities of estimating individual-specific BSPs for each HAT segment.

Our team has recently obtained detailed BSPs from a single cadaver to calculate the moments at spinal joints using a multi-segment HAT model for a male individual during perturbed sitting [56]. However, the obtained kinetic results might be considerably affected by the heterogeneity of BSPs among individuals. Later, we presented a novel method to optimize the estimation of individual-specific BSPs of the HAT segments and proposed it for accurate measurement of the 3D inter-segmental moments of the spinal column. Building upon these efforts, the purpose of this study is to calculate the 3D inter-segmental moments using multi-segment HAT model with (a) optimized participant-specific BSPs; and (b) corrected kinematic parameters after compensation the effect of STA during multi-directional trunk-bending tasks. By minimizing the influence of STA and inaccurate BSPs, we were then able to investigate how these moments vary across the spinal column, and among different trunk-bending directions and speeds.

4.3 Method

4.3.1 Experiment Procedures

The experimental procedures were described in detail in our previous study [136] and, thus, are only briefly described here. Eleven non-disabled individuals (4 females; age: 28.5±3.3 years; trunk height: 0.75±0.04 m) with no history of persistent back pain or spine-related musculoskeletal or neuromuscular impairments participated in the experiment. All participants provided written consent prior to participating in the study. Research Ethics Board approval was received from the local ethics committee.

Participants were asked to sit naturally on a rigid, elevated force-plate with no constraints or support to restrict the participant's movement, and the lower legs freely hanging. Five targets were placed anterior of the participant, with the distances and heights adjusted based on the participant's trunk height to elicit angular trunk motions of 45° (Figure 9). Each participant was instructed to lean toward the target, touch the target with his/her head, and then return to the initial upright

sitting position. Each participant randomly performed the tasks with three different speeds for each target and three times for each speed. The arms were crossed motionless over the chest throughout each trunk-bending trial.

4.3.2 Data acquisition

The measurement setup described in Chapter 3 was used.

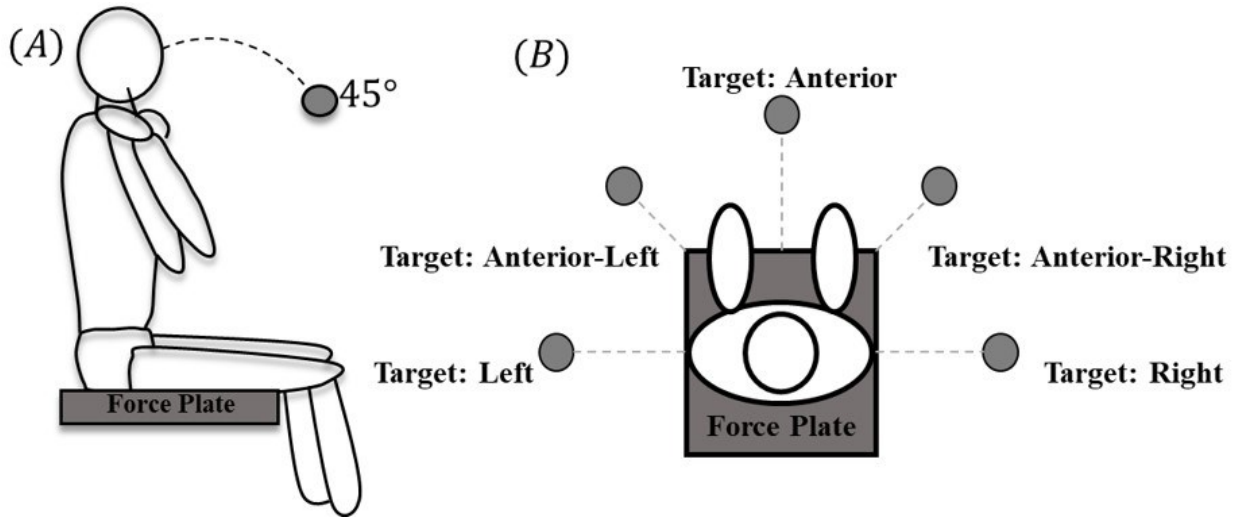

Figure 9. (A) Subject-specific distance and height representing an angular motion of 45° of the trunk as an inverted pendulum. (B) Targets for movement tasks. Targets were placed in the transverse plane at 45° intervals, anteriorly and laterally of the participant.

4.3.3 Multi-segment HAT modeling

4.3.3.1 Multi-segment model of the HAT

The seven rigid segments and the multi-segment model of the HATdefined in Chapter 3 (Figure 6) were used in the present study.

4.3.3.2 Modeling and compensation algorithm for STA induced errors

STA were modeled to compensate the error induced by relative motion between skin-mounted markers and actual bony anatomical landmarks during trunk-bending trials. For this purpose, the model suggested in our previous study [19] was used. This model assumed that the relative displacement between the actual bony landmark and the skin-mounted marker was proportional to the trunk bending angle. It was also assumed that the minimum (zero) and maximum relative

displacements occurred at the upright sitting and maximum trunk-bending posture, respectively. The instantaneous trunk bending angle (θ_t) was defined as the angle between the line formed by the $S1$ and $C7$ markers and the upright position. The instantaneous soft tissue artifact of marker i in segment j calculated in the segment's local frame ($STA_i^j(\theta_t)$) was then obtained by using equation (1):

$$STA_i^j(\theta_t) = STA_i^j(\theta_{max})\frac{\theta_t}{\theta_{max}} \quad \text{(Eq. 4.1)}$$

where $STA_i^j(\theta_{max})$ is the soft tissue artifact at the maximum trunk bending angle (θ_{max}). We used $STA_i^j(\theta_{max})$ measured by palpating actual bony anatomical landmarks for each marker at maximum trunk-bending posture in a previous study [19] and scaled the reported $STA_i^j(\theta_{max})$ values for each individual by participant's trunk height. Subsequently, the trajectory of each marker was calculated by using equation (2):

$$C_i^j(t) = {}^G_L R_j(t)[\,{}^G_L R_j{}^{-1}(t).P_i^j(t) - STA_i^j(\theta_t)] \quad \text{(Eq. 4.2)}$$

where $P_i^j(t)$ and $C_i^j(t)$ are the preliminary and corrected trajectory of marker i in segment j at the time index t, respectively, and ${}^G_L R_j(t)$ is the instantaneous rotation matrix from the segment-fixed frame to the lab-fixed frame. The seven-segment model of the HAT was then reconstructed using corrected marker trajectories, and 3D inter-segmental angles were calculated based on standard joint coordinate system conventions [180].

4.3.4 Inverse dynamics

3D inter-segmental forces and moments were calculated through both bottom-up and top-down inverse dynamics approaches similar to Chapter 3.

4.3.5 Optimized estimation of individual-specific BSPs for inverse dynamics

3D inter-segmental forces and moments were calculated through both bottom-up and top-down inverse dynamics approaches. For this purpose, an initial guess of the BSPs (i.e., mass, COM, JCR, and moments of inertia of each HAT segment) was obtained by individual-specific scaling of

cadaveric data from the Male Visible Human images reported by Vette et al. [51] using body weight and trunk height of each participant. However, such scaling methods are error-prone when the data are applied to individuals with a different range of age, body type, sex and ethnicity [50], [166]. Since scaling induces inaccuracies in the estimation of the BSPs, the top-down and bottom-up inverse dynamics approaches were expected to result in different values for the net joint moments, mostly due to inaccurate estimation of BSPs for HAT segments. Thus, we adjusted the scaled BSPs to estimate an optimal individual-specific set of BSPs as well as compensating systematic offset in the force plate center of pressure measurement by employing a nonlinear, multi-step, optimization-based, non-invasive method that minimizes the difference between the joint moments at all inter-segmental levels obtained by top-down and bottom-up inverse dynamics approaches.

4.3.6 Data Analysis

The Kolmogorov-Smirnov test was used to determine whether the calculated moments across the participants came from a normal distribution. Moreover, the Levene's test was used to assess the equality of variance in case of normality. Statistical analysis of the inter-segmental moments in the sagittal, coronal, and transverse planes were separately conducted using a three-way analysis of variance (ANOVA). The independent variables were joint level (seven joints: SC~LL to UT~HD), target direction (five directions), and bending speed (three speeds), with the 3D joint moment being the dependent variable. In addition, to investigate the influence of STA on the net joint moments, a two-way ANOVA was performed on the root-mean-square (RMS) difference between the net joint moment before and after STA error compensation. The independent variables were joint level and target direction, with the test being performed for both bottom-up and top-down inverse dynamic approaches.

All statistical analyses were performed on the absolute peak values of the 3D joint moments with the significance level set at 0.01 when applying Bonferroni correction. A multiple comparison post-hoc test was performed to investigate main effects on the joint moments of the multi-segment HAT.

4.4 Results

All participants were able to successfully perform the bending tasks for different directions except for the targets placed laterally (left and right targets, Figure 9) which no participant could touch the target with his/her head. Therefore, these motions were considered as the maximum voluntary lateral bending for each individual.

The effect of the STA error compensation on the inter-segmental joint moment at each joint-level and trunk-bending direction was investigated as presented in Table 5 as the RMS difference between the net joint moment (resultant of the sagittal, coronal, and transverse moments) calculated with and without STA error compensation for both bottom-up and top-down inverse dynamics approaches. We observed significant main effects of joint-level (Table 7) and trunk-bending direction (Table 8) as well as their interaction effect on the RMS difference between the inter-segmental net joint moment calculated before and after STA error compensation, and for both bottom-up and top-down approaches (Table 5). Results also reflected a significant difference between the results obtained via two inverse dynamics approaches.

Table 6 and Figure 10 to Figure 12 present the peak joint moments in the sagittal, coronal, and transverse planes for different joint levels and target directions. According to Table 6, CV%, defined as $CV\% = \frac{standard\ deviation}{mean} \times 100$, of the peak moments among all participants varied from 27.3 to 82.1%, 7.5 to 72.2%, and 27.9 to 59.3% (the range of CV% across different joints) for the sagittal, coronal, and transverse moments, respectively.

A main effect of joint level and trunk-bending direction was observed for moments in the sagittal, coronal, and transverse planes (Table 6, Table 9, and Table 10).

Effect of joint level: The sagittal moments of the lumbar joints (SC~LL, LL~UL, and UL~LT) were significantly larger ($p<0.01$) compared to all other superior (thoracic and cervical) joints (Table 6 and Table 9.a). Among the lumbar joints, the sagittal moment at LL~UL tended to be the largest among all joints. Similarly, larger coronal moments were observed at inferior joints relative to their superior joints, except for the coronal moment at SC~LL, which was larger than that of

other joints, but the LL~UL joint. The transverse moment at the two most superior joints (MUT~UT and UT~HD) tended to be larger compared to the inferior joints while no significant differences were found among the transverse moments at the inferior joints. The transverse moment in UT~HD was significantly larger compared to all inferior joints, except MUT~UT.

Effect of trunk-bending direction: The sagittal moment across different joints decreased in more lateral trunk-bending directions compared to more anterior directions, as it was larger (smaller) in anterior (lateral: left and right) direction than all other directions ($p<0.01$). No significant bilateral asymmetry was observed in the sagittal moments ($p=1.00$) (Table 10.a). We observed the opposite main effect of trunk-bending direction for the coronal moments: The largest (smallest) coronal moments were observed for trunk-bending in the lateral (anterior) direction. Again, no significant bilateral asymmetry was observed in the coronal moments (Table 10.b)

Effect of speed: Results of the ANOVA for the inter-segmental sagittal moment (Figure 10) reflected no main effect of speed ($p = 0.1499$) and no significant two-way interaction effects for joint-speed ($p = 0.999$) and direction-speed ($p = 0.3808$) on the sagittal moment. Therefore, the voluntary speed of trunk-bending does not change the sagittal moment of the trunk joints. We observed that the slowest speed of trunk bending led to significantly smaller coronal moments compared to the faster speeds. However, no significant difference was seen between speed levels 2 and 3. We also observed that the transverse moment increased significantly by increasing the speed of the bending tasks, implying that the participants tended to have faster axial-rotation of the neck while they increased their trunk-bending pace.

Table 5. RMS difference between the inter-segmental net joint moment calculated before and after STA error compensation at each joint level of the proposed HAT model (Figure 6) for five trunk-bending directions (Figure 9 b). Results are expressed as mean ± standard deviation among all participants and obtained through both (a) bottom-up and (b) top-down inverse dynamics approaches. The average of the three trials and three speeds are presented. Moments (N.m) were normalized by participant's body weight and trunk height.

(a) Bottom-up approach

	SC~LT	**LL~UL**	**UL~LT**	**LT~MLT**	**MLT~MUT**	**MUT~UT**	**UT~HD**
Left	7.4 ±1.4	7.5 ±1.2	6.5 ±0.9	5.5 ±0.7	4.6 ±0.9	3.9 ±1	2.8 ±1
Anterior-Left	8.2 ±1.3	8.4 ±0.9	7 ±1.1	5.4 ±0.9	3.7 ±0.7	2.7 ±0.8	2 ±1
Anterior	8.4 ±1.8	8.8 ±1.3	6.8 ±1.4	4.8 ±1	2.8 ±0.8	1.5 ±0.7	1.4 ±0.7
Anterior-Right	8.2 ±1.5	8.5 ±1.1	7 ±1.1	5.3 ±0.7	3.7 ±0.6	2.8 ±0.7	2.2 ±0.8
Right	7.4 ±1.1	7.5 ±1	6.6 ±0.7	5.6 ±0.7	4.8 ±1	4.1 ±1.1	2.9 ±1.3

(b) Top-down approach

(b) Top-down	**SC~LT**	**LL~UL**	**UL~LT**	**LT~MLT**	**MLT~MUT**	**MUT~UT**	**UT~HD**
Left	5.4 ±2	5.5 ±1.8	4.5 ±1.2	3.5 ±0.9	2.6 ±0.7	1.8 ±0.8	0.6 ±0.4
Anterior-Left	6.6 ±2.1	6.9 ±1.8	5.5 ±1.6	4 ±1.2	2.4 ±0.7	1.4 ±0.5	0.6 ±0.4
Anterior	7.5 ±2.5	7.9 ±2.1	6 ±1.8	4.2 ±1.3	2.2 ±0.8	1 ±0.6	0.6 ±0.3
Anterior-Right	6.8 ±2.5	7.1 ±2.1	5.6 ±1.9	4 ±1.2	2.4 ±0.7	1.4 ±0.5	0.6 ±0.3
Right	5.4 ±1.7	5.5 ±1.5	4.5 ±1.1	3.5 ±0.8	2.6 ±0.7	1.9 ±0.7	0.6 ±0.3

Table 6. Peak joint moments calculated via a bottom-up inverse dynamics approach using optimized individual-specific BSPs and STA-induced error compensation. The results are expressed as mean (coefficient of variations %) across all participants for inter-segmental joint moments at the sagittal, coronal, and transverse plane for five trunk-bending directions (see Figure 6 and Figure 9). The average of the three trials were used. Moments (N.m) were normalized by participant's body weight and trunk height.

		SC~LT	LL~UL	UL~LT	LT~MLT	MLT~MUT	MUT~UT	UT~HD
Left	**Sagittal**	6.6 (31.7)	6.6 (33.7)	5.3 (38.0)	4.7 (48.4)	4.8 (47.9)	4.7 (44.3)	3.4 (81.5)
	Coronal	15.2 (10.8)	16.0 (8.9)	14.4 (9.2)	12.2 (9.5)	10.2 (12.0)	8.4 (15.9)	6.3 (30.0)
	Transverse	1.5 (28.6)	1.6 (27.9)	1.5 (30.2)	1.4 (31.3)	1.3 (32.9)	1.3 (33.9)	1.5 (30.9)
Anterior-Left	**Sagittal**	13.4 (40.0)	14.7 (34.4)	12.7 (40.5)	10.0 (39.6)	7.7 (39.5)	6.1 (37.6)	4.7 (60.9)
	Coronal	13.0 (13.3)	14.3 (14.5)	12.3 (16.0)	9.0 (19.5)	6.7 (26.6)	5.1 (33.9)	4.1 (48.7)
	Transverse	1.3 (41.5)	1.3 (42.2)	1.3 (43.4)	1.2 (45.2)	1.2 (46.5)	1.2 (47.8)	1.4 (45.1)
Anterior	**Sagittal**	17.3 (33.3)	18.9 (27.3)	15.3 (34.1)	10.7 (42.8)	7.6 (46.3)	5.9 (47.4)	4.6 (60.4)
	Coronal	1.8 (48.0)	1.8 (61.6)	1.5 (72.2)	1.5 (64.1)	1.4 (53.1)	1.4 (44.1)	1.3 (50.8)
	Transverse	0.9 (58.5)	0.9 (59.3)	0.9 (58.7)	1.0 (58.1)	1.2 (56.7)	1.3 (54.6)	1.5 (52.1)
Anterior-Right	**Sagittal**	13.5 (40.8)	15.0 (35.4)	12.8 (39.8)	9.6 (43.2)	7.2 (49.4)	5.7 (52.1)	4.5 (69.0)
	Coronal	13.5 (10.3)	14.9 (7.6)	12.7 (7.5)	8.8 (11.9)	6.1 (16.5)	4.1 (28.6)	3.1 (49.8)
	Transverse	1.8 (32.2)	1.8 (33.8)	1.9 (34.7)	2.0 (35.4)	2.1 (35.2)	2.3 (34.8)	2.6 (33.4)
Right	**Sagittal**	6.5 (29.7)	6.4 (30.9)	5.5 (44.1)	5.1 (53.9)	4.9 (59.5)	4.8 (57.6)	3.6 (82.1)
	Coronal	15.4 (13.6)	16.2 (13.6)	14.3 (12.1)	11.6 (15.5)	9.2 (20.1)	7.0 (28.5)	4.8 (52.9)
	Transverse	1.7 (35.3)	1.8 (35.4)	1.7 (37.6)	1.7 (38.5)	1.8 (39.5)	1.9 (39.0)	2.1 (34.8)

Table 7. The main effect of joint level on the net joint moment calculated via (a) bottom-up, and (b) top-down approaches. * indicates significant differences ($p < 0.01$) in the moments between individual pairs of joints. – indicates no significant differences.

(a) Effect on the net moment calculated via bottom-up approach

Joints	**SC~LL**	**LL~UL**	**SC~LL**	**LL~UL**	**MLT~MUT**	**MUT~UT**	**UT~HD**
SC~LL		-	*	*	*	*	*
LL~UL	-		*	*	*	*	*
UL~LT	*	*		*	*	*	*
LT~MLT	*	*	*		*	*	*
MLT~MUT	*	*	*	*		*	*
MUT~UT	*	*	*	*	*		-
UT~HD	*	*	*	*	*	*	

(b) Effect on the net moment calculated via top-down approach							
Joints	**SC~LL**	**LL~UL**	**SC~LL**	**LL~UL**	**MLT~MUT**	**MUT~UT**	**UT~HD**
SC~LL		-	*	*	*	*	*
LL~UL	-		*	*	*	*	*
UL~LT	*	*		*	*	*	*
LT~MLT	*	*	*		*	*	*
MLT~MUT	*	*	*	*		*	*
MUT~UT	*	*	*	*	*		-
UT~HD	*	*	*	*	*	*	

Table 8. The main effect of trunk-bending direction on the net joint moment calculated via (a) bottom-up, and (b) top-down approaches. * indicates significant differences ($p < 0.01$) in the moments between two directions. – indicates no significant differences.

(a) Effect on the net moment calculated via bottom-up approach					
Directions	**Left**	**Anterior-Left**	**Anterior**	**Anterior-Right**	**Right**
Left		-	*	-	-
Anterior-Left	-		-	-	
Anterior	*	-		-	*
Anterior-Right	-		-		-
Right	-	-	*	-	

(b) Effect on the net moment calculated via top-down approach					
Directions	**Left**	**Anterior-Left**	**Anterior**	**Anterior-Right**	**Right**
Left		-	*	-	-
Anterior-Left	-		-	-	-
Anterior	*	-		-	*
Anterior-Right	-	-	-		-
Right	-	-	*	-	

Table 9. The main effect of joint level on the sagittal moment (a), coronal moment (b), transverse moment (c), and net sagittal-coronal moment (d). * indicates significant differences ($p < 0.01$) in moments between individual pairs of joints. – indicates no significant differences.

(a) Effect on the sagittal moment

Joints	SC~LL	LL~UL	UL~LT	LT~MLT	MLT~MUT	MUT~UT	UT~HD
SC~LL		-	-	*	*	*	*
LL~UL	-		*	*	*	*	*
UL~LT	-	*		*	*	*	*
LT~MLT	*	*	*		*	*	*
MLT~MUT	*	*	*	*		-	*
MUT~UT	*	*	*	*	-		-
UT~HD	*	*	*	*	*	-	

(b) Effect on the coronal moment

Joints	SC~LL	LL~UL	UL~LT	LT~MLT	MLT~MUT	MUT~UT	UT~HD
SC~LL		*	*	*	*	*	*
LL~UL	*		*	*	*	*	*
UL~LT	*	*		*	*	*	*
LT~MLT	*	*	*		*	*	*
MLT~MUT	*	*	*	*		*	*
MUT~UT	*	*	*	*	*		*
UT~HD	*	*	*	*	*	*	

(c) Effect on the transverse moment

Joints	SC~LL	LL~UL	UL~LT	LT~MLT	MLT~MUT	MUT~UT	UT~HD
SC~LL		-	-	-	-	*	*
LL~UL	-		-	-	-	*	*
UL~LT	-	-		-	-	-	*
LT~MLT	-	-	-		-	-	*
MLT~MUT	-	-	-	-		-	*
MUT~UT	*	*	-	-	-		-
UT~HD	*	*	*	*	*	-	

(d) Effect on the net sagittal-coronal moment

Joints	SC~LL	LL~UL	UL~LT	LT~MLT	MLT~MUT	MUT~UT	UT~HD
SC~LL		*	*	*	*	*	*
LL~UL	*		*	*	*	*	*
UL~LT	*	*		*	*	*	*
LT~MLT	*	*	*		*	*	*
MLT~MUT	*	*	*	*		*	*
MUT~UT	*	*	*	*	*		*
UT~HD	*	*	*	*	*	*	

Table 10. The main effect of trunk-bending direction on the sagittal moment (a), coronal moment (b), transverse moment (c), and net sagittal-coronal moment (d). * indicates significant differences ($p < 0.01$) in moments between two directions. – indicates no significant differences.

(a) Effect on the sagittal moment

Directions	Left	Anterior-Left	Anterior	Anterior-Right	Right
Left		*	*	*	-
Anterior-Left	*		*	-	*
Anterior	*	*		*	*
Anterior-Right	*	-	*		*
Right	-	*	*	*	

(b) Effect on the coronal moment

Directions	Left	Anterior-Left	Anterior	Anterior-Right	Right
Left		*	*	*	-
Anterior-Left	*		*	-	*
Anterior	*	*		*	*
Anterior-Right	*	-	*		*
Right	-	*	*	*	

(c) Effect on the transverse moment

Directions	Left	Anterior-Left	Anterior	Anterior-Right	Right
Left		-	-	*	*
Anterior-Left	-		-	*	*
Anterior	-	-		*	*
Anterior-Right	*	*	*		*
Right	*	*	*	*	

(d) Effect on the net sagittal-coronal moment

Directions	Left	Anterior-Left	Anterior	Anterior-Right	Right
Left		-	*	-	-
Anterior-Left	-		*	-	-
Anterior	*	*		*	*
Anterior-Right	-	-	*		-
Right	-	-	*	-	

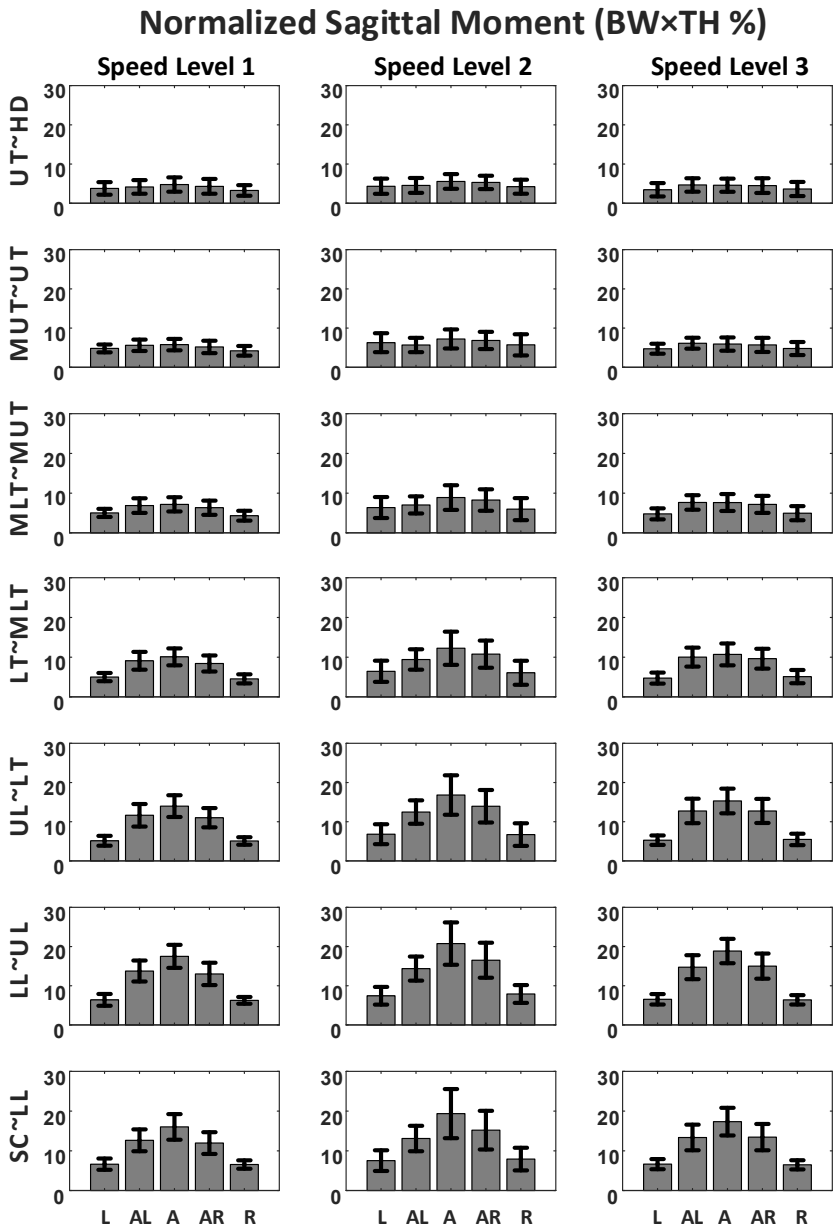

Figure 10. Peak joint moment at sagittal plane calculated via the bottom-up approach using optimized individual-specific BSPs and STA error compensation for different joint levels, trunk-bending directions, and speed levels. Results are presented as bar and error bar plots. Bars represent the mean value of the peak joint moment among participants, with the error bar depicting the range of plus to minus standard error of mean. Moments (N.m) were normalized by participant's body weight and trunk height. (L: left, AL: anterior-left, A: anterior, AR: anterior-right, R: right)

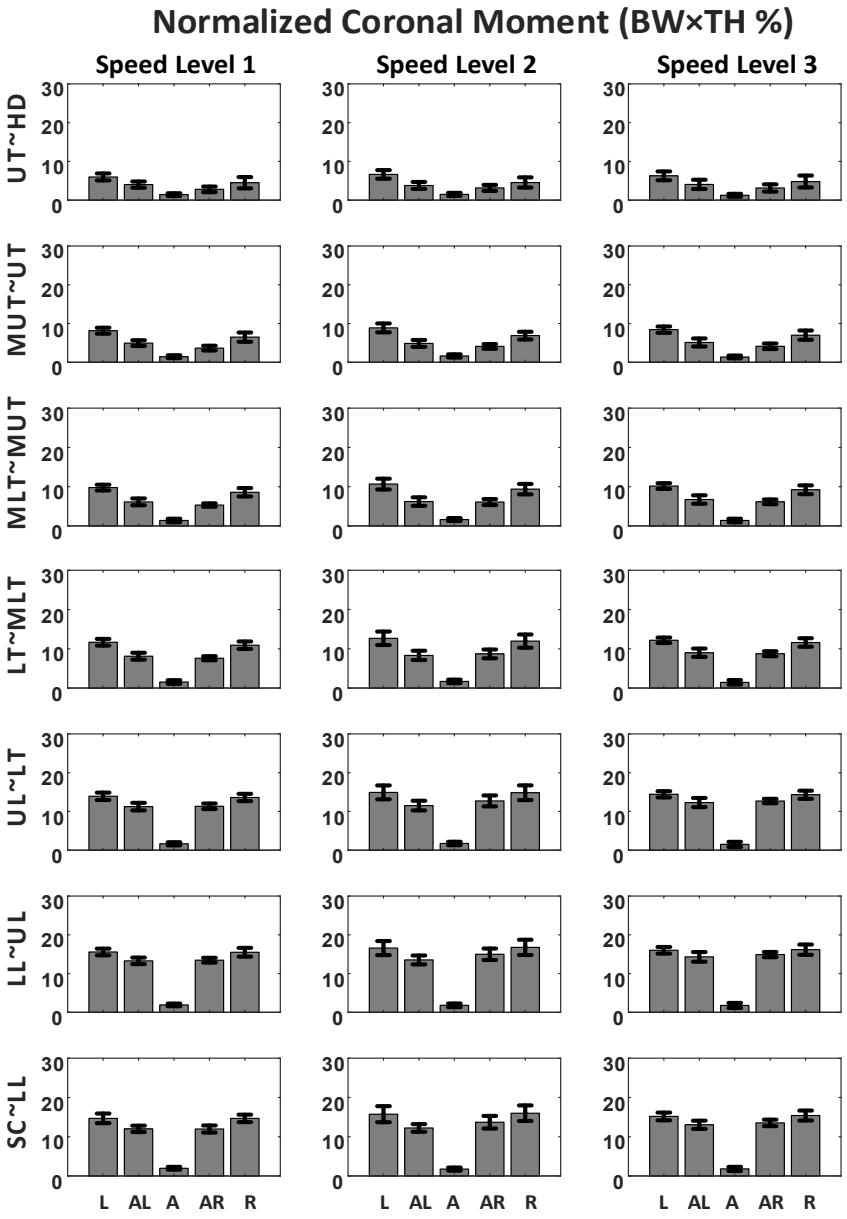

Figure 11. Peak joint moment at coronal plane calculated via the bottom-up approach using optimized individual-specific BSPs and STA error compensation for different joint levels, trunk-bending directions, and speed levels. Results are presented as bar and error bar plots. Bars represent the mean value of the peak joint moment among participants, with the error bar depicting the range of plus to minus standard error of mean. Moments (N.m) were normalized by participant's body weight and trunk height. (L: left, AL: anterior-left, A: anterior, AR: anterior-right, R: right)

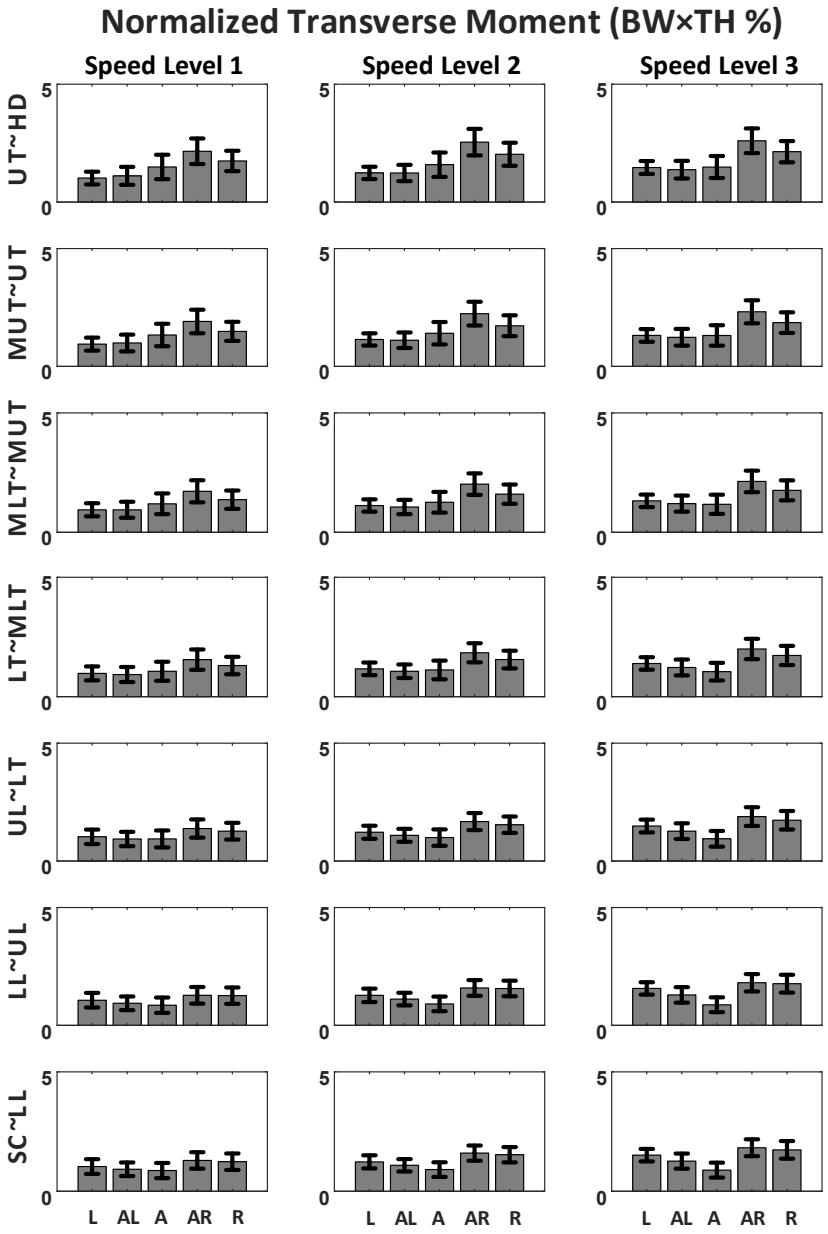

Figure 12. Peak joint moment at transverse plane calculated via the bottom-up approach using optimized individual-specific BSPs and STA error compensation for different joint levels, trunk-bending directions, and speed levels. Results are presented as bar and error bar plots. Bars represent the mean value of the peak joint moment among participants, with the error bar depicting the range of plus to minus standard error of mean. Moments (N.m) were normalized by participant's body weight and trunk height. (L: left, AL: anterior-left, A: anterior, AR: anterior-right, R: right)

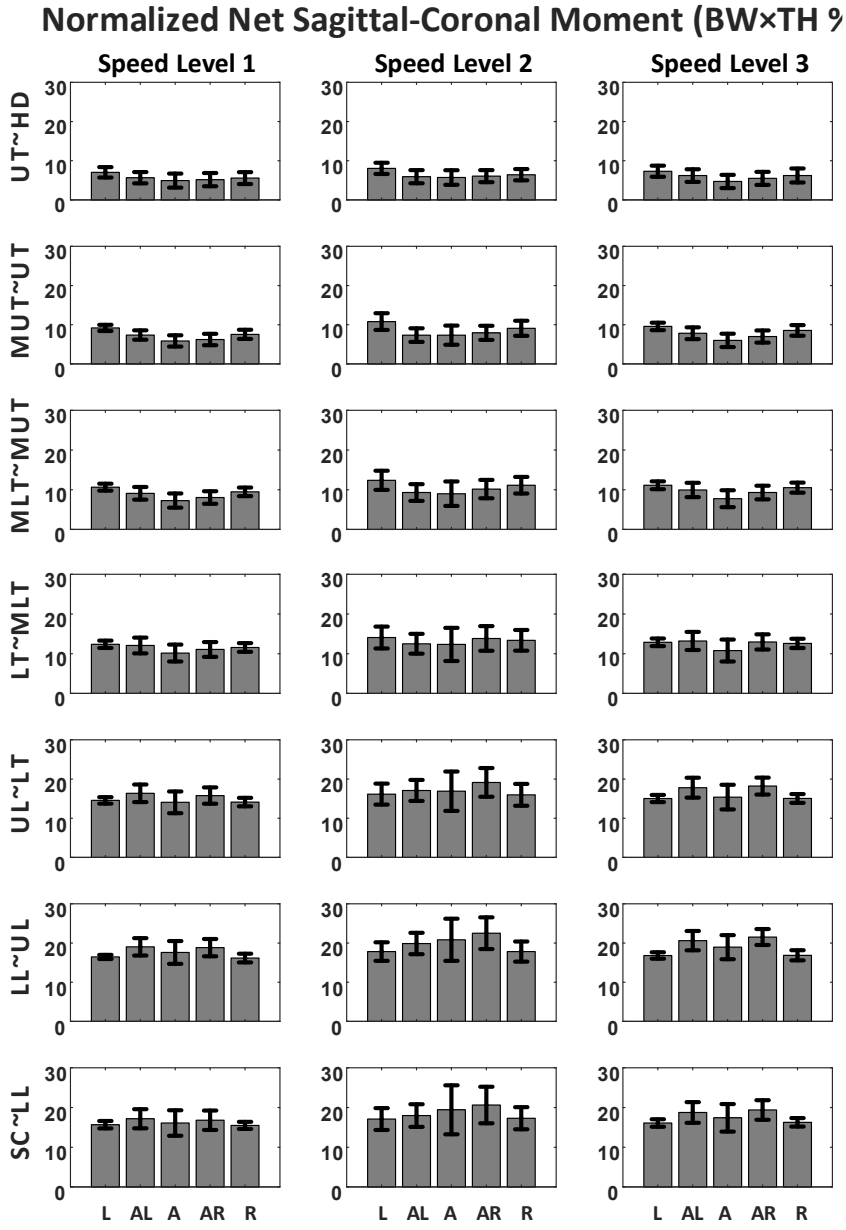

Figure 13. Peak joint moment at net sagittal-coronal plane (plane of movement) calculated via the bottom-up approach using optimized individual-specific BSPs and STA error compensation for different joint levels, trunk-bending directions, and speed levels. Results are presented as bar and error bar plots. Bars represent the mean value of the peak joint moment among participants, with the error bar depicting the range of plus to minus standard error of mean. Moments (N.m) were normalized by participant's body weight and trunk height. (L: left, AL: anterior-left, A: anterior, AR: anterior-right, R: right)

4.5 Discussion

Inverse dynamics approaches have been extensively used to estimate the lumbo-sacral joint moment using a single-segment trunk model along with regressions [39], [54], [55], [140], scaling equations [31], or geometrical models [1] for estimating BSPs. The accuracy of 3D joint moments obtained via a multi-segment HAT model can be affected by two major sources of error, and compensation strategies for minimizing the effect of these inaccuracies have not been addressed to date. First, previous studies have shown considerable effects of STA on the lower limb kinetics. However, no study has investigated the STA effects on the kinetics of the multi-segment HAT model. We have recently developed a methodology to compensate for the STA effects on the kinematics of the multi-segment HAT model that can subsequently be used for joint moment calculation. Second, previous studies have shown the effects of inaccurate BSPs on lower limb kinetics. Accurate estimation of BSPs has been the major challenge in the kinetics assessment of the multi-segment HAT model because of their inter-participant heterogeneity and the lack of palpable anatomical landmarks for JCR locations. We have recently proposed a non-linear, optimization-based method for minimizing the errors in joint moment calculation by estimating the individual-specific BSPs of a multi-segment HAT model. These two recent findings enable us to perform, for the first time in the present study, an inclusive assessment of a 3D multi-segment HAT kinetics during multi-directional trunk-bending. In the present study, we obtained 3D joint moments based on optimized individual-specific BSPs along with compensation of STA-induced errors, and subsequently investigated the effects of the joint level, bending direction, and bending speed on joint moments in the sagittal, coronal, and transverse planes. Notably, the magnitudes of the peak moments obtained in this study are in good agreement with previous studies which reported the $L5/S1$ joint moment during lifting [54] as well as lifting and lowering [141].

4.5.1 STA effect on inter-segmental net joint moment

The RMS difference for both the SC~LL and LL~UL joints was significantly larger compared to the superior joints. Although no significant differences were found between the SC~LL and LL~UL joints, the LL~UL joint tended to have a larger RMS difference. Moreover, the RMS

difference significantly decreased from the inferior joints to the superior joints, implying that the most superior joints had the smallest RMS difference. This finding suggests that STA correction is more essential for kinetics assessment of the inferior joints compared to the superior joints (for both bottom-up and top-down inverse dynamics approaches).

The interaction effect of joint level and trunk-bending direction showed that the RMS difference between the lumbar joint (SC~LL, LL~UL) moments calculated before and after STA error compensation tended to decrease with more lateral trunk-bending directions. Moreover, this RMS difference for mid-upper thoracic levels (MLT~MUT and MUT~UT) tended to be larger for more lateral trunk-bending directions. This [19]could be explained as the muscles in the thoracic region (such as trapezius muscle) are more involved in lateral movements [19]. This could result in increasing the STA induced error in this region.

In addition, the RMS difference between the joint moments calculated before and after STA error compensation was significantly smaller in the top-down approach compared to the bottom-up approach, implying that the top-down approach is less sensitive to the STA-induced error for spinal joint moment assessment. This is reasonable since, in the top-down approach, the kinematics of the inferior segment were calculated with respect to the superior segment. Then, since the motion and moments of superior joints were significantly less affected by STA induced errors compared to the inferior joints, error propagation was smaller for the top-down approach compared to the bottom-up approach.

4.5.2 3D inter-segmental moments and effect of joint level and trunk-bending direction

The sagittal and coronal moments increased from the superior joints caudally toward LL~UL joint. These results were expected since the inferior joints bear more weight during trunk bending. A significantly larger coronal moment was generated at LL~UL compared to SC~LL. A similar trend was observed for the sagittal moments, but was found to be non-significant. This observation could result from the fact that, during trunk bending (especially in the lateral directions), the lumbar spine's curvature is maximum at the LL~UL joint.

At the same time, dependency of the sagittal and coronal moments on trunk-bending direction is justified by the fact that, during trunk bending in the anterior (lateral) direction, the moment component associated with weight bearing is projected into the sagittal (coronal) plane. In this light, we observed a two-way interaction effect between joint level and trunk-bending direction on both sagittal and coronal moments, indicating that the difference between the sagittal (coronal) moments at different joint levels diminished for lateral (anterior) trunk-bending directions. For the left and right directions, no significant difference was found among all joint levels for sagittal moments. In contrast, bending towards more anterior directions led to significantly larger sagittal moments at the SC~LL, LL~UL, UL~LT, and LT~MLT joints compared to more lateral bending directions. In addition, the sagittal moments at more superior joints (MLT~MUT, MUT~UT, UT~HD) were not significantly affected by trunk-bending direction. In summary, we found that, although for trunk-bending in the anterior (lateral) direction the sagittal (coronal) moments increased from the top to the bottom joint, this assumption for sagittal (coronal) moment is of limited use for movement toward more laterally-placed targets (anterior target).

Statistical analyses of the moment magnitudes showed that the sagittal and coronal moments were significantly larger than the transverse moment, and the transverse moment generated at each joint level was negligible compared to the other components. This likely reflects the nature of the trunk-bending task in which the participants were asked to maintain the spine's torsional direction during the task to reach that target. The larger transverse moment in UT~HD compared to all other joints could have occurred since the participants axially rotated their neck to visually fixate a target while moving towards the target, which could require a transverse moment that was not required in other joints for the trunk-bending task.

To investigate whether the sagittal and coronal moment components essentially reflect the upper body weight bearing moment projected in the sagittal and coronal plane, we calculated the net sagittal-coronal moment (Table 9.d and Table 10.d and Figure 13) during trunk-bending in different directions. We observed that the effect of joint level on the net sagittal-coronal moment was very similar for the sagittal and coronal moments, and that this net moment significantly decreased from LL~UL to UT~HD. The net sagittal-coronal moment at the SC~LL joint was significantly larger compared to all superior joints, except for the LL~UL joint. Interestingly, there

was no significant difference among the net sagittal-coronal moments across the directions except the anterior direction, which tended to be smaller. However, the contribution of the sagittal (coronal) moment increased with more anterior (lateral) trunk-bending directions. Interestingly, unlike coronal and sagittal moments, no significant interaction effects between joint level and trunk-bending direction were found on the net sagittal-coronal moment. These observations suggest that the sagittal and coronal moment components are both projections of the same upper body weight bearing moment in different trunk-bending directions. Additionally, the net sagittal-coronal moment at LT~MLT joint reflected a transition between the lumbar and mid-thoracic levels: The joints inferior and superior to LT~MLT had significantly larger and smaller moments, respectively, than the net sagittal-coronal moment at LT~MLT, whereas no significance was found within these groups of joints. These findings imply that the pattern of the net sagittal-coronal moments is more likely to change across the spinal joint levels rather than across the directions. The results also showed that the slowest speed of trunk bending led to significantly smaller net sagittal-coronal moments compared to the faster speeds ($p < 0.01$). However, no significant difference was seen between speed levels 2 and 3.

4.5.3 Inter-participant variability

Our results showed that inter-segmental joint moments obtained using a multi-segment model of the HAT have complex, task-specific patterns across different joint levels and trunk-bending directions. These patterns cannot be observed using a single-segment HAT model. We investigated the variability of these moments among the participants to find any potential patterns in individuals with no history of spine-related impairment. In spite of the homogeneous population, the peak moments showed high inter-participant variability (coefficient of variation) (CV% of up to 82.1%, 72.2%, and 59.3% for the sagittal, coronal, and transverse moments, respectively). Previous studies reported high inter-participant variability for spine motion [140], while the present study reported the inter-participant variability of the joint moments in a multi-segment HAT model for the first time. Notably, high inter-participant variability of inter-vertebral motion and moment is an impediment in finding consistent normal or pathological patterns for clinical evaluations. Nevertheless, a higher inter-participant variability is expectable for voluntary tasks (e.g., trunk bending) compared to semi-automatic motor tasks (e.g., walking). Nonetheless, the bilaterally symmetrical moment patterns found in this study could be useful for clinical evaluations to

recognize any asymmetrical patterns at different spinal column levels. Preuss et al. [136] suggested that symmetrical movement patterns might be useful in identifying individuals at risk of developing low-back pain. Finally, the data used in this study was collected from a mixed-gender, relatively small population, which limits any generalization for representing neither healthy male nor female populations. A larger population would be needed to identify any clinically meaningful patterns for either non-disabled or patient populations.

4.6 Conclusion

The kinetics assessment of the spinal column using multi-segment HAT models is currently challenging and error-prone. The present study proposed a procedure for accurate estimation of the 3D inter-segmental moments at different levels of the spinal column based on optimized estimation of individual-specific BSPs along with compensation of STA-induced errors. This study investigated (a) the effect of STA-induced error compensation on the inter-segmental moments during trunk-bending towards different directions, and (b) the pattern of the 3D inter-segmental moments at different joint levels, target directions, and speed levels after compensating the errors induced by STA and BSPs inaccuracy. The results of this study revealed complex, task-dependent patterns for the 3D inter-segmental moments at different levels of the spinal column, which could not be studied using single-segment models or without such error compensations. Our findings show that multi-segment assessment of the spine kinetics is of great importance and could be beneficial for understanding pathological conditions related to the trunk movements.

Chapter 5

5 Conclusions and Future Perspectives

5.1 General Results and Main Contributions

The main objective of this thesis project was to develop a methodology for more accurate estimation of three-dimensional (3D) intervertebral joint moments in a multi-segment model of the head-arms-trunk complex (HAT), via an inverse dynamics approach. To this end, our developed methodology minimized the errors due to inaccuracies in (a) kinematic data due to soft tissue artifacts (STA), (b) COP offset, in force plate measurements, and (c) body segment parameters (BSPs). Our first original contribution was to propose a non-invasive, non-linear, two-step optimization-based method to estimate individual-specific BSPs and COP offset that minimizes the error in HAT joint moment estimation. Our second original contribution was (a) to apply the method proposed for optimal estimation of individual-specific BSPs and COP offset and another method previously proposed to compensate the error induced by STA to more accurately assess the pattern of the joint moments at different levels of the spinal column during multi-directional seated bending with different speeds, and (b) to enable investigation of the effect of factors such as joint level, trunk bending direction, and bending speed, on the intersegmental moments of the HAT. The main results and contributions of this thesis are summarized in the following sections.

5.1.1 Optimization Method for Estimating BSPs and COP Offset

Many approaches have been proposed in the past for estimating BSPs. Some studies employed medical imaging techniques to accurately obtain individual-specific BSPs. Although such methods are highly accurate, radiation exposure, cost, and complexity limit the feasibility of their real-world application, particularly for clinical evaluations. Some studies provided regression equations, scaling equations, or geometrical models based on either medical images or data from a limited number of cadavers. However, none of these methods provide high accuracy in estimation of

individual-specific BSPs, which could result in errors in estimating joint moments of the HAT, because of high inter-participant variability in the shape and composition of the segments in a multi-segment HAT model. Optimization methods have been employed as a mathematical technique to compensate such inaccuracies; however, their cost function usually minimized the difference between measured and calculated GRF and did not contain information on the net joint moments at a majority of body joints. Therefore, the error in the net joint moment could not be minimized by their proposed optimization cost function. Moreover, the available methods only targeted the lower limbs while assuming the upper body as a single segment. They neither modeled the spinal column using multiple segments, nor attempted to estimate the BSPs for each of these segments. For the first time, the present study addressed inaccuracies in BSPs and COP offset for assessing the kinetics of a multi-segment HAT model. First, we assigned BSPs for each segment of the HAT, scaled from cadaveric data as approximated individual-specific BSPs. Subsequently, we proposed a two-step optimization method to minimize the difference between the joint moments calculated via bottom-up and top-down approaches at all inter-segmental levels during trunk bending in the anterior direction, as the calibration task. Our optimization method significantly reduced the error (defined as the difference between calculated joint moment via bottom-up and top-down approaches) in joint moments at all levels of the spinal column, and provided more accurate, optimized individual-specific BSPs and COP offset.

5.1.2 Multi-Directional Kinetics of the Multi-Segment HAT: STA Compensation

In the past, the kinetics of the human trunk have been widely investigated to calculate the lumbo-sacral joint moment for various motor tasks using single-segment kinematic models of the trunk. These studies used regression equations, scaling equations, or geometrical models to estimate BSPs, and no study has employed an accurate estimation of individual-specific BSPs for a multi-segment HAT. Moreover, many studies investigated the effect of the induced error due to STA on the kinematics and kinetics of the lower limbs. A recent study proposed a methodology to model and compensate for the effect of STA on the kinematics measurement of the HAT segments; however, no study investigated STA effects on the kinetics of the HAT. For the first time, the present study proposed to compensate for the effects of STA in kinematics measurements for a comprehensive kinetics assessment of the multi-segment HAT during multi-directional seated trunk bending using individual-specific BSPs and suppressed COP offset. Consequently, this study

enabled, for the first time, estimation of the 3D intervertebral moment patterns at different levels of the spinal column, for different trunk bending directions, and for different trunk bending speeds. The results revealed complex, task-specific patterns which could not be captured by a single-segment trunk model, without compensating the effect of STA on kinematic parameters, and without estimation of optimized individual-specific BSPs. As such, by compensating the major sources of errors, our proposed method facilitates the assessment of multi-segment HAT kinetics for clinical evaluations, and for understanding pathological conditions related to the trunk.

5.2 Future Perspectives

5.2.1 Postural Balance and Risk of Falling Assessment

Characterization of postural balance and risk of falling during seated posture (e.g., during wheeling in a wheelchair) requires the highest level of accuracy in estimating the kinetics of the multi-segment HAT, which has been enabled by the present study. In the future, the methodology proposed by this study can be applied to investigate dynamic sitting balance using a multi-segment HAT model during different daily or work-related conditions (e.g., sitting perturbations and reaching tasks). This can provide insight into the mechanisms and strategies employed by the central nervous system to maintain sitting balance.

5.2.2 Ambulatory Assessment of Trunk Kinetics

This study was based on in-lab measurements using a stationary motion capture system and a force plate. However, recent developments in wearable technologies could be used to assess kinematics and kinetics of the multi-segment HAT in an unconstraint environment. The outcome of the present study can be implemented to improve the accuracy of kinematics and kinetics measurements of the multi-segment HAT using wearable technologies.

5.2.3 Clinical Evaluation of Pathological Conditions

Evaluation of neuro-musculoskeletal conditions pertaining to the spinal column, and injury prevention and treatment strategies require accurate and reliable estimation of the inter-spinal interactions. Evaluation of several pathological conditions such as low-back pain, herniated disc,

scoliosis, and kyphosis as well as of pre- and post-operational treatment can also benefit from assessment of the inter-vertebral interactions. Therefore, the methodology proposed by this study can be used for evaluating clinical conditions by providing a more accurate estimation of the inter-spinal interactions, which can be used for routine clinical evaluations. Moreover, this study provides insight into moment patterns along the spinal column (e.g., bilaterally symmetrical moment patterns), which could be used in diagnosis of any pathological asymmetrical patterns; for example, in individuals who are at risk of developing low-back pain.

References

[1] N. Arjmand, D. Gagnon, A. Plamondon, A. Shirazi-Adl, and C. Larivière, "Comparison of trunk muscle forces and spinal loads estimated by two biomechanical models," *Clin. Biomech.*, vol. 24, no. 7, pp. 533–541, 2009.

[2] C. Fortin, S. Nadeau, and H. Labelle, "Inter-trial and test-retest reliability of kinematic and kinetic gait parameters among subjects with adolescent idiopathic scoliosis," *Eur. Spine J.*, vol. 17, no. 2, pp. 204–216, 2008.

[3] S. Scherrer, M. Begon, A. Leardini, C. Coillard, C. Rivard, and P. Allard, "Three-Dimensional Vertebral Wedging in Mild and Moderate Adolescent Idiopathic Scoliosis," *PLoS One*, vol. 8, no. 8, pp. 1–7, 2013.

[4] M. Nishida, T. Nagura, N. Fujita, N. Hosogane, T. Tsuji, M. Nakamura, M. Matsumoto, and K. Watanabe, "Position of the major curve influences asymmetrical trunk kinematics during gait in adolescent idiopathic scoliosis," *Gait Posture*, vol. 51, pp. 142–148, 2017.

[5] R. M. Holewijn, I. Kingma, M. De Kleuver, J. J. P. Schimmel, and N. L. W. Keijsers, "Spinal fusion limits upper body range of motion during gait without inducing compensatory mechanisms in adolescent idiopathic scoliosis patients," *Gait Posture*, vol. 57, no. February, pp. 1–6, 2017.

[6] J. Cholewicki and S. M. McGill, "Mechanical stability of the in vivo lumbar spine: Implications for injury and chronic low back pain," *Clin. Biomech.*, vol. 11, no. 1, pp. 1–

15, 1996.

[7] T. Lund, T. Nydegger, D. Schlenzka, and T. R. Oxland, “Three-Dimensional Motion Patterns During Active Bending in Patients with Chronic Low Back Pain,” *Spine (Phila. Pa. 1976).*, vol. 27, no. 17, pp. 1865–1874, 2002.

[8] Linda R. Van Dillen, Shirley A. Sahrmann, Barbara J. Norton, Cheryl A. Caldwell, Mary Kate McDonnell, and Nancy J. Bloom, “Movement System Impairment-Based Categories for Low Back Pain : Stage 1 Validation,” *J. Orthop. Sport. Phys. Ther.*, vol. 33, pp. 126–142, 2003.

[9] R. Preuss and J. Fung, “Can acute low back pain result from segmental spinal buckling during sub-maximal activities ? A review of the current literature,” *Man. Ther.*, vol. 10, pp. 14–20, 2005.

[10] L. R. Van Dillen, S. P. Gombatto, D. R. Collins, J. R. Engsberg, and S. A. Sahrmann, “Symmetry of Timing of Hip and Lumbopelvic Rotation Motion in 2 Different Subgroups of People With Low Back Pain,” *Arch Phys Med Rehabil*, vol. 88, pp. 351–360, 2007.

[11] E. Nelson-wong, B. Alex, D. Csepe, D. Lancaster, and J. P. Callaghan, “Altered muscle recruitment during extension from trunk flexion in low back pain developers,” *JCLB*, vol. 27, no. 10, pp. 994–998, 2012.

[12] G. Christe, L. Redhead, T. Legrand, B. M. Jolles, and J. Favre, “Multi-segment analysis of spinal kinematics during sit-to-stand in patients with chronic low back pain,” *J. Biomech.*,

vol. 49, no. 10, pp. 2060–2067, 2016.

[13] X. Guan, S. Kuai, L. Ji, R. Wang, and R. Ji, “Trunk muscle activity patterns and motion cord injury at T8 and T10 walking with different Trunk muscle activity patterns and motion patterns of patients with motor complete spinal cord injury at T8 and T10 walking with different un-powered exoskeletons,” *J. Spinal Cord Med.*, vol. 0, no. 0, pp. 1–8, 2017.

[14] J. Lobo-prat, J. M. Font-llagunes, C. Gómez-pérez, J. Medina-Casanovas, and R. M. Angulo-barroso, “New biomechanical model for clinical evaluation of the upper extremity motion in subjects with neurological disorders : an application case,” *Computer Methods in Biomechanics and Biomedical Engineering*, vol. 17, no. 10. Taylor & Francis, pp. 1144–1156, 2014.

[15] M. Lalumiere, D. H. Gagnon, F. Routhier, L. Bouyer, and G. Desroches, “Upper Extremity Kinematics and Kinetics During the Performance of a Stationary Wheelie in Manual Wheelchair Users With a Spinal Cord Injury,” *J. Appl. Biomech.*, vol. 30, pp. 574–580, 2014.

[16] C. Gauthier, D. Gagnon, G. Jacquemin, C. Duclos, K. Masani, and M. R. Popovic, “Which trunk inclination directions best predict multidirectional-seated limits of stability among individuals with spinal cord injury ?,” *J. Spinal Cord Med.*, vol. 35, no. 5, pp. 343–350, 2012.

[17] J. L. Garrido-Castro, R. Medina-Carnicer, R. Schiottis, A. M. Galisteo, E. Collantes-Estevez, and C. Gonzalez-Navas, “Assessment of spinal mobility in ankylosing spondylitis

using a video-based motion capture system," *Man. Ther.*, vol. 17, no. 5, pp. 422–426, 2012.

[18] H.-C. H. Lan, H.-Y. Chen, L.-C. Kuo, J.-Y. You, W.-C. Li, and S.-K. Wu, "The shift of segmental contribution ratio in patients with herniated disc during cervical lateral bending," *BMC Musculoskelet. Disord.*, vol. 15, no. 1, p. 273, 2014.

[19] S. Mahallati, H. Rouhani, R. Preuss, K. Masani, and M. R. Popovic, "Multisegment Kinematics of the Spinal Column: Soft Tissue Artifacts Assessment," *J. Biomech. Eng.*, vol. 138, no. 7, p. 71003, 2016.

[20] P. Lundgren, C. Nester, A. Liu, A. Arndt, R. Jones, A. Stacoff, P. Wolf, and A. Lundberg, "Invasive in vivo measurement of rear-, mid- and forefoot motion during walking," *Gait Posture*, vol. 28, no. 1, pp. 93–100, 2008.

[21] A. Rozumalski, M. H. Schwartz, R. Wervey, A. Swanson, D. C. Dykes, and T. Novacheck, "The in vivo three-dimensional motion of the human lumbar spine during gait.," *Gait Posture*, vol. 28, pp. 378–384, 2008.

[22] P. G. Passias, S. Wang, M. Kozanek, Q. Xia, W. Li, B. Grottkau, K. B. Wood, and G. Li, "Segmental lumbar rotation in patients with discogenic low back pain during functional weight-bearing activities.," *J. Bone Joint Surg. Am.*, vol. 93, no. 1, pp. 29–37, 2011.

[23] M. R. Popovic, I. P. I. Pappas, K. Nakazawa, T. Keller, M. Morari, and V. Dietz, "Stability criterion for controlling standing in able-bodied subjects," *J. Biomech.*, vol. 33, no. 11, pp. 1359–1368, 2000.

[24] R. A. Preuss and M. R. Popovic, “Quantitative analysis of the limits of stability in sitting,” *J. Appl. Biomech.*, vol. 26, no. 3, pp. 265–272, 2010.

[25] E. Grimpampi, V. Bonnet, A. Taviani, and C. Mazzà, “Estimate of lower trunk angles using gyroscope data in pathological gait,” *Biosyst. Biorobotics*, vol. 1, pp. 747–751, 2013.

[26] A. H. Huntley, A. Schinkel-Ivy, A. Aqui, and A. Mansfield, “Validation of simplified centre of mass models during gait in individuals with chronic stroke,” *Clin. Biomech.*, vol. 48, no. July, pp. 97–102, 2017.

[27] J. J. Craig, A. P. Bruetsch, S. G. Lynch, and J. M. Huisinga, “The relationship between trunk and foot acceleration variability during walking shows minor changes in persons with multiple sclerosis,” *Clin. Biomech.*, vol. 49, no. July, pp. 16–21, 2017.

[28] G. K. Lenton, T. L. A. Doyle, D. J. Saxby, and D. G. Lloyd, “An alternative whole-body marker set to accurately and reliably quantify joint kinematics during load carriage,” *Gait Posture*, vol. 54, no. December 2016, pp. 318–324, 2017.

[29] A. Leardini, F. Biagi, A. Merlo, C. Belvedere, and M. G. Bendetti, “Multi-segment trunk kinematics during locomotion and elementary exercises,” *Clin. Biomech.*, vol. 26, no. 6, pp. 562–571, 2011.

[30] S. Ayatollahzadeh, “Human Trunk Multi-segment Kinematics : Sensitivity to Experimental Errors,” University of Toronto, 2014.

[31] T. Robert, L. Chèze, R. Dumas, and J. P. Verriest, “Validation of net joint loads calculated

by inverse dynamics in case of complex movements: Application to balance recovery movements," *J. Biomech.*, vol. 40, no. 11, pp. 2450–2456, 2007.

[32] A. D. Kuo, "A Least-Squares Estimation Approach to Improving the Precision of Inverse Dynamics Computations," *J. Biomech. Eng. ASME*, vol. 120, pp. 149–159, 1998.

[33] V. Cahouet, M. Luc, and A. David, "Static optimal estimation of joint accelerations for inverse dynamics problem solution," *J. Biomech.*, vol. 35, pp. 1507–1513, 2002.

[34] R. Riemer and E. T. Hsiao-Wecksler, "Improving joint torque calculations: Optimization-based inverse dynamics to reduce the effect of motion errors," *J. Biomech.*, vol. 41, no. 7, pp. 1503–1509, 2008.

[35] P. D. Steven T. McCaw, "Errors in Alignment of Center of Pressure and Foot Coordinates Affect Predicted Lower Extremity Torques," *J. Biomech.*, vol. 28, no. 8, pp. 985–988, 1995.

[36] G. Rao, D. Amarantini, E. Berton, and D. Favier, "Influence of body segments ' parameters estimation models on inverse dynamics solutions during gait," *J. Biomech.*, vol. 39, pp. 1531–1536, 2006.

[37] R. Riemer, E. T. Hsiao-Wecksler, and X. Zhang, "Uncertainties in inverse dynamics solutions: A comprehensive analysis and an application to gait," *Gait Posture*, vol. 27, no. 4, pp. 578–588, 2008.

[38] D. Kiernan, M. Walsh, R. O. Sullivan, T. O. Brien, and C. K. Simms, "The influence of estimated body segment parameters on predicted joint kinetics during diplegic cerebral

palsy gait," *J. Biomech.*, vol. 47, no. 1, pp. 284–288, 2014.

[39] P. Desjardins, A. Plamondon, and M. Gagnon, "Sensitivity analysis of segment models to estimate the net reaction moments at the L5/S1 joint in lifting," *Med. Eng. Phys.*, vol. 20, no. 2, pp. 153–158, 1998.

[40] C. Larivière and D. Gagnon, "The L5/S1 joint moment sensitivity to measurement errors in dynamic 3D multisegment lifting models," *Hum. Mov. Sci.*, vol. 18, no. 4, pp. 573–587, 1999.

[41] L. Chiari, U. Della, A. Leardini, and A. Cappozzo, "Human movement analysis using stereophotogrammetry Part 2 : Instrumental errors," *Gait Posture*, vol. 21, pp. 197–211, 2005.

[42] U. Della, A. Leardini, L. Chiari, A. Cappozzo, and I. Sistemistica, "Human movement analysis using stereophotogrammetry Part 4 : assessment of anatomical landmark misplacement and its effects on joint kinematics," *Gait Posture*, vol. 21, pp. 226–237, 2005.

[43] A. Leardini, L. Chiari, U. Della, and A. Cappozzo, "Human movement analysis using stereophotogrammetry Part 3 . Soft tissue artifact assessment and compensation," *Gait Posture*, vol. 21, pp. 212–225, 2005.

[44] K. B. Smale, B. M. Potvin, M. S. Shourijeh, and D. L. Benoit, "Knee joint kinematics and kinetics during the hop and cut after soft tissue artifact suppression: Time to reconsider ACL injury mechanisms?," *J. Biomech.*, pp. 1–8, 2017.

[45] T. Y. Tsai, T. W. Lu, M. Y. Kuo, and C. C. Lin, “Effects of soft tissue artifacts on the calculated kinematics and kinetics of the knee during stair-ascent,” *J. Biomech.*, vol. 44, no. 6, pp. 1182–1188, 2011.

[46] M. Y. Kuo, T. Y. Tsai, C. C. Lin, T. W. Lu, H. C. Hsu, and W. C. Shen, “Influence of soft tissue artifacts on the calculated kinematics and kinetics of total knee replacements during sit-to-stand,” *Gait Posture*, vol. 33, no. 3, pp. 379–384, 2011.

[47] K. Matsui, K. Shimada, and P. D. Andrew, “Deviation of skin marker from bone target during movement of the scapula,” *J. Orthop. Sci.*, vol. 11, no. 2, pp. 180–184, 2006.

[48] F. Mörl and R. Blickhan, “Three-dimensional relation of skin markers to lumbar vertebrae of healthy subjects in different postures measured by open MRI,” *Eur. Spine J.*, vol. 15, no. 6, pp. 742–751, 2006.

[49] R. Zemp, R. List, T. Gülay, J. P. Elsig, J. Naxera, W. R. Taylor, and S. Lorenzetti, “Soft tissue artefacts of the human back: Comparison of the sagittal curvature of the spine measured using skin markers and an open upright MRI,” *PLoS One*, vol. 9, no. 4, pp. 1–8, 2014.

[50] R. N. Hinrichs, “Regression Equations to Predict Segmental Moments Inertia From Anthropometric Measurements: Extension Of The Data Of Chandler Et Al. (1975),” *J. Biomech.*, vol. 18, no. 8, pp. 621–624, 1985.

[51] A. H. Vette, T. Yoshida, T. A. Thrasher, K. Masani, and M. R. Popovic, “A complete, non-

lumped, and verifiable set of upper body segment parameters for three-dimensional dynamic modeling," *Med. Eng. Phys.*, vol. 33, no. 1, pp. 70–79, 2011.

[52] R. Riemer and E. T. Hsiao-Wecksler, "Improving Net Joint Torque Calculations Through a Two-Step Optimization Method for Estimating Body Segment Parameters," *J. Biomech. Eng.*, vol. 131, no. 1, p. 11007, 2009.

[53] C. L. Vaughan, J. G. Andrews, and J. G. Hay, "Selection of Body Segment Parameters by Optimization Methods," *J. Biomech. Eng. ASME*, vol. 104, pp. 38–44, 1982.

[54] A. Plamondon, M. Gagnon, and P. Desjardins, "Validation of two 3-D segment models to calculate the net reaction forces and moments at the L5/S1 joint in lifting," *Clin. Biomech.*, vol. 11, no. 2, pp. 101–110, 1996.

[55] I. Kingma, M. P. De Looze, H. M. Toussaint, H. G. Klijnsma, and T. B. M. Bruijnen, "Validation of a full body 3-D dynamic linked segment model," *Hum. Mov. Sci.*, vol. 15, no. 6, pp. 833–860, 1996.

[56] A. H. Vette, T. Yoshida, T. A. Thrasher, K. Masani, and M. R. Popovic, "A comprehensive three-dimensional dynamic model of the human head and trunk for estimating lumbar and cervical joint torques and forces from upper body kinematics," *Med. Eng. Phys.*, vol. 34, no. 5, pp. 640–649, 2012.

[57] D. A. Winter, *Biomechanics and Motor Control of Human Movement*, Fourth Edi. Hoboken, NJ, USA: John Wiley & Sons, Inc., 2009.

[58] F. Gholibeigian, “Quantitative Characterization of Dynamic Sitting Control during Continuous Multi-Directional Perturbations,” University of Alberta, 2017.

[59] A. Cappozzo, U. Della, A. Leardini, and L. Chiari, “Human movement analysis using stereophotogrammetry Part 1 : theoretical background,” *Gait Posture*, vol. 21, pp. 186–196, 2005.

[60] A. Leardini, F. Biagi, C. Belvedere, and M. G. Benedetti, “Quantitative comparison of current models for trunk motion in human movement analysis,” *Clin. Biomech.*, vol. 24, no. 7, pp. 542–550, 2009.

[61] R. H. Brown, A. H. Burstein, C. L. Nash, and C. C. Schock, “Spinal analysis using a three-dimensional radiographic technique,” *J. Biomech.*, vol. 9, no. 6, 1976.

[62] A. M. J. Bull, F. H. Berkshire, and A. A. Amis, “Accuracy of an electromagnetic measurement device and application to the measurement and description of knee joint motion,” *Proc. Inst. Mech. Eng. Part H J. Eng. Med.*, vol. 212, no. 5, pp. 347–355, 1998.

[63] K. N. An, M. C. Jacobsen, L. J. Berglund, and E. Y. S. Chao, “Application of a magnetic tracking device to kinesiolgic studies,” *J. Biomech.*, vol. 21, no. 7, pp. 613–620, 1988.

[64] M. J. Pearcy and R. J. Hindle, “New method for the non-invasive three-dimensional measurement of human back movement,” *Clin. Biomech.*, vol. 4, no. 2, pp. 73–79, 1989.

[65] P. B. Shull, W. Jirattigalachote, M. A. Hunt, M. R. Cutkosky, and S. L. Delp, “Quantified self and human movement: A review on the clinical impact of wearable sensing and

feedback for gait analysis and intervention," *Gait Posture*, vol. 40, no. 1, pp. 11–19, 2014.

[66] A. Salarian, H. Russmann, F. J. G. Vingerhoets, C. Dehollain, Y. Blanc, P. R. Burkhard, and K. Aminian, "Gait assessment in Parkinson's disease: Toward an ambulatory system for long-term monitoring," *IEEE Trans. Biomed. Eng.*, vol. 51, no. 8, pp. 1434–1443, 2004.

[67] A. M. Sabatini, "Quaternion-based strap-down integration method for applications of inertial sensing to gait analysis," *Med. Biol. Eng. Comput.*, vol. 43, no. 1, pp. 94–101, 2005.

[68] J. R. Rebula, L. V. Ojeda, P. G. Adamczyk, and A. D. Kuo, "Measurement of foot placement and its variability with inertial sensors," *Gait Posture*, vol. 38, no. 4, pp. 974–980, 2013.

[69] J. K. Lee and E. J. Park, "3D spinal motion analysis during staircase walking using an ambulatory inertial and magnetic sensing system," *Med. Biol. Eng. Comput.*, vol. 49, no. 7, pp. 755–764, 2011.

[70] H. Dejnabadi, B. M. Jolles, E. Casanova, P. Fua, and K. Aminian, "Estimation and visualization of sagittal kinematics of lower limbs orientation using body-fixed sensors," *IEEE Trans. Biomed. Eng.*, vol. 53, no. 7, pp. 1385–1393, 2006.

[71] A. Schmitz, M. Ye, R. Shapiro, R. Yang, and B. Noehren, "Accuracy and repeatability of joint angles measured using a single camera markerless motion capture system," *J. Biomech.*, vol. 47, no. 2, pp. 587–591, 2014.

[72] A. Schmitz, M. Ye, G. Boggess, R. Shapiro, R. Yang, and B. Noehren, "The measurement of in vivo joint angles during a squat using a single camera markerless motion capture

system as compared to a marker based system," *Gait Posture*, vol. 41, no. 2, pp. 694–698, 2015.

[73] S. Corazza, L. MUNDERMANN, A. M. Chaudhari, T. Demattio, C. Cobelli, and T. P. Andriacchi, "A markerless motion capture system to study musculoskeletal biomechanics: Visual hull and simulated annealing approach," *Ann. Biomed. Eng.*, vol. 34, no. 6, pp. 1019–1029, 2006.

[74] G. JO., "Instrumentation in video-based three-dimensional systems.," *Allard P, Stokes IAF, Blanchi JP, Ed. Three-dimensional Anal. Hum. movement. Champaign Hum. Kinet.*, pp. 41–54, 1995.

[75] R. Huiskes, J. Kremers, A. de Lange, H. J. Woltring, G. Selvik, and T. J. G. van Rens, "Analytical stereophotogrammetric determination of three-dimensional knee-joint geometry," *J. Biomech.*, vol. 18, no. 8, pp. 559–570, 1985.

[76] W. P. Stevens, "Reconstruction of three-dimensional anatomical landmark coordinates using video-based stereophotogrammetry," *J. Anat.*, vol. 191, no. 1997, pp. 277–284, 1997.

[77] K. D. Taylor, F. M. Mottier, D. W. Simmons, W. Cohen, R. J. Pavlak, D. P. Cornell, and G. B. Hankins, "An automated motion measurement system for clinical gait analysis," *J. Biomech.*, vol. 15, no. 7, pp. 505–516, 1982.

[78] G. Ferrigno, N. A. Borghese, and A. Pedotti, "Pattern recognition in 3D automatic human motion analysis," *ISPRS J. Photogramm. Remote Sens.*, vol. 45, no. 4, pp. 227–246, 1990.

[79] D. NI and M. AS, Eds., *Virtual reality: scientific and technological challenges*. Washington DC: National Academy Press, 1995.

[80] H. Rouhani, S. Mahallati, R. Preuss, K. Masani, and M. R. Popovic, "Sensitivity of intersegmental angles of the spinal column to errors due to marker misplacement.," *J. Biomech. Eng.*, vol. 137, no. 7, p. 74502, 2015.

[81] L. Mündermann, S. Corazza, and T. P. Andriacchi, "The evolution of methods for the capture of human movement leading to markerless motion capture for biomechanical applications.," *J. Neuroeng. Rehabil.*, vol. 3, p. 6, 2006.

[82] B. Bonnechère, B. Jansen, P. Salvia, H. Bouzahouene, L. Omelina, F. Moiseev, V. Sholukha, J. Cornelis, M. Rooze, and S. Van Sint Jan, "Validity and reliability of the Kinect within functional assessment activities: Comparison with standard stereophotogrammetry," *Gait Posture*, vol. 39, no. 1, pp. 593–598, 2014.

[83] C. Wong, Z. Q. Zhang, B. Lo, and G. Z. Yang, "Wearable Sensing for Solid Biomechanics: A Review," *IEEE Sens. J.*, vol. 15, no. 5, pp. 2747–2760, 2015.

[84] W. Zijlstra and K. Aminian, "Mobility assessment in older people: New possibilities and challenges," *Eur. J. Ageing*, vol. 4, no. 1, pp. 3–12, 2007.

[85] S. Patel, H. Park, P. Bonato, L. Chan, and M. Rodgers, "A review of wearable sensors and systems with application in rehabilitation," *J. Neuroeng. Rehabil.*, vol. 9, no. 1, p. 21, 2012.

[86] A. Pantelopoulos and N. G. Bourbakis, "A survey on wearable sensor-based systems for

health monitoring and prognosis," *IEEE Trans. Syst. Man Cybern. Part C Appl. Rev.*, vol. 40, no. 1, pp. 1–12, 2010.

[87] Q. Wang, P. Markopoulos, B. Yu, W. Chen, and A. Timmermans, "Interactive wearable systems for upper body rehabilitation: a systematic review," *J. Neuroeng. Rehabil.*, vol. 14, no. 1, p. 20, 2017.

[88] a Cappozzo, F. Catani, U. Della Croce, and a Leardini, "Position and orietnation in space of bones during movement," *Clin. Biomech.*, vol. 10, no. 4, pp. 171–178, 1995.

[89] C. J. Craig, *Introduction to robotics: mechanics and control*, 3rd Editio. New Jersey: Pearson, 2005.

[90] D. G. E. Robertson, G. E. Caldwell, J. Hamill, G. Kamen, and S. N. Whittlesey, *Research Methods in Biomechanics*, 2nd Editio., no. January. Champaign,IL: Human Kinetics, 2004.

[91] R. Y. W. Lee, J. Laprade, and E. H. K. Fung, "A real-time gyroscopic system for three-dimensional measurement of lumbar spine motion," *J. Med. Eng. Phys.*, vol. 25, pp. 817–824, 2003.

[92] S. J. Edmondston, M. Aggerholm, S. Elfving, N. Flores, C. Ng, R. Smith, and K. Netto, "Influence of posture on the range of axial rotation and coupled lateral flexion of the thoracic spine," *J. Manipulative Physiol. Ther.*, pp. 193–199, 2007.

[93] M. Troke, A. Moore, F. Maillardet, A. Hough, and E. Cheek, "A new , comprehensive normative database of lumbar spine ranges of motion," *Clin. Rehabil.*, vol. 2155, no. 1, pp.

371–379, 2001.

[94] Y.-C. Pai and J. Patton, “Center of Mass Velocity-Position Predictions for Balance Control,” *J. Biomech.*, vol. 30, no. 4, pp. 347–354, 1997.

[95] K. Iqbal and Y. C. Pai, “Predicted region of stability for balance recovery: Motion at the knee joint can improve termination of forward movement,” *J. Biomech.*, vol. 33, no. 12, pp. 1619–1627, 2000.

[96] Y. C. Pai and K. Iqbal, “Simulated movement termination for balance recovery: Can movement strategies be sought to maintain stability in the presence of slipping or forced sliding?,” *J. Biomech.*, vol. 32, no. 8, pp. 779–786, 1999.

[97] M. J. Pavol, E. F. Runtz, and Y. C. Pai, “Diminished stepping responses lead to a fall following a novel slip induced during a sit-to-stand,” *Gait Posture*, vol. 20, no. 2, pp. 154–162, 2004.

[98] Y. Pai, J. D. Wening, E. F. Runtz, K. Iqbal, and M. J. Pavol, “Role of Feedforward Control of Movement Stability in Reducing Slip-Related Balance Loss and Falls Among Older Adults Role of Feedforward Control of Movement Stability in Reducing Slip-Related Balance Loss and Falls Among Older Adults,” *J. Neurophysiol.*, vol. 90, no. 2, pp. 755–762, 2007.

[99] M. J. Pavol and Y. C. Pai, “Deficient limb support is a major contributor to age differences in falling,” *J. Biomech.*, vol. 40, no. 6, pp. 1318–1325, 2007.

[100] F. Yang, F. C. Anderson, and Y. C. Pai, “Predicted threshold against backward balance loss following a slip in gait,” *J. Biomech.*, vol. 41, no. 9, pp. 1823–1831, 2008.

[101] R. J. Peterka, P. J. Loughlin, R. J. Peterka, and P. J. Loughlin, “Dynamic Regulation of Sensorimotor Integration in Human Postural Control,” *J. Neurohysiology*, pp. 410–423, 2010.

[102] A. D. Goodworth and R. J. Peterka, “Influence of Stance Width on Frontal Plane Postural Dynamics and Coordination in Human Balance Control,” *J. Neurophysiol.*, vol. 104, no. 2, pp. 1103–1118, 2010.

[103] R. J. Peterka, P. J. Loughlin, R. J. Peterka, and P. J. Loughlin, “Dynamic Regulation of Sensorimotor Integration in Human Postural Control,” pp. 410–423, 2010.

[104] H. Van Der Kooij and R. J. Peterka, “Non-linear stimulus-response behavior of the human stance control system is predicted by optimization of a system with sensory and motor noise,” *J. Comput. Neurosci.*, vol. 30, no. 3, pp. 759–778, 2011.

[105] T. Kiemel, Y. Zhang, and J. J. Jeka, “Identification of Neural Feedback for Upright Stance in Humans: Stabilization rather than Sway Minimization,” *J. Neurosci.*, vol. 31, no. 42, pp. 15144–15153, 2011.

[106] A. D. Goodworth and R. J. Peterka, “Sensorimotor integration for multisegmental frontal plane balance control in humans,” *J. Neurophysiol.*, vol. 107, no. 1, pp. 12–28, 2012.

[107] R. J. Peterka and M. S. Benolken, “Role of somatosensory and vestibular cues in attending

visually induced human postural sway," *Exp. Brain Res.*, vol. 105, pp. 101–110, 1995.

[108] M. Lauk, C. C. Chow, A. E. Pavlik, and J. J. Collins, "Human Balance out of Equilibrium: Nonequilibrium Statistical Mechanics in Posture Control," *Phys. Rev. Lett.*, vol. 80, no. 2, pp. 413–416, 1998.

[109] D. M. Merfeld, L. Zupan, and R. J. Peterka, "Humans use internal models to estimate gravity and linear acceleration.," *Nature*, vol. 398, no. 6728, pp. 615–618, 1999.

[110] R. J. Peterka, "Sensorimotor Integration in Human Postural Control," *J. Neurophysiol.*, vol. 88, pp. 1097–1118, 2002.

[111] R. J. Peterka, A. D. Goodworth, P. Mellodge, R. J. Peterka, D. Volpe, M. G. Giantin, R. Maestri, G. Frazzitta, C. Rehabil, C. F. Honeycutt, and T. R. Nichols, "Sensorimotor Integration in Human Postural Control," *J. Neurophysiol.*, vol. 88, no. 3, pp. 1097–1118, 2002.

[112] T. Mergner, C. Maurer, and R. J. Peterka, "A multisensory posture control model of human upright stance," *Prog. Brain Res.*, vol. 142, no. I, pp. 189–201, 2003.

[113] J. Jeka, T. Kiemel, R. Creath, F. Horak, and R. Peterka, "Controlling human upright posture: velocity information is more accurate than position or acceleration.," *J. Neurophysiol.*, vol. 92, no. 4, pp. 2368–79, 2004.

[114] C. Maurer and R. J. Peterka, "A new interpretation of spontaneous sway measures based on a simple model of human postural control," *J. Neurohysiology*, vol. 93, pp. 189–200, 2005.

[115] H. Van Der Kooij, E. Van Asseldonk, and F. C. T. Van Der Helm, "Comparison of different methods to identify and quantify balance control," *J. Neurosci. Methods*, vol. 145, no. 1–2, pp. 175–203, 2005.

[116] C. Maurer, T. Mergner, and R. J. Peterka, "Multisensory control of human upright stance," *Exp. Brain Res.*, vol. 171, no. 2, pp. 231–250, 2006.

[117] H. van der Kooij and E. de Vlugt, "Postural responses evoked by platform pertubations are dominated by continuous feedback," *J. Neurophysiol.*, vol. 98, no. 2, pp. 730–43, 2007.

[118] T. Kiemel, A. J. Elahi, and J. J. Jeka, "Identification of the Plant for Upright Stance in Humans: Multiple Movement Patterns From a Single Neural Strategy," *J. Neurophysiol.*, vol. 100, no. 6, pp. 3394–3406, 2008.

[119] K. Masani, V. W. Sin, A. H. Vette, T. Adam Thrasher, N. Kawashima, A. Morris, R. Preuss, and M. R. Popovic, "Postural reactions of the trunk muscles to multi-directional perturbations in sitting," *Clin. Biomech.*, vol. 24, no. 2, pp. 176–182, 2009.

[120] A. D. Goodworth and R. J. Peterka, "Contribution of Sensorimotor Integration to Spinal Stabilization in Humans," *J. Neurophysiol.*, vol. 102, no. 1, pp. 496–512, 2009.

[121] A. D. Goodworth and R. J. Peterka, "Influence of bilateral vestibular loss on spinal stabilization in humans," *J Neurophysiol*, vol. 103, no. 4, pp. 1978–1987, 2010.

[122] K. P. Granata and W. S. Marras, "An EMG-assisted model of loads on the lumbar spine during asymmetric trunk extensions," *J. Biomech.*, vol. 26, no. 12, pp. 1429–1438, 1993.

[123] K. P. Granata and W. S. Marras, “An EMG-assisted model of trunk loading during free-dynamic lifting,” *J. Biomech.*, vol. 28, no. 11, pp. 1309–1317, 1995.

[124] K. P. Granata and S. E. Wilson, “Trunk posture and spinal stability,” *Clin. Biomech.*, vol. 16, no. 8, pp. 650–659, 2001.

[125] M. M. Panjabi, R. A. Brand, and A. A. White, “Three-dimensional flexibility and stiffness properties of the human thoracic spine,” *J. Biomech.*, vol. 9, no. 4, pp. 185–192, 1976.

[126] M. M. Panjabi, A. M. Pearson, S. Ito, P. C. Ivancic, and J. L. Wang, “Cervical spine curvature during simulated whiplash,” *Clin. Biomech.*, vol. 19, no. 1, pp. 1–9, 2004.

[127] M. P. Kadaba, H. K. Ramakrishnan, and M. E. Wootten, “Measurement of Lower Extremity Kinematics During Level Walking,” *J. Orthop. Res.*, vol. 8, no. 3, pp. 383–392, 1990.

[128] H. K. Ramakrishnan and M. P. Kadaba, “Technical note on the estimation of joint kinematics during gait,” *J. Biomech.*, vol. 24, no. 10, pp. 969–977, 1991.

[129] C. N. Armitano, S. Morrison, and D. M. Russell, “Upper body accelerations during walking are altered in adults with ACL reconstruction.,” *Gait Posture*, vol. 58, no. August, pp. 401–408, 2017.

[130] C. Mazzà, M. Donati, J. McCamley, P. Picerno, and A. Cappozzo, “An optimized Kalman filter for the estimate of trunk orientation from inertial sensors data during treadmill walking,” *Gait Posture*, vol. 35, no. 1, pp. 138–142, 2012.

[131] R. J. Konz, S. Fatone, R. L. Stine, A. Ganju, S. A. Gard, and S. L. Ondra, “A Kinematic Model to Assess Spinal Motion During Walking,” *Spine (Phila. Pa. 1976).*, vol. 31, no. 24, pp. 898–906, 2006.

[132] M. B. Syczewska, T. Oberg, and D. Karlsson, “Segmental movements of the spine during treadmill walking with normal speed,” *Clin. Biomech.*, vol. 14, no. 6, pp. 384–388, 1999.

[133] M. L. Gatton and M. J. Pearcy, “Kinematics and movement sequencing during ¯ exion of the lumbar spine,” *Clin. Biomech.*, vol. 14, pp. 376–383, 1999.

[134] E. Al-Eisa, D. Egan, K. Deluzio, and R. Wassersug, “Effects of Pelvic Skeletal Asymmetry on Trunk Movement Three-Dimensional Analysis in Healthy Individuals Versus Patients With Mechanical Low Back Pain,” *Spine (Phila. Pa. 1976).*, vol. 31, no. 3, pp. 71–79, 2006.

[135] R. Preuss and J. Fung, “Musculature and biomechanics of the trunk in the maintenance of upright posture,” *J. Electromyogr. Kinesiol.*, vol. 18, pp. 815–828, 2008.

[136] R. A. Preuss and M. R. Popovic, “Three-dimensional spine kinematics during multidirectional, target-directed trunk movement in sitting,” *J. Electromyogr. Kinesiol.*, vol. 20, no. 5, pp. 823–832, 2010.

[137] P. S. Sung and P. M. Leininger, “A kinematic and kinetic analysis of spinal region in subjects with and without recurrent low back pain during one leg standing,” *Clin. Biomech.*, vol. 30, no. 7, pp. 696–702, 2015.

[138] S. Schmid, B. Bruhin, D. Ignasiak, J. Romkes, W. R. Taylor, S. J. Ferguson, R. Brunner,

and S. Lorenzetti, “Spinal kinematics during gait in healthy individuals across different age groups,” *Hum. Mov. Sci.*, vol. 54, no. April, pp. 73–81, 2017.

[139] L. Christian and G. Denis, “A Comparison between two dynamic methods to estimate triaxial net reaction moments at the L5/S1 joint during lifting,” *Clin. Biomech.*, vol. 13, no. 1, pp. 36–47, 1998.

[140] J. P. Callaghan, A. E. Patla, and S. M. McGill, “Low back three dimensional joint forces, kinematics, and kinetics during walking,” *Clin. Biomech.*, vol. 14, pp. 203–216, 1999.

[141] C. Larivière, D. Gagnon, and P. Loisel, “A biomechanical comparison of lifting techniques between subjects with and without chronic low back pain during freestyle lifting and lowering tasks,” *Clin. Biomech.*, vol. 17, no. 2, pp. 89–98, 2002.

[142] B. D. Hendershot and E. J. Wolf, “Three-dimensional joint reaction forces and moments at the low back during over-ground walking in persons with unilateral lower-extremity amputation,” *Clin. Biomech.*, vol. 29, no. 3, pp. 235–242, 2014.

[143] B. D. Hendershot and E. J. Wolf, “Persons with unilateral transfemoral amputation have altered lumbosacral kinetics during sitting and standing movements,” *Gait Posture*, vol. 42, no. 2, pp. 204–209, 2015.

[144] G. S. Faber, C. C. Chang, I. Kingma, J. T. Dennerlein, and J. H. Van Dieën, “Estimating 3D L5 / S1 moments and ground reaction forces during trunk bending using a full-body ambulatory inertial motion capture system,” *J. Biomech.*, vol. 49, no. 6, pp. 904–912, 2016.

[145] J. Seay, W. S. Selbie, and J. Hamill, “In vivo lumbo-sacral forces and moments during constant speed running at different stride lengths.,” *J. Sports Sci.*, vol. 26, no. 14, pp. 1519–29, 2008.

[146] D. J. Pearsall, J. G. Reid, and L. a Livingston, “Segmental inertial parameters of the human trunk as determined from computed tomography.,” *Ann. Biomed. Eng.*, vol. 24, no. 2, pp. 198–210, 1996.

[147] D. Lenzi, A. Cappello, and L. Chiari, “Influence of body segment parameters and modeling assumptions on the estimate of center of mass trajectory,” *J. Biomech.*, vol. 36, no. 9, pp. 1335–1341, 2003.

[148] T. C. Nguyen and K. J. Reynolds, “The effect of variability in body segment parameters on joint moment using Monte Carlo simulations,” *Gait Posture*, vol. 39, no. 1, pp. 346–353, 2014.

[149] K. J. Ganley and C. M. Powers, “Determination of lower extremity anthropometric parameters using dual energy X-ray absorptiometry : the influence on net joint moments during gait,” *Clin. Biomech.*, vol. 19, pp. 50–56, 2004.

[150] M. Kay Lee, N. Sang Le, A. C. Fang, and M. T. H. Koh, “Measurement of body segment parameters using dual energy X-ray absorptiometry and three-dimensional geometry : An application in gait analysis,” *J. Biomech.*, vol. 42, pp. 217–222, 2009.

[151] S. Chen, H. Hsieh, T. Lu, and C. Tseng, “A method for estimating subject-specific body

segment inertial parameters in human movement analysis," *Gait Posture*, vol. 33, no. 4, pp. 695–700, 2011.

[152] K. J. Ganley and C. M. Powers, "Anthropometric parameters in children: A comparison of values obtained from dual energy x-ray absorptiometry and cadaver-based estimates," *Gait Posture*, vol. 19, no. 2, pp. 133–140, 2004.

[153] R. K. Jensen, "Changes in segment inertia proportions between 4 and 20 years," *J. Biomech.*, vol. 22, no. 6–7, pp. 529–536, 1989.

[154] D. J. Pearsall and P. A. Costigan, "The effect of segment parameter error on gait analysis results," *Gait Posture*, vol. 9, no. 3, pp. 173–183, 1999.

[155] M. Damavandi, N. Farahpour, and P. Allard, "Determination of body segment masses and centers of mass using a force plate method in individuals of different morphology," *Med. Eng. Phys.*, vol. 31, no. 9, pp. 1187–1194, 2009.

[156] P. E. Martin, M. Mungiole, and J. M. Longhill, "The Use of Magnetic Resonance Imaging for Measuring Segment Inertial Properties," *J. Biomech.*, no. 4, pp. 367–376, 1989.

[157] P. E. M. Michael Mungiole, "Estimating Segment Inertial Properties: Comparison of Magnetic Resonance Imaging With Existing Methods," *J. Biomech.*, vol. 23, no. 10, pp. 1039–1046, 1990.

[158] D. J. Pearsal, J. G. Reid, and R. Rosst, "Inertial Properties of the Human Trunk of Males Determined from Magnetic Resonance Imaging," *Ann. Biomed. Eng.*, vol. 22, pp. 692–706,

1994.

[159] C. Cheng, H. Chen, C. Chen, C. Lee, and C. Chen, “Segment inertial properties of Chinese adults determined from magnetic resonance imaging,” *Clin. Biomech.*, vol. 15, pp. 559–566, 2000.

[160] P. De Leva, “Adjusments to Zatiorsky-Seluyanov’s Segment Inertia Parameters,” *J. Biomech.*, vol. 29, no. 9, pp. 1223–1230, 1996.

[161] J. L. Durkin, J. J. Dowling, and D. M. Andrews, “The measurement of body segment inertial parameters using dual energy X-ray absorptiometry,” *J. Biomech.*, vol. 35, pp. 1575–1580, 2002.

[162] J. Wicke and G. A. Dumas, “Estimating Segment Inertial Parameters Using Fan-Beam DXA,” *J. Appl. Biomech.*, vol. 24, pp. 180–184, 2008.

[163] J. L. Durkin and J. J. Dowling, “Analysis of Body Segment Parameter Differences Between Four Human Populations and the Estimation Errors of Four Popular Mathematical Models,” *J. Biomech. Eng. ASME*, vol. 125, no. August 2003, pp. 515–522, 2003.

[164] R. K. Jensen, “Estimation of the biomechanical properties of three body types using a photogrammetric method,” *J. Biomech.*, vol. 11, no. 8–9, pp. 349–358, 1978.

[165] R. Dumas, L. Chèze, and J. P. Verriest, “Adjustments to McConville et al. and Young et al. body segment inertial parameters,” *J. Biomech.*, vol. 40, no. 3, pp. 543–553, 2007.

[166] T. C. Pataky, V. M. Zatsiorsky, and J. H. Challis, “A simple method to determine body segment masses in vivo : reliability , accuracy and sensitivity analysis,” *Clin. Biomech.*, vol. 18, pp. 364–368, 2003.

[167] C. Hansen, G. Venture, N. Rezzoug, P. Gorce, and B. Isableu, “An individual and dynamic Body Segment Inertial Parameter validation method using ground reaction forces,” *J. Biomech.*, vol. 47, no. 7, pp. 1577–1581, 2014.

[168] D. G. Heiss and G. Pagnacco, “Effect of center of pressure and trunk center of mass optimization methods on the analysis of whole body lifting mechanics,” *Clin. Biomech.*, vol. 17, pp. 106–115, 2002.

[169] A. Karlsson and G. Frykberg, “Correlations between force plate measures for assessment of balance,” *Clin. Biomech.*, vol. 15, pp. 365–369, 2000.

[170] A. Ruhe, R. Fejer, and B. Walker, “The test-retest reliability of centre of pressure measures in bipedal static task conditions - A systematic review of the literature,” *Gait Posture*, vol. 32, no. 4, pp. 436–445, 2010.

[171] R. Pàmies-Vilà, J. M. Font-Llagunes, J. Cuadrado, and F. J. Alonso, “Analysis of different uncertainties in the inverse dynamic analysis of human gait,” *Mech. Mach. Theory*, vol. 58, pp. 153–164, 2012.

[172] H. B. Schmiedmayer and J. Kastner, “Parameters influencing the accuracy of the point of force application determined with piezoelectric force plates,” *J. Biomech.*, vol. 32, no. 11,

pp. 1237–1242, 1999.

[173] H. B. Schmiedmayer and J. Kastner, “Enhancements in the accuracy of the center of pressure (COP) determined with piezoelectric force plates are dependent on the load distribution.,” *J. Biomech. Eng.*, vol. 122, no. 5, pp. 523–527, 2000.

[174] D. Barbado, J. Moreside, and F. J. Vera-garcia, “Reliability and Repetition Effect of the Center of Pressure and Kinematics Parameters That Characterize Trunk Postural Control During Unstable Sitting Test,” *PM&R*, vol. 9, no. 3, pp. 219–230, 2017.

[175] R. Dumas, E. Nicol, and L. Chèze, “Influence of the 3D Inverse Dynamic Method on the Joint Forces and Moments During Gait,” *J. Biomech. Eng. ASME*, vol. 129, pp. 786–790, 2007.

[176] A. G. Schache and R. Baker, “On the expression of joint moments during gait,” *Gait Posture*, vol. 25, pp. 440–452, 2007.

[177] J. P. Holden and S. J. Stanhope, “The effect of variation in knee center location estimates on net knee joint moments,” *Gait Posture*, vol. 7, pp. 1–6, 1998.

[178] A. Cappozzo, “Minimum measured-input models for the assessment of motor ability,” *J. Biomech.*, vol. 35, pp. 437–446, 2002.

[179] C. Mazzà and A. Cappozzo, “An optimization algorithm for human joint angle time-history generation using external force data,” *Ann. Biomed. Eng.*, vol. 32, no. 5, pp. 764–772, 2004.

[180] L. to the Editor, “ISB recommendation on definitions of joint coordinate system of various joints for the reporting of human joint motion—part I: ankle, hip, and spine,” *J. Biomech.*, vol. 35, pp. 543–548, 2002.

Appendices

Appendix A: Inter-segmental Moments after Error Compensation

Figure A. 1 to Figure A. 5 show the inter-segmental moment (Nm) normalized by body weight and trunk height of the participants (BW×TH %). Given are the moments at all joint levels for five trunk-bending directions after compensating errors due to soft tissue artifacts and using individual-specific BSPs and COP offset. Results are presented as *mean* (solid line) and *mean* ± *standard deviation* (shaded area) for sagittal, coronal, and transverse planes.

Figure A. 1

Normalized Joint Moment (BW×TH %) Bending toward Left Target

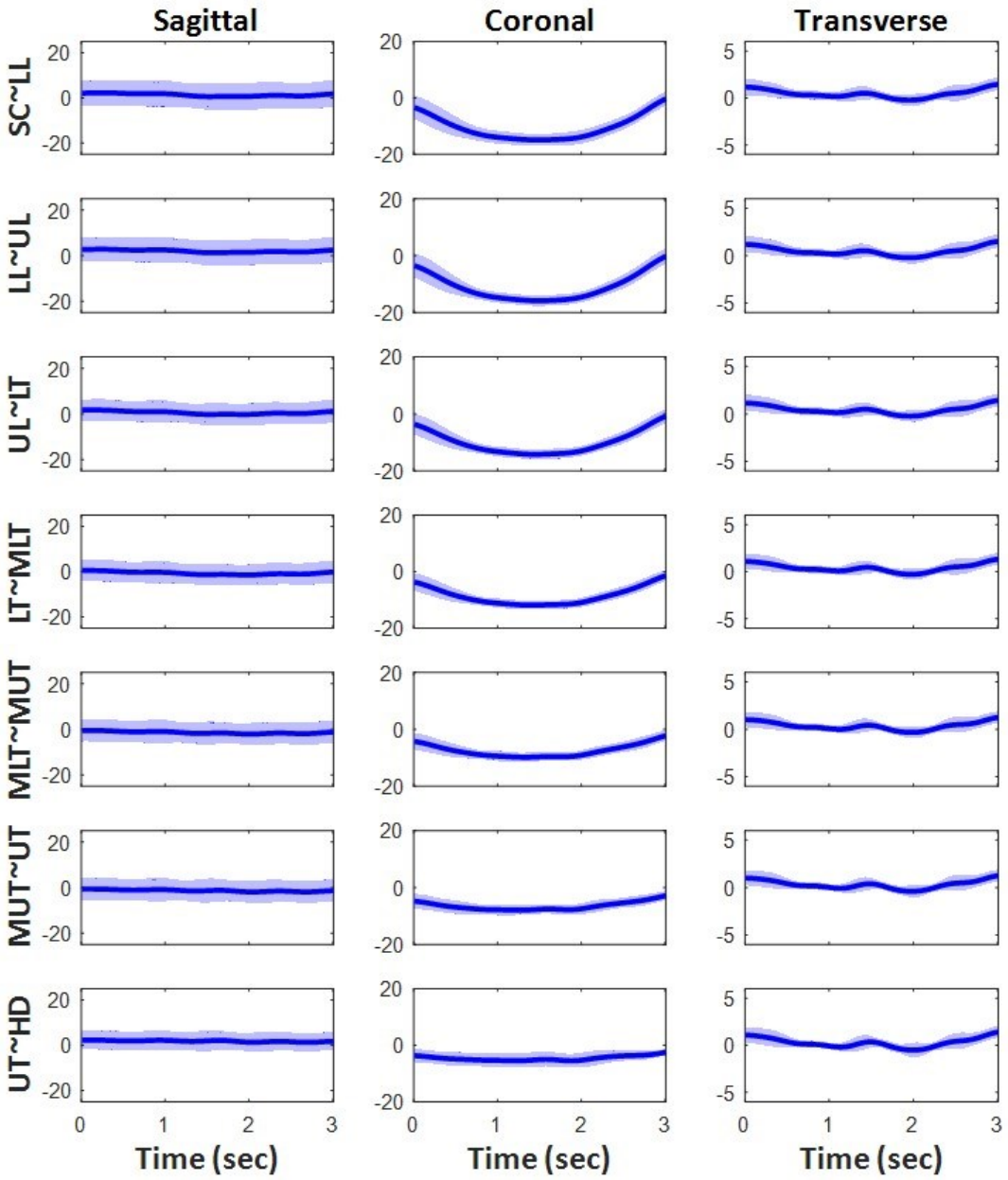

Figure A. 2

Normalized Joint Moment (BW×TH %) Bending toward Anterior-Left Target

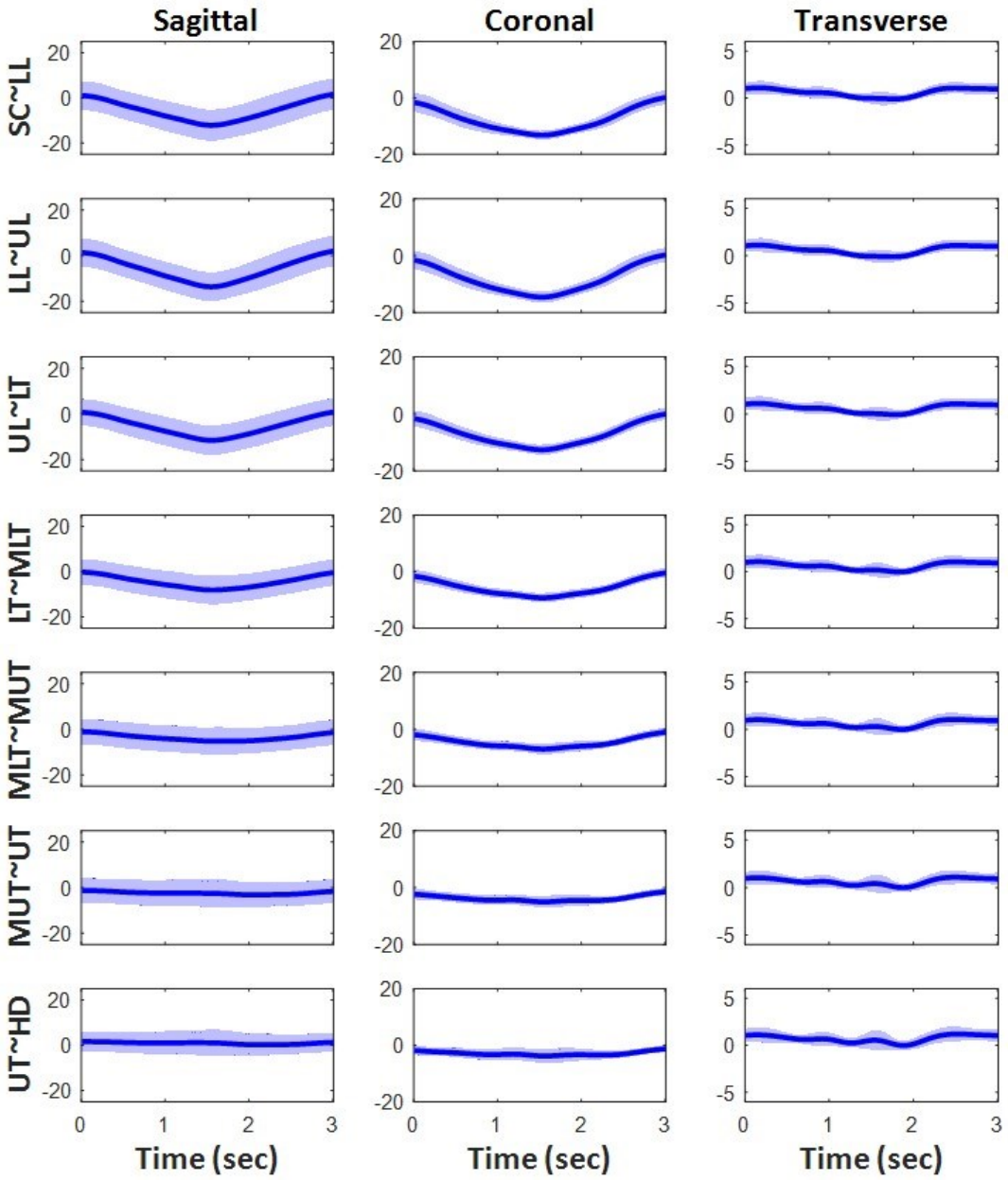

Figure A. 3

Normalized Joint Moment (BW×TH %) Bending toward Anterior Target

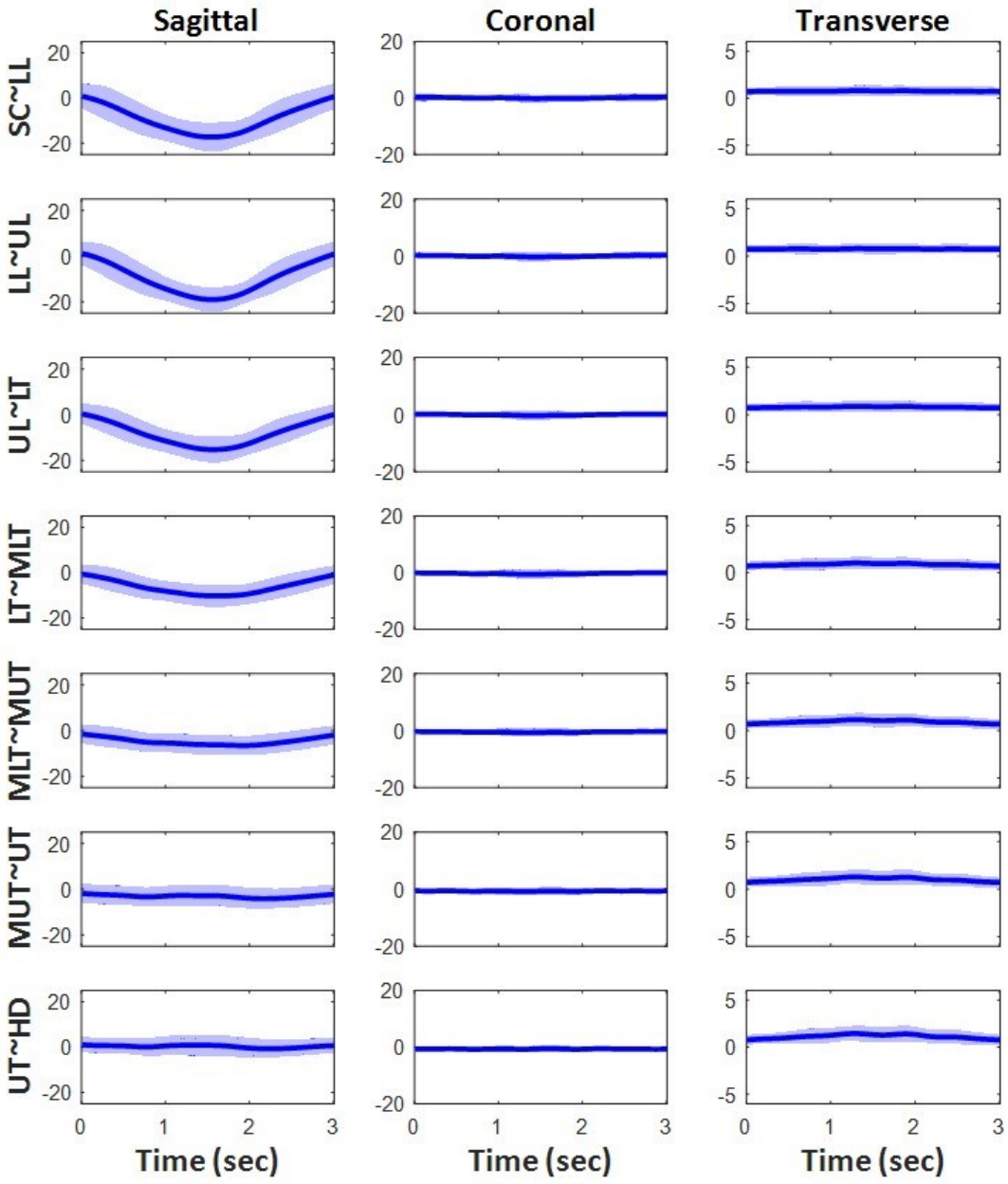

Figure A. 4

Normalized Joint Moment (BW×TH %) Bending toward Anterior-Right Target

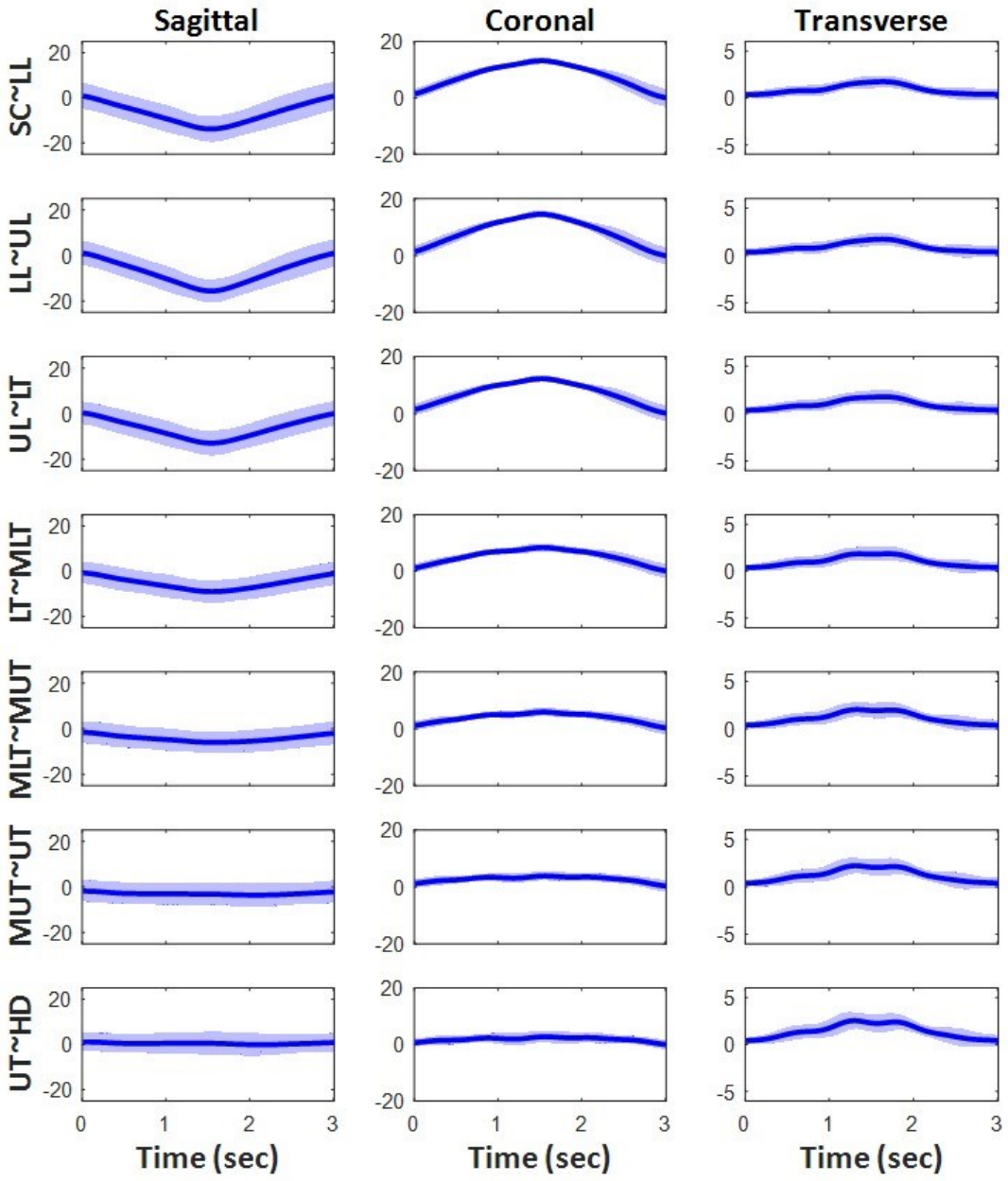

Figure A. 5

Normalized Joint Moment (BW×TH %) Bending toward Right Target